Reverse Genetic Analysis of Coronavirus Replication

Dissertation

zur

Erlangung der naturwissenschaftlichen Doktorwürde

(Dr. sc. nat.)

vorgelegt der

Mathematisch-naturwissenschaftlichen Fakultät

der Universität Zürich

von

Roland Züst

aus Lutzenberg, AR

2008

Promotionskomitee

PD Dr. V. Thiel (Supervisor)

Prof. Dr. M. O. Hottiger (Leiter der Dissertation)

Prof. Dr. M. O. Hengartner

PD Dr. B. Ludewig

Table of contents

Table of contents **2**

1 Summary **5**

2 Zusammenfassung **7**

3 Abbreviations **9**

4 Introduction **12**

4.1 Coronavirus classification 12

4.2 Coronavirus morphology 15

4.3 Coronavirus genome organization and replication 15

4.3.1 The coronavirus genome 15

4.3.2 Coronavirus replication cycle 17

4.4 Coronavirus genes 21

4.4.1 Coronavirus structural genes 21

4.4.2 Coronavirus accessory genes 23

4.4.3 Coronavirus replicase gene 23

4.4.3.1 Nonstructural protein 1 (nsp1) 24

4.4.3.2 Nonstructural protein 2 (nsp2) 24

4.4.3.3 Nonstructural protein 3 (nsp3) 24

4.4.3.4 Nonstructural protein 4 (nsp4) 26

4.4.3.5 Nonstructural protein 5 (nsp5) 26

4.4.3.6 Nonstructural protein 6 (nsp6) 26

4.4.3.7 Nonstructural proteins 7-11 (nsps7-11) 26
4.4.3.8 Nonstructural protein 12 (nsp12) 27
4.4.3.9 Nonstructural protein 13 (nsp13) 27
4.4.3.10 Nonstructural protein 14 (nsp14) 28
4.4.3.11 Nonstructural protein 15 (nsp15) 28
4.4.3.12 Nonstructural protein 16 (nsp16) 29
4.5 Coronavirus *cis*-acting elements 29
4.5.1 The coronavirus ribosomal frameshift element 29
4.5.2 *Cis*-acting elements regulating sg mRNA synthesis 30
4.5.3 *Cis*-acting elements regulating genome RNA replication 32
4.6 Coronavirus reverse genetics 34
4.7 Innate immunity and coronavirus 35
5 Aim of the thesis 37
6 Original research articles 38
7 Unpublished data 74
7.1 Introduction 74
7.2 Results 75
7.2.1 The role of nsp14 in viral replication 75
7.2.2 The role of nsp15 in viral replication 78
7.2.3 The role of nsp16 in viral replication 79
8 Discussion 81
8.1 Summary of own findings 81
8.2 Interactions of replicase gene products with 3' UTR 82

8.3 Coronavirus interaction with the type I IFN system 83

8.4 The role of nsp1 in viral replication.....84

9 Future perspectives 87

10 References.....88

11 Curriculum Vitae.....108

12 Acknowledgements.....110

1 Summary

Coronaviruses are large positive-stranded RNA viruses that are able to infect a broad range of vertebrates and are mainly associated with respiratory, enteric, and sometimes, systemic diseases. Human coronaviruses are known to generally cause mild upper-respiratory tract disease including common cold, and occasional enteric infections. The emergence of a novel coronavirus causing severe acute respiratory syndrome (SARS) highlighted the potential of coronaviruses to seriously impact on human health.

The functions of a large number of coronavirus-encoded proteins and *cis*-acting RNA elements are poorly understood or unknown. The major aim of this thesis was to investigate the role of replicase-encoded gene products in the context of both viral RNA replication and host interactions. We mainly focused on the replicase-encoded non-structural proteins (nsps) nsp1, nsp8 and nsp9. In addition to the characterization of viral functions we also studied coronavirus-host interactions in the context of host innate immune responses.

Nsp8 and nsp9 have been recently described to bind RNA molecules but the exact function(s) and RNA substrate specificities remained elusive. The analysis of an MHV mutant (Alb391) that carries a 6 nucleotide insertion in an essential 3' *cis*-acting RNA element allowed us to provide conclusive genetic evidence that this 3' *cis*-acting element interacts with nsp8 and nsp9. Our data furthermore indicate that the extreme 3'-end of the MHV genomic RNA is involved in this interaction and that a large portion of the 3' untranslated region of MHV is dispensable for viral RNA replication. Collectively, our studies led us to propose a substantially refined model for the initiation of coronavirus negative strand RNA synthesis.

There is accumulating evidence that a number of coronavirus gene products are involved in virus-host interactions. Our studies on the impact of host innate immune responses revealed that coronaviruses are very poor inducers of type I interferons (IFNs). However, the infection of type I IFN receptor-deficient mice with mouse hepatitis virus (MHV) revealed that a swift induction of type I IFNs is essential to combat coronavirus infections. We could demonstrate that plasmacytoid dendritic cells (pDCs) are able to sense coronavirus infections through toll-like receptor 7

(TLR7) and that pDCs are in fact the main producers of protective type I IFNs early after infection. The impact of pDC-derived type I IFNs was demonstrated by antibody-mediated depletion of pDCs in mice which results in increased virus replication, spread and severity of disease.

Finally, we have generated and characterized an MHV mutant bearing a deletion in the C-terminal region of nsp1. We showed that this nsp1 mutant can grow to high viral titers in tissue culture, but is strongly attenuated in mice. Attenuation was abolished in mice lacking the type I IFN receptor, suggesting a pivotal role of nsp1 in modulating host innate immune responses. Additionally we demonstrated that this virus retained the ability to replicate in professional antigen presenting cells and, consequently, was found to be highly immunogenic. Immunization with this nsp1 mutant virus elicited potent cytotoxic T cell responses and protected mice against homologous and heterologous virus challenge. Taken together, the presented attenuation strategy has implications for the rational design of live attenuated coronavirus vaccines aimed at preventing coronavirus-induced diseases of veterinary and medical importance, including the potentially lethal SARS.

2 Zusammenfassung

Cornaviren sind grosse positiv-strängige RNS Viren, die ein breites Spektrum von Wirbeltieren infizieren und hauptsächlich Atmungs-, Magen-Darm- und manchmal Systemische Krankheiten verursachen. Humane Coronaviren sind dafür bekannt, meist milde Infektionen der oberen Atemwege zu verursachen, können aber gelegentlich auch Krankheiten des Verdauungstrakts hervorrufen. Das Auftauchen eines neuen Coronavirus, das das schwere akute respiratorische Syndrom (SARS), eine schwere Form der Lungenentzündung, verursacht, legte das Potential dieser Viren, ernsthaft die menschliche Gesundheit zu gefährden, an den Tag.

Die Funktionen vieler Coronavirus-kodierter Proteine und *cis*-wirkende RNS Elemente sind kaum verstanden oder gar unbekannt. Das wichtigste Ziel dieser Thesis war es, die Rolle der Replikase-kodierten Genprodukte sowohl im Kontext der viralen Replikation, als auch deren Interaktionen mit dem Wirt zu untersuchen. Wir schenkten unsere Aufmerksamkeit hauptsächlich den Replikase-kodierten nicht-strukturellen Proteinen (nsps) nsp1, nsp8 und nsp9. Nebst der Charakterisierung der viralen Funktionen haben wir uns auch zum Ziel gesetzt, Coronavirus-Wirt-Interaktionen im Rahmen der angeborenen Immunantwort zu untersuchen.

Nsp8 und nsp9 wurden kürzlich als RNS-bindende Moleküle beschrieben, aber ihre exakte(n) Funktion(en) und RNS Substratspezifitäten sind unbekannt. Die Analyse einer MHV Mutante (Alb391), die eine Insertion von 6 Nukleotiden in einem essentiellen 3‘ *cis*-wirkenden RNS Element hat, hat aufgezeigt, dass dieses 3‘ *cis*-wirkende RNS Element mit nsp8 und nsp9 interagiert. Des weiteren weisen unsere Daten darauf hin, dass das extreme 3‘ Ende der genomischen MHV RNS an dieser Interaktion beteiligt ist, und dass grosse Teile der 3‘ nicht-translatierten viralen RNS für die virale Replikation entbehrlich sind. Unsere Studien erlauben uns ein substanziell verfeinertes Modell der Initiierung der negativ-strang RNS Synthese der Coronaviren vorzuschlagen.

Die Anzeichen, dass etliche Coronavirale Gene in Virus-Wirt Interaktionen beteiligt sind, häufen sich. Unsere Studien über die Bedeutung der angeborenen Immunantwort des Wirts zeigten auf, dass Coronaviren sehr wenig Typ I Interferone (IFN) induzieren. Dennoch zeigt die Infektion von Mäusen, die den Typ I IFN Rezeptor nicht haben, dass eine rasche IFN Antwort essentiell für das Überleben des

Wirts und die Bekämpfung des Virus‘ ist. Wir konnten auch aufzeigen, dass plasmacytoide dendritische Zellen (pDCs) eine Cornavirusinfektion durch den Toll-like Rezeptor 7 (TLR7) erkennen, und dass diese pDCs die hauptsächliche Quelle für das protektive IFN sind. Der Einfluss des durch pDCs produzierten IFNs konnte durch die Depletion der pDCs mittels Antikörper demonstriert werden. MHV infizierte pDC-depletierte Mäuse erholten sich langsamer von der Krankheit und das Virus konnte besser replizieren und sich in verschiede Organe ausbreiten.

Schliesslich generierten und charakterisierten wir eine MHV Mutante, deren C-terminale Region des nsp1 deletiert wurde. Wir zeigten, dass diese Nsp1-Mutante zu hohen Titern in Zellkultur wachsen kann, aber in der Maus stark abgeschwächt ist. Diese Schwächung ist in Mäusen, die den Typ I IFN-Rezeptor nicht haben, wieder aufgehoben, wodurch eine zentrale Rolle von nsp1 in der Regulierung der angeborenen Immunantwort des Wirts verdeutlicht wird. Desweiteren konnten wir zeigen, dass das Virus immer noch in professionellen Antigen-präsentierenden Zellen wachsen konnte und infolgedessen hoch immunogen ist. Immunisierung von Mäusen mit der nsp1 Mutante rief eine starke zytotoxische T-Zell Antwort hervor, und konnte die Mäuse sowohl vor einer homologen als auch einer heterologen viralen Infektion schützen. Zusammenfassend hat die beschriebene Attenuationsstrategie Einfluss auf die zukünftige rationale Entwicklung von attenuierten coronaviralen Lebendimpfstoffen und könnte helfen, medizinisch und veterinärmedizinisch bedeutsame Coronaviren, einschliesslch des SARS-Coronavirus, wirksam zu bekämpfen.

3 Abbreviations

°C	Degree celsius
3CL	Poliovirus 3C like proteinase
A	Adenine
aa	Amino acid
ACE2	Angiotensin converting enzyme 2
ALT	Alanine 2-oxoglutarate-aminotransferase
BAC	Bacterial artificial chromosome
BCoV	Bovine coronavirus
BHK	Baby hamster kidney
Bp	Base pair
BSA	Bovine serum albumin
BtCoV	Bat coronavirus
C	Cytosine
cDC	Conventional dendritic cells
cDNA	Complementary (copy) DNA
CEACAM	Carcinoembryonic antigen-related cell adhesion molecule
CoV	Coronavirus
CPE	Cytopathogenic effect
C-terminus	Carboxyl-terminus
CTL	Cytotoxic T lymphocyte
CV1	African green monkey cells
d	Day
DMEM	Dulbecco´s Modified Eagles Medium
DMSO	Dimethylsulfoxid
DMV	Double membrane vesicles
DNA	Desoxyribonucleicacid
dNTP	Desoxynucleoside triphosphate
DTT	Dithiothreitol
E protein	Envelope protein
E. coli	*Escherichia coli*
e.g.	*Exempli gratia* (for example)
EDTA	Ethylendiamine tetraacetic acid
ELISA	Enzyme-linked immunosorbent assay
ER	Endoplasmatic reticulum
ERGIC	Endoplasmatic reticulum-Golgi intermediate compartment
FACS	Fluorescent activated cell sorter
FCS	Fetal calf serum
FeCoV	Feline Coronavirus
Fig.	Figure
FIPV	Feline infectious peritonitis virus
G	Guanine
g	Gram
GAPDH	Glyceraldehyde 3-phosphate dehydrogenase

GFP	Green fluorescent protein
gmRNA	Genomic mRNA
gpt	Guanine phosphoribosyltransferase
h	Hour
hAPN	human aminopeptidase N
HCoV	Human coronavirus
HCoV-229E	Human coronavirus 229E
HCoV-HKU1	Human coronavirus HKU1
HCoV-NL63	Human coronavirus NL63
HCoV-OC43	Human coronavirus OC43
HE	Hemagglutinin esterase
Hel	Helicase
His	Histidine
HVR	Hypervariable region
i.c.	Intra cranially
i.e.	*Id est* (that is)
i.p.	Intraperitoneally
IBV	Infectious Bronchitis Virus
IFN	Interferon
IRF7	Interferon regulatory factor 7
ISRE	Interferon stimulated response element
kb	Kilo base
kDa	Kilo Dalton
L	Liter
L929	Mouse fibroblast cells
LB	Luria Bertani Medium
LCMV	Lymphocytic choriomeningitis virus
M	Molar
M protein	Membrane protein
mAb	Monoclonal antibody
MEM	Minimal essential medium
MHV	Murine hepatitis virus
min	Minute
mL	Milliliter
mM	Millimolar
MOI	Multiplicity of infection
Mpro	Main proteinase
mRNA	Messenger RNA
N protein	Nucleocapsid protein
NendoU	Nidoviral uridylate-specific enoribonuclease
Nsp	Non-structural protein
nt	Nucleotide
N-terminus	Amino-terminus
ORF	Open reading frame
p.i.	Post infection

pAPC	Professional antigen presenting cell
PBMC	Peripheral blood mononuclear cells
PBS	Phophate buffered saline
PCR	Polymerase chain reaction
pDC	plasmacytoid dendritic cells
PEDV	Porcine epidemic diarrhea virus
PFU	Plaque forming units
pp	Polyprotein
PLP	Papain like proteinase
RL	Renilla luciferase
RNA	Ribonucleic acid
rnp	Ribonucleprotein
rpm	Revolutions per minute
RPMI 1640	Roswell Park Memorial Institute (cell culture medium)
RT	Reverse transcriptase
s	Second
S protein	Spike protein
SARS	Severe acute respiratory syndrome
SARS-CoV	SARS coronavirus
SD	Standard deviation
SDS	Sodium dodecylsulfate
sg	Subgenomic
sg mRNA	Subgenomic mRNA
SL-CoV	SARS-like coronavirus
SV40	Simian Virus 40
T	Thymine
TBE buffer	Tris borate EDTA buffer
TGEV	Transmissible gastroenteritis virus
TLR	Toll-like receptor
TRS	Transcription regulating sequence
ts	Temperature sensitive
U	Uracil
UTR	Untranslated region
V	Volts
vlp	Virus like particle
w/v	Weight per volume
µg	Microgram
µL	Microliter

4 Introduction

4.1 Coronavirus classification

The *Coronaviridae* family (genus Coronavirus (CoV) and genus Torovirus) belongs together with the families *Arteriviridae* and *Roniviridae* to the order *Nidovirales* (39, 48) (Table 1). Coronaviruses are positive stranded RNA viruses with a genome size of 27 to 31 kilobases (kb). They can infect numerous mammalian and avian species and mainly cause respiratory and enteric diseases. They have long been recognized as important pathogens of livestock and companion animals. In humans, coronaviruses are usually associated with upper respiratory tract infections and can cause the common cold.

In 2003, during the outbreak of the severe acute respiratory syndrome (SARS) in China, the causative agent of this disease was identified as a formerly unknown coronavirus (SARS-CoV). This virus was responsible for more than 8,000 documented cases, with a fatality rate of 10%, and spread to more than 30 countries. The resulting renewed interest in coronavirus research subsequently led to the discovery of two additional human coronaviruses HCoV-NL63 and HCoV-HKU1 (87, 154, 263, 278).

Initially, coronaviruses have been classified into three groups based on serological cross reactivity that were, more recently, supported by phylogenetic analyses. These analyses and the availability of an increasing number of coronavirus genome sequences, led to the concept to divide coronavirus groups I and II to subgroups Ia/Ib and IIa/IIb, respectively (94, 96, 215, 232). However, it should be noted that the recent detection of numerous group I and II and yet unclassified coronaviruses in bats most likely will lead to a further revision of the current coronavirus classification (49, 69, 89, 185).

Order	Family	Genus			Species
Nidovirales	Arteriviridae	Arterivirus			Equine arteritis virus (EAV) Lactate dehydrogenase- elevating virus (LDV) Porcine respiratory and reproductive syndrome virus (PRRSV) Simian hemorrhagic fever virus (SHFV)
	Roniviridae	Okavirus			Gill-associated virus (GAV) Yellow head virus (YHV)
	Coronaviridae	Torovirus			Equine torovirus (ETV) Bovine torovirus (BTV) Porcine torovirus (BTV) Human torovirus (HTV)
		Coronavirus	Group I	a	Transmissible gastroenteritis virus (TGEV) Feline infectious peritonitis virus (FIPV) Canine coronavirus (CCV)
				b	Human coronavirus NL63 (HCoV-NL63) Human coronavirus 229 E (HCoV-229E) Porcine diarrhea virus (PEDV) Bat coronavirus (BtCoV)*
			Group II	a	Human coronavirus OC43 (HCoV-OC43) Bovine coronavirus (BCoV) Murine coronavirus (MHV) Human coronavirus HKU1 (HCoV-HKU1)
				b	SARS coronavirus (SARS-CoV) SARS-like bat coronavirus (BtCoV) *
			Group III		Infectious bronchitis virus (IBV) Turkey coronavirus (TCoV)

Table 1: Overview of *Nidovirales* families, genera and species.

* Recently, numerous bat coronaviruses have been identified that are not yet classified or grouped according to their RNA-dependent RNA polymerase sequence into group Ib or group IIb.

Group I coronaviruses include the long-known human coronavirus 229E (HCoV-229E) as well as the porcine transmissible gastroenteritis virus (TGEV), feline coronaviruses (FeCoVs), and porcine diarrhea virus (PEDV). New group I coronaviruses include the human coronavirus NL63 (HCoV-NL63) (83, 87, 263) and several bat coronaviruses detected in China, Africa, Europe and America (69, 89, 185, 247, 274). HCoV-NL63 was isolated from a 7-month-old child suffering from bronchiolitis and conjunctivitis. HCoV-NL63 is distributed worldwide and can be responsible for up to 20% of human respiratory tract infections (common cold) during

winter time. Occasionally, HCoV-NL63 infections can also cause more severe clinical signs of disease especially in children, in adults with underlying disease or in elderly (reviewed in (262)).

The most extensively studied members of group II coronaviruses are murine hepatitis virus (MHV), bovine coronavirus (BCoV), and SARS-CoV. MHV (group IIa) can cause enteritis, pneumonia, hepatitis, and demyelinating encephalomyelitis in mice and is widely used as animal model for a number of diseases of medical importance, such as acute viral hepatitis or multiple sclerosis (17, 179). BCoV (group IIa) causes diarrhea in calves and cattles and mixed infection with other pathogens results in serious disease. The involvement of BCoV in respiratory tract diseases has also been reported (105, 106, 244). Interestingly, BCoV and HCoV-OC43 are highly homologous suggesting a relatively recent zoonotic transmission event about 100 years ago (271).

SARS-CoV, a group IIb member, mainly infects the lower respiratory tract and causes fever, dry cough, headache, hypoxemia and dyspnoea (51, 72, 199, 200, 215). The search of a reservoir for SARS-CoV has led to the discovery of a similar virus in bats, termed SARS-like bat coronavirus. Taking in consideration the diversity of species and the habitats bats occupy, large population sizes and densities, and the ability to migrate, bats appear to be ideal candidates for the natural reservoirs of many coronaviruses (74).

Group III coronaviruses include the avian coronavirus infectious bronchitis virus (IBV) that was the first coronavirus to be discovered in the 1930s. IBV is responsible for considerable economic losses in poultry and causes severe bronchiolitis and nephritis (38, 129). Although, IBV infections are usually not lethal, secondary microbial infections can increase disease severity and fatality. Other group III coronaviruses, that are genetically and antigenically related to IBV, cause enteric disease in turkeys (Turkey coronavirus), and respiratory and kidney disease in pheasants (Pheasant coronavirus). Recently IBV-like viruses have also been reported in several other *Gallinaceous* (avian fowl-like species) (reviewed in (40, 252).

4.2 Coronavirus morphology

The coronavirus RNA genome associates with the nucleocapsid protein (N) to form a helical ribonucleocapsid, which is surrounded by a membrane envelope. The size of the pleiomorphic coronavirus virion is 80 to 150 nm. Embedded within the envelope, there are three structural proteins expressed by all coronaviruses, i.e. the membrane (M) protein, the envelope (E) protein and the spike (S) protein. Some group IIa coronaviruses additionally encode a hemagglutininesterase (HE) which is also embedded into the viral envelope (174, 230). In electron microscopical images coronaviruses display a crown-like structure that gave rise to the name “Coronaviruses” (corona; latin: crown) and are formed by about 17 – 20 nm projections of S protein homotrimers (Fig. 1).

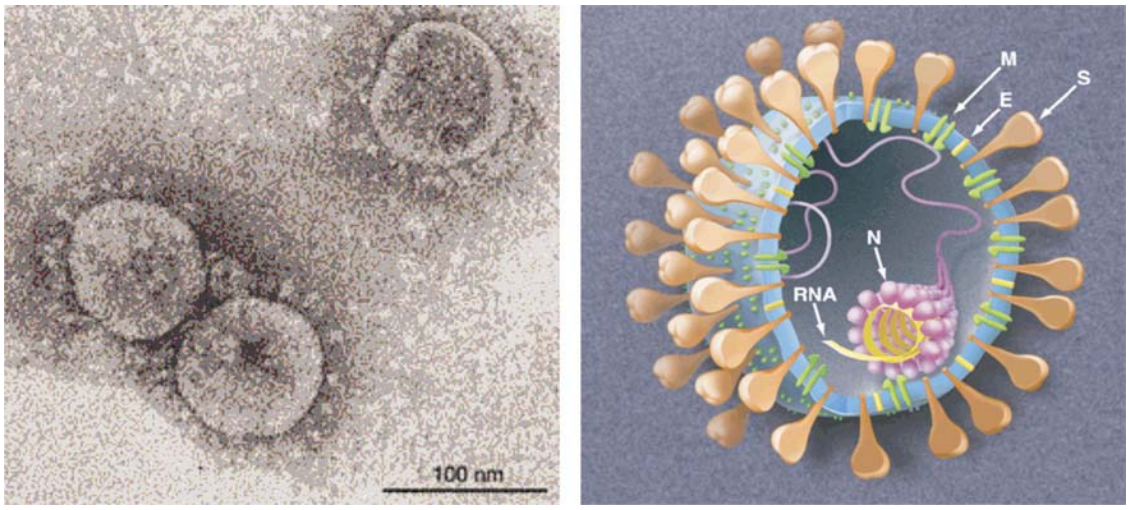

Fig1. Electron micrograph and schematic representation of a coronavirus.

Figures from Holmes and Enjuanes (79) and Stadler et al. (240).

4.3 Coronavirus genome organization and replication

4.3.1 The coronavirus genome

The coronavirus RNA genome is a linear, non-segmented, single stranded positive-sense RNA. The 5’ end is capped and the 3’ end is polyadenylated (150, 151). With a genome size of 27 kb to more than 31 kb, coronaviruses possess the largest known RNA genome among all RNA viruses.

Furthermore, all coronaviruses encode:

1. A 5’ untranslated region (UTR) of 209 nts (MHV-A59) to 528 nts (IBV-Beaudette) containing a so-called “leader sequence” of 65-98 nts at the extreme 5’ terminus and a short open reading frame (ORF) downstream the leader sequence that potentially encodes short peptides of 3-11 amino acids (aa) of unknown function.
2. A 3’ UTRs of 279 nts (TGEV) to 506 nts (IBV-Beaudette) followed by a poly(A) tail.
3. A replicase gene comprised of two overlapping ORFs, ORF1a and ORF1b spanning about two thirds of the coronavirus genome (approx. 20 kb). Coronavirus replicase gene expression is complex and involves a ribosomal frameshift mechanism to express ORF1b and extensive proteolytic processing of large replicase polyproteins (see below).
4. Four structural genes within the 3’-proximal one-third of the genome in the order (5’->3’) S-E-M-N.
5. One to seven accessory genes (formerly called group-specific genes) interspersed between the structural genes.

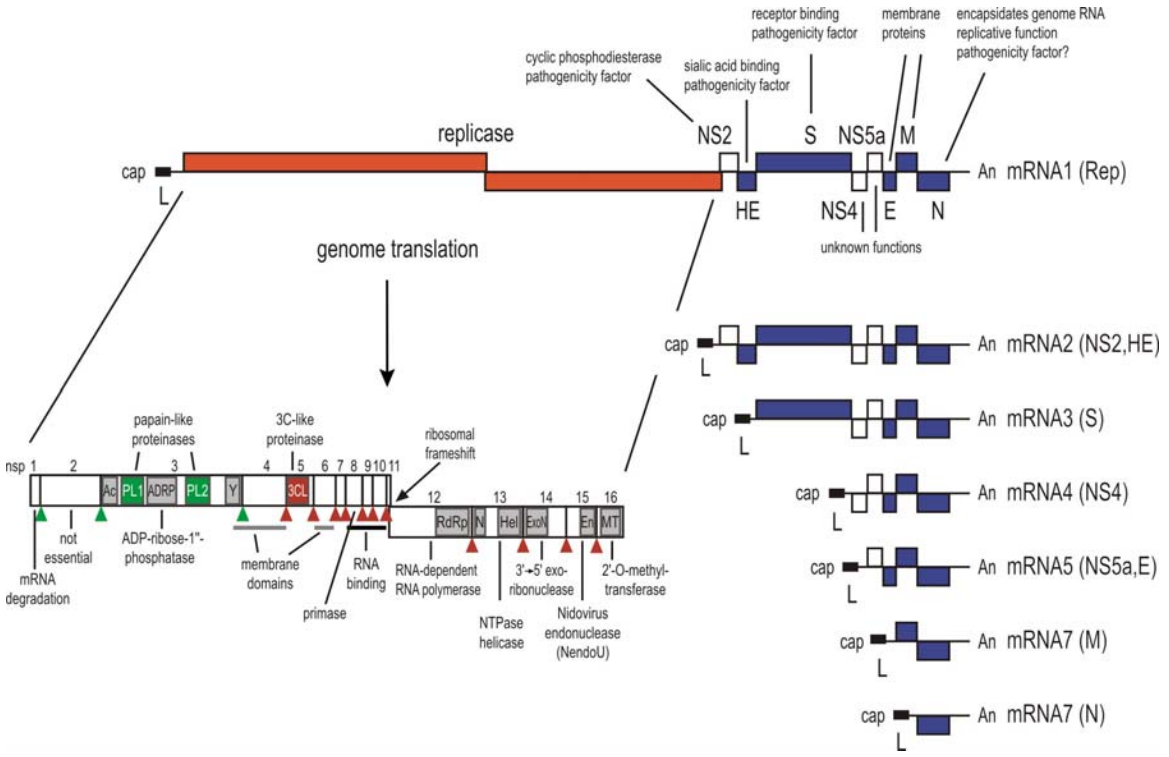

Fig. 2: Organization and expression of MHV-A59 genome

Structural relationship of the MHV-A59 genome and subgenomic RNAs are shown. The virus ORFs are depicted in red (replicase), white (accessory proteins) and blue (structural proteins). The black box represents the common 5' capped leader sequence, An indicates the poly(A)-tail. The ribosomal frameshift is indicated with an arrow. The autoproteolytic processing of ORF1a/ORF1ab polyprotein into the 16 nsps is shown. Nsp1-3 are processed by PL1/PL2 (green triangles), whereas nsp4-16 are processed by 3CL (red triangle). Known or putative protein functions are written above or below the corresponding box. Ac, acidic domain; L, leader; Y, Y domain, containing several transmembrane regions.

4.3.2 Coronavirus replication cycle

Replication of coronavirus begins with the association of the spike protein to its appropriate receptor and subsequent fusion of the lipid bilayer of the viral envelope with the host cell membrane and entry into the cell. Group IIa coronavirus MHV uses murine carcinoembryonic antigen-related cell adhesion molecules (CEACAMs), members of the immunoglobulin superfamily of receptors, whereas a number of group I coronaviruses, for example HCoV-229E, TGEV and FIPV require the zinc metalloprotease aminopeptidase N (APN, CD13) for entry into their target cells.

Human angiotensin-converting enzyme 2 (ACE2) has been identified as the receptor for SARS-CoV, a group IIb member and for HCoV-NL63, a group I member. For the most studied group III member, IBV, no specific and required host receptor has been identified, but preferential binding to sialic acid moieties could be demonstrated. (65, 73, 113, 163, 260, 277, 282).

After infection, the first ORF in the genome is translated as two large polyproteins pp1a and pp1ab of 495- or 803-kDa of size (for MHV), respectively (158). The distal positioned ORF 1b is expressed as a fusion protein with ORF 1a as a result from a -1 pseudoknot-induced ribosomal frameshift at a slippery sequence (25, 27-30, 66, 78, 109, 233). These large polyproteins are proteolytically processed by two or three functional proteinases into 15 (for group III coronaviruses) or 16 nonstructural proteins, nsp1-nsp16 (for group I and II coronaviruses) (Fig. 2). Coronaviruses usually posses 2 papain-like proteinases ($PL1^{pro}$ and $PL2^{pro}$; encoded in nsp3) and one poliovirus 3C-like proteinase ($3CL^{pro}$; encoded in nsp5). Exceptions are group III coronaviruses (e.g. IBV expresses an inactive form of $PL1^{pro}$) and group IIb coronaviruses (e.g. SARS-CoV and SARS-like CoV do not encode a $PL1^{pro}$ domain). The released processing products form the viral replicase/transcriptase complex that is engaged in the synthesis of the genomic and subgenomic RNAs.

Coronavirus RNA synthesis takes place in double membrane vesicles (DMV) most likely generated by the association of coronavirus non-structural proteins with host intracellular membranes (97, 104, 204, 228, 234). Shortly after replicase/transcriptase complex assembly, genomic and sg minus-strand RNAs are synthesized that serve as templates for the production of positive-strand genomic and sg mRNAs. Initially, it had been suggested, that the coronaviral replicase/transcriptase synthesizes only one minus-strand template of genome length that serves as template for all (genomic and sg) positive strand mRNAs. (149). However, the fact that coronavirus replicative intermediates of sg length function in RNA synthesis (220) and the discovery of minus-strand sg mRNA containing an anti-leader sequence at their 3'-end in TGEV infected cells (225, 226), led Sawicki and colleagues to propose a model termed "discontinuous extension of minus-strand RNA" (221). In this model the genomic RNA is the template for the synthesis of a set of genomic and sg minus strand RNAs. During minus strand synthesis, the viral replicase/transcriptase complex is suggested to pause at a transcription regulatory

sequence (TRS) and then relocate to the 5' end and re-initiate minus strand synthesis to add the anti-leader sequence to the nascent RNA chain. TRSs appear repeatedly in the genomic RNA, near the 5' end of the genome (downstream the leader sequence; "leader TRS") and at various positions downstream the replicase gene ("body TRSs"). Therefore, the discontinuous extension of minus strand RNAs results in a set of sg minus strand RNAs that differ in length according to the position of TRS elements within the genomic RNA template. Each minus strand sg RNA can serve a template for the production of a particular sg positive strand mRNA. As a result of this transcription mechanism a characteristic nested set of 3'-coterminal sg mRNAs with a common structure (a leader sequence of ~60-90 nts at the 5' end, followed by a TRS and a so-called "body" sequence at the 3' end) is produced. The model of discontinuous extension of minus-strand RNA has received support from a number of studies on Arteriviruses and Coronaviruses that demonstrated that the TRSs found in sg mRNAs of arteri- and coronaviruses are derived from the corresponding body TRSs (266, 267, 298). It is believed that only the 5'-terminal ORFs of coronavirus mRNAs are translated. Thus, although coronavirus mRNAs are structurally polycistronic (except the smallest sg mRNA), they most likely function as monocistronic mRNAs with only the 5'-ORF being translated (35, 128, 159).

Coronavirus sg mRNAs encode for accessory proteins that are usually dispensable for virus replication in tissue culture and for structural proteins that are needed to assemble progeny virus particles. Coronaviruses particle assembly and budding takes place at the *cis*-Golgi network also known as Endoplasmatic-Reticulum-Golgi-Intermediate-Compartment (ERGIC) (218, 258, 259). The E and M proteins play an important role during virus budding and have been proposed to induce virus envelope curvature during MHV and SARS-CoV infection (7, 47, 169, 208). Co-expression of E and M from MHV, TGEV, IBV, and SARS-CoV in mammalian expression systems results in formation of virus-like particles (VLP) (16, 47, 145, 183, 268). Furthermore it has been shown, that both MHV and IBV E are sufficient for the generation of VLPs (47, 169) suggesting that neither N nor S are needed for viral budding. In contrast Huang et al. described that M and N are sufficient for the formation of SARS-CoV pseudoparticles (118) suggesting a minor role of E in viral release. Notably, the dependence of E for virus particle formation may vary amongst coronaviruses, or coronavirus groups, since MHV and SARS-CoV

mutants lacking the entire E gene are viable, but at variance E gene-deleted TGEV mutants were not viable (64, 147, 197).

In order to produce infectious particles the genomic RNA has to be incorporated into the virions. This is assisted by the formation of a complex of N and viral genomic RNA called ribonucleoprotein (RNP) complex. The nucleocapsid protein condenses the large RNA molecule so that it fits into the relatively small virus particle. It has been reported that the MHV N protein specifically recognizes a packaging signal encoded within ORF1b of MHV. However, N protein was also reported to bind to TRS elements, leader RNA and even unspecifically to any RNA (46, 54, 173, 182, 194, 214, 243, 293). Alternatively, it has been proposed that, at least for MHV, the M protein might interact with the packaging signal. The specificity is granted by the finding that M coimmunoprecipitates only N bound to genomic RNA but not N bound to sg mRNA (191-193). Recent work demonstrated that M and E proteins from MHV can incorporate a heterologous RNA molecule only if it contained the packaging signal. The direct selection of packaging signal RNA has been attributed to M, making this protein to the key player in viral assembly (189).

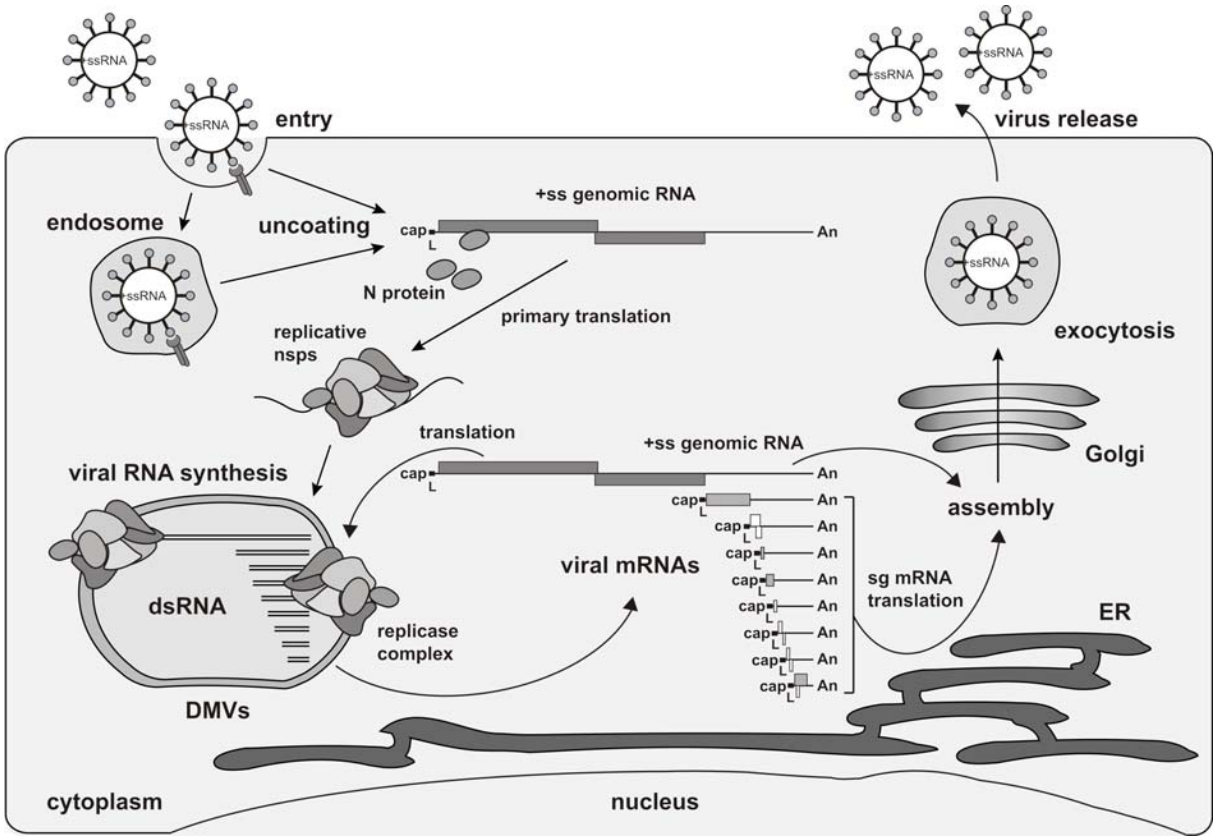

Fig. 3: The coronavirus replication cycle

After adsorption of viral particles the positive-stranded RNA genome is uncoated and replication starts in the cytosol. A nested set of subgenomic mRNA is produced in double membrane vesicles by discontinuous transcription during minus-strand synthesis resulting in structural (spike (S), envelope (E), membrane (M), nucleocapsid (N)) and non-structural proteins (nsps). Viral proteins assemble and bud at the ER Golgi intermediate compartment (ERGIC) and are processed in the Golgi apparatus. Newly produced viral particles are incorporated in vesicles and released by exocytosis. Picture adapted from (257).

4.4 Coronavirus genes

4.4.1 Coronavirus structural genes

Conservation of the N protein among coronaviruses is relatively poor, but sequence comparison revealed three domains of which the middle one possesses RNA binding capacity (152, 176, 194, 299). After reverse genetic systems have been established, it has been reported, that the recovery of recombinant coronaviruses is critically facilitated by N protein expression (3, 13, 37, 45, 223, 253-256, 285-287).

This effect may be related to the finding that N protein is required for efficient genome RNA replication (3, 223). Thus, in addition to the function as a structural protein, N is also involved in coronavirus RNA synthesis.

The M protein is a key player of virus assembly and budding and is able to interact with S, E, and N (61, 107, 119, 273). It is a triple spanning membrane protein and has a short glycosylated ectodomain and a large C-terminus endodomain. MHV M gene mutants encoding an M protein that lacks two aa at the carboxyterminus have been generated. These mutants formed initially tiny plaques but after several passages in tissue culture gained fitness. Isolated clones contained compensatory mutations in N indicating a direct protein-protein interaction between M and N (146). This interaction has been further corroborated: clustered charged-to-alanine N gene mutants have been constructed, and indeed, some second-site revertants contained mutations within the M gene (119).

Another membrane protein is E which has low abundance in infected cells. Nonetheless it plays a pivotal role in coronavirus assembly (23, 268). Reverse genetic studies of TGEV revealed an indispensable role of E in TGEV propagation (50, 197). However, recombinant and viable MHV and SARS-CoV mutants lacking E have been reported, although the mutant MHV virus displayed a small plaque phenotype and grew to greatly reduced titers (64, 147). Notably, the MHV E gene could functionally be replaced by BCoV, SARS-CoV (group II coronaviruses) or IBV (group III coronavirus) E genes, but not by the TGEV (group I coronavirus) E gene (145). Whether the requirement of E in particle formation differs amongst coronavirus groups remain to be elucidated.

The most intensively studied coronavirus structural protein is the heavily glycosylated S protein with a molecular weight of 150-200 kDa. It is responsible for the corona-like shape of the virion as perceived by electron microscopy. It plays an important role in receptor binding, membrane fusion, tropism and pathogenesis. A seminal experiment performed by Kuo et al. showed that S determines the tropism. They fused the carboxyterminal 64 residues of MHV S protein (representing the endo- and tansmembrane-domains) to the FIPV spike ectodomain. This virus termed feline MHV (fMHV) lost the ability to infect murine cells but could now infect feline cells (144). The fMHV virus is now used in a modified protocol of the targeted recombination-based reverse genetic system (177).

4.4.2 Coronavirus accessory genes

A variety of genes encoding accessory proteins are interspersed between the structural genes. Their number and location varies within coronavirus genomes and their functions are largely unknown. Some concordance, also regarding the positions where these genes are encoded within the genome, can be observed within groups or subgroups of coronaviruses. For one accessory protein, namely the NS2 protein encoded in mRNA2 of MHV and some other group IIa coronaviruses, a cyclic phosphodiesterase (CPD) activity has been predicted (232). This activity may rather play a role *in vivo* than *in vitro*, since a single aa substitution (Leu94Pro) resulted in attenuation in mice, whereas no significant difference in tissue culture could be observed (237). Even the deletion of NS2 in MHV-JHM led to no significant differences in growth in cell lines (224). In general it can be stated, that accessory proteins are not required for viral replication *in vitro* but may support growth in the respective host (36, 60, 86, 102, 110, 112, 174, 198, 288).

4.4.3 Coronavirus replicase gene

The replicase gene is encoded at the 5'-end of the genomic RNA and is comprised of two large ORFs, ORF1a and ORF1b. As mentioned above, coronavirus replicase gene expression is complex and involves the expression of two large polyproteins, pp1a and pp1ab that are extensively processed by viral proteinases. Here, functional details of the resulting 16 polyprotein processing end products are summarized. However, it should be noted that in addition to the final processing products (i.e. nsp1-16), intermediate processing products may also have significant impact on viral replication. This idea is supported by analyses of a large panel of temperature sensitive (ts) MHV mutants that are defective in RNA synthesis. Complementation analyses indicated that a large portion of ORF1a-encoded replicase gene products encompassing nsp4 to nsp10 may constitute a single complementation group (cistron I), whereas ORF1b-encoded gene products could be complemented in *trans* and therefore form individual cistrons (222).

4.4.3.1 Nonstructural protein 1 (nsp1)

Nsp1 is encoded at the 5' end of the replicase gene and is, thus, the first mature viral protein expressed in the host cell cytoplasm (294). Therefore an important role in coronavirus replication has been suggested. It is encoded by all mammalian coronaviruses known to date (coronavirus group Ia, Ib, IIa, and IIb), but has not been identified in avian coronaviruses (coronavirus group III). nsp1 is processed by the papain-like proteinases (98) and can be detected in SARS-CoV- and MHV-infected cells as early as 6h post infection (p.i.) Immunofluorescence experiments revealed that MHV and SARS-CoV nsp1 molecules co-localize with other replicase proteins into discrete cytoplasmic foci that were both perinuclear and dispersed throughout the cytoplasm. These cytoplasmic foci likely represent coronavirus replication complexes, where viral RNA synthesis occurs (104, 205). It has been shown, that the carboxy-terminal half of MHV nsp1 is dispensable for virus replication in tissue culture, whereas deletion of residues amino-terminal to amino acid (aa) 123 failed to produce infectious virus (32). It remains to be determined, whether the amino-terminal half of nsp1 is required for MHV replication, or if essential 5'-*cis*-acting elements located within the nsp1-coding sequence (34) have been deleted. A recent *in vitro* study suggested that SARS-CoV nsp1 may be associated with host cell mRNA degradation and may counteract innate immune responses (133, 190). Nsp1 was shown to be a major pathogenicity factor (see chapter 6) and it has been suggested that partial deletion of nsp1 may be an efficient and secure system for the rational design of attenuated coronavirus vaccines (275, 300).

4.4.3.2 Nonstructural protein 2 (nsp2)

For coronavirus nsp2 there has yet no function been proposed. Deletions using reverse genetic systems indicate that nsp2 is dispensable in both SARS-CoV and MHV (99, 100). Noteworthy, the entire nps2-encoding region could be deleted with only moderate changes in growth and RNA synthesis. It has also been shown, that nsp2 of MHV co-localizes with replicase complexes, but similar studies on nsp2 from other coronaviruses are required to determine whether these cleavage products display the same cellular localization pattern (24, 31, 33, 97, 204, 228, 264).

4.4.3.3 Nonstructural protein 3 (nsp3)

Based on sequence comparisons a multidomain organization with five conserved domains (listed in the order N- to C-terminal bellow) has been revealed: Ac (acidic

domain), $PL1^{pro}$, ADRP (ADP-ribose-1"-monophosphatase, also called X-domain), $PL2^{pro}$, and Y (containing several trans-membrane regions) (255, 297). The Ac, ADRP, $PL2^{pro}$, and Y domains are conserved in all coronaviruses, but $PL1^{pro}$ is in some coronaviruses either not active (IBV) or is lacking completely (SARS-CoV and SARS-like CoVs) (207, 232). PL^{pro}s are responsible for the proteolytic release of nsp1, nsp2, nsp3 and the aminoterminus of nsp4. It has been shown that coronavirus PL^{pro}s have slightly different substrate specificities that are best illustrated by their ability to release nsp1 from replicase polyproteins. Four different patterns of nsp1 processing have been identified: (i) no nsp1 and a single active $PL2^{pro}$ (IBV; group III coronaviruses), (ii) a group IIa-specific processing pattern where nsp1 is processed by $PL1^{pro}$ but not by $PL2^{pro}$ (MHV), (iii) a group IIb-specific processing pattern, where no $PL1^{pro}$ is present and hence nsp1 is processed by $PL2^{pro}$ (SARS-CoV), and (iv) a group I-specific processing pattern where nsp1 is released by $PL1^{pro}$ but is assisted by $PL2^{pro}$ (HCoV-229E) (21, 22, 56, 67, 135, 250, 295, 297). These patterns represent the four major phylogenetic lineages of coronaviruses. Besides the proteolytic activity a deubiquitinating activity could be demonstrated for SARS-CoV and HCoV-NL63 $PL2^{pro}$ (14, 15, 56, 211). Another role for SARS-CoV $PL2^{pro}$ may be the inhibition of IFN response independently of the protease activity via interaction with IRF3 (68). Recently the crystal structure of SARS-CoV ADRP has been resolved and the SARS-CoV and HCoV-229E ADRP domains were shown to indeed display a ADP-ribose-1"-monophosphatase processing activity (77, 207, 211, 217). Interestingly, the ADRP-domain of HCoV-229E was demonstrated to be dispensable for virus RNA synthesis (207), suggesting a possible role *in vivo*. Indeed we could demonstrate that an MHV ADRP mutant grows to slightly reduced titers in the liver but, strikingly, did not induce liver disease. Moreover, the mutant virus induced only low levels of inflammatory cytokines TNF-α and IL-6, but increased level of IFN-α in plasmacytoid dendritic cells (pDCs) (Eriksson et al, in revision). Recently it has been reported, that MHV nsp3 has 4 membrane-spanning regions, allowing the protein to insert into the ER membranes co-translationally. It has been shown, that the transmembrane (TM) is important for membrane association of the replicase and tethering the $PL2^{pro}$ domain for viral polyprotein processing (121, 135).

4.4.3.4 Nonstructural protein 4 (nsp4)

Nsp4 is a very hydrophobic protein. Bioinformatic studies have shown, that nsp4 and nsp6 have membrane spanning helices (296). Biochemical fractionation studies revealed that nsp4 is a integral membrane protein (97, 135, 196, 236). It has been shown that MHV nsp4 is required for virus replication, as the nsp4 coding region cannot be deleted from the ORF1a. Additionally, it has been demonstrated that the carboxy terminus of MHV nsp4 is dispensable for virus replication in culture, whereas deletions of regions within nsp4 containing residues amino terminal to P335 prevented recovery of infectious virus (196, 236). Using an MHV ts mutant described by Sawicki et al. (222), Baker and colleagues suggested that nsp4 is involved in DMV formation (44).

4.4.3.5 Nonstructural protein 5 (nsp5)

Nsp5, the main proteinase is a cysteine proteinase with a serine proteinase-like structure (6). It is responsible for the processing of nsp4-nsp16 and is distantly related to picornaviral 3C proteinases (93, 296). Crystal structures of several coronavirus nsp5 have been resolved, and a high degree of substrate specificity and structure could be demonstrated (6, 108, 281). Since several inhibitors are available for related proteinases and due to the fact, that nsp5 is involved pivotally in virus replication and transcription it has become a key target in the search for antiviral agents (280).

4.4.3.6 Nonstructural protein 6 (nsp6)

Like nsp4, nsp6 is a highly hydrophobic protein and is predicted to be an integral membrane protein. Hence, it is, together with nsp3 and nsp4, likely to function in anchoring the replication complexes to the lipid bilayer (196).

4.4.3.7 Nonstructural proteins 7-11 (nsps7-11)

Biochemical and structural data on nsps 7-10 indicate, that these proteins are nucleic acid binding proteins (76, 120, 131, 178, 245, 246, 290). SARS-CoV nsp8 has been demonstrated to possess an RNA-dependent RNA polymerase (RdRp) activity, enabling the synthesis of small RNAs *in vitro* (120). It has been proposed that nsp8 may act as a primase. The model suggests that nsp8 initiates viral RNA replication by producing small RNA primers utilized by the “main” RdRp (nsp12). It is not clear whether nsps7-10 recognize specific coronaviral RNA sequences, but

evidence from our work indicate that MHV nsp8 and nsp9 may interact with an essential 3' *cis*-acting element at the 3' UTR and with the extreme 3' end of the MHV genome (see chapter 6) (301). The analysis of an MHV ts mutant encoding a mutation in nsp10 demonstrated that nsp10 is involved in viral RNA synthesis (222, 229, 284). A further analysis of this ts mutant revealed that the defect in RNA synthesis at the restrictive temperature may be based on a potential function of nsp10 as a cofactor for $3CL^{pro}$ activity and plays a critical role in negative-strand elongation (70, 71).

4.4.3.8 Nonstructural protein 12 (nsp12)

Nsp12 encodes the RNA-dependent RNA polymerase domain that differs substantially from its homologs in other positive-strand RNA viruses. RNA-dependent RNA polymerase activity could be demonstrated for *in vitro* expressed SARS-CoV nsp12 (57). An MHV ts mutant, termed Alb ts22, was found to encode a mutation in nsp12 and to be defective in RNA synthesis at the restrictive temperature. This mutant carries a mutation (His868Arg) in a predicted thumb subdomain of MHV RNA-dependent RNA polymerase, which has been implicated in other RNA polymerases with polymerase activity (222). Thus, upon a shift to the restrictive temperature both, plus- and minus-strand synthesis stopped immediately. Given the crucial role of RNA-dependent RNA polymerase in the virus life cycle and the success obtained with polymerase inhibitors in the treatment of other viral diseases, nsp12 is an attractive target for antiviral drugs (279).

4.4.3.9 Nonstructural protein 13 (nsp13)

By computational analysis nsp13 has been classified as belonging to superfamiliy 1 (SF1) helicases (95). nsp13 has a zinc-binding domain at its N-terminus, which is known to be required for the enzymatic activity of the protein (227). Using recombinant HCoV-229E and SARS-CoV nsp13, it was demonstrated, that the helicase efficiently unwinds both partial-duplex RNA and DNA with 5'-to-3' polarity and that the energy needed for this process may be provided through the NTPase activity encoded within the aminoproximal region in nsp13 (123, 124, 255). The NTPase activity of nsp13 might be involved in capping of viral RNAs (124). The 5'-to-3' polarity of the helicase activity argues against a role of nsp13 in separation of secondary RNA structures arising during RNA synthesis. By reverse genetics a

domain with undefined functions has been targeted, leading to a lethal IBV in cell culture (84).

4.4.3.10 Nonstructural protein 14 (nsp14)

Bioinformatics studies demonstrated a homology of nsp14 to known cellular RNA processing 3'-5' exonucleases (ExoN) of the DEDD superfamily (232). The ExoN activity has been demonstrated for HCoV-229E and SARS-CoV nsp14 (55, 181). It has been shown that the coronavirus ExoN activity can efficiently process single-stranded and double-stranded RNA to final products of 8-12 nucleotides, but not DNA or ribose-2'-O-methylated RNA (181). Recombinant HCoV-229E ExoN mutants showed drastically reduced RNA synthesis and the common molar ratio of individual sg mRNAs was altered. The findings were consistent with the failure to recover infectious HCoV-229E progenies (55, 181). However, Eckerle et al. demonstrated that MHV mutants encoding ExoN-inactivating mutations are viable but, remarkably, displayed decreased polymerase fidelity (75). This observation support the idea that coronaviruses may possess a mechanism of RNA proofreading to stably maintain their extraordinary large RNA genome (94). In addition to the ExoN domain, coronavirus nsp14 may encode an additional function. Support for this hypothesis was provided by the description of an MHV nsp14 mutant that grew like wild type MHV in tissue culture but was severely attenuated in mice (237). The responsive mutation is located in the carboxyterminal part of nsp14 that may constitute a second functional domain of nsp14.

4.4.3.11 Nonstructural protein 15 (nsp15)

Snijder and colleagues proposed that nsp15 encodes a domain that has similarities to the poly(U)-specific cellular endoribonuclease XendoU (232). This domain is encoded in all Nidoviruses and was designated NendoU. The NendoU activity has been confirmed by a study where SARS-CoV nsp15 has been expressed in *E.coli* and the manganese-dependent enzyme activity has been shown (19). Further studies revealed that MHV nsp15 forms a hexamer and can process both double and single-stranded RNA. Like for the ExoN activity of nsp14, 2'-O-ribose-methylated RNA appeared to be resistant to cleavage by the NendoU enzyme. This observation supports a functional link of nsp14, nsp15 and the 2'-O methyltransferase (2'-O-MT) encoded in nsp16 (20, 122, 132, 213). Likewise, these activities, i.e. XendoU, ExoN and 2'-O-MT, are functionally linked in the cellular

snoRNA processing pathway (232). Notably, reverse genetic studies revealed that MHV mutants bearing alanine substitutions in the NendoU catalytic pocket were easily recovered, and showed little or no delay in virus growth kinetics, indicating that the NendoU activity may not be essential for viral RNA synthesis (134).

4.4.3.12 Nonstructural protein 16 (nsp16)

Nsp16 has been predicted to possess 2'-O-MT activity. Extensive attempts to demonstrate methyltransferase activity of recombinant expressed nsp16 initially failed to produce conclusive evidence (85, 232, 272). However, a recent report from Decroly et al. conclusively showed that recombinant expressed FIPV nsp16 exclusively bound N7-methylated capped RNAs and mediated AdoMet-dependent methyl transfer from AdoMet to the 2'-O position of $^{7Me}GpppAC_{3-6}$ RNAs resulting in a cap-1 formation (2'-O methylation at nucleotide position 1) (63). These results further corroborate the idea that nsp16 is (probably in conjunction with the NTPase activity of nsp13) involved in coronavirus cap structure formation and further indicate that coronavirus mRNAs may carry a cap-1 structure.

4.5 Coronavirus *cis*-acting elements

RNAs of positive strand RNA viruses are known to contain *cis*-acting elements that regulate viral replication, transcription, and gene expression. The term "*cis*-acting element" refers to the Latin word *cis*, which means "on the same side as". For coronaviruses various *cis*-acting elements are known. First, a ribosomal frameshift element comprised of a slippery sequence and a pseudoknot structure is known to be involved in a programmed -1 frameshift event during ORF1a/ORF1b translation. Second, coronaviruses harbor *cis*-acting elements at their 5'- and 3'-genomic termini that are specifically recognized by the viral replicase complex in order to replicate the genomic RNA. Finally, the process of coronavirus discontinuous transcription is regulated by TRS elements that direct the synthesis of sg minus strand RNAs.

4.5.1 The coronavirus ribosomal frameshift element

Coronavirus replicase gene expression is mediated by translation of ORF1a and ORF1b of the genomic RNA. This event is regulated co-translationally (ribosomal

frameshifting) and post-translationally (polyprotein processing). In order to translate the ORF1b region, a fraction of the ribosomes translating ORF1a from the genomic RNA must shift into the -1 reading frame to produce pp1ab. The coronavirus frameshift signal was first described for IBV and consists of a so-called slippery sequence, where the ribosomes can “slip” into the -1 frame, and a higher-order RNA structure, i.e. an RNA pseudoknot, downstream the slippery sequence. The coronavirus slippery sequence consists of seven nucleotides with the consensus sequence UUUAAAC (where UUU is the postslippage P-site and AAA the postslippage A-site) (26, 203). Coronavirus pseudoknot structures involved in ribosomal frameshifting have either been described as a classical pseudoknot, i.e. two stem loop structures where the two loop regions can form an additional stem region (also described as kissing loops), or as elaborated pseudoknots involving an additional loop and stem region (109). Most likely pseudoknots adapt a quasi-helical overall structure making them difficult to unwind during translation. Consequently the pseudoknot impedes the progress of the elongating ribosome. The delay required to melt down this secondary structure allows the simultaneous slippage of the P and A site tRNAs by one base in the -1 direction. *In vitro* studies revealed that up to 30% of translation products result from a ribosomal frameshift event at coronavirus frameshift elements. Both, modification of the slippery sequence and destabilizing mutations in pseudoknot stem regions have been shown to greatly reduce frameshifting efficacy (10, 28, 127, 188, 249).

4.5.2 *Cis*-acting elements regulating sg mRNA synthesis

Coronaviruses have evolved an unusual process of discontinuous transcription to express the 3’-proximal third of their genomes. They produce a characteristic set of 3’-coterminal sg mRNAs and each sg mRNA contains a 5’ leader sequence corresponding to the leader sequence at the 5’ end of the genome. Thus, during coronavirus sg mRNA synthesis sequences derived from the 5’ end of the genome (i.e. the leader sequence) and sequences derived from the 3’ third of the genome (i.e. the body sequence) are fused by a discontinuous step during minus strand sg RNA synthesis. TRS elements are known to be critically involved in this step as they determine the border of leader and body sequences.

It is still not known, how the process is regulated in detail, but during negative-strand synthesis a number of consecutive events have been proposed:

1. Recruitment of the replication-transcription complex (RTC) to the 3' end of the genomic RNA and initiation of minus-strand synthesis.
2. Elongation of minus-strand synthesis until the first functional TRS is found. A proportion of the RTC will ignore the TRS and continue to elongate the nascent RNA. Alternatively, the RTC will stop synthesis of the negative-strand RNA, relocate and bind to the leader TRS and reinitiate negative strand RNA synthesis by adding the anti-leader sequence to the nascent RNA strand.

The relocation is believed to be guided by complementary base-pairing between the 3'end of the newly synthesized RNA (minus strand copy of the body TRS) and the leader TRS located at the 5' end of the genome. This step necessarily implicates that 5'- and 3'-end derived sequences form a complex to bring the leader region and the newly synthesized minus RNA into proximity. Protein-RNA and protein-protein interactions probably mediate such an interaction. Heterogeneous nuclear ribonucleoprotein (hnRNP) A1, polypyrimidine tract-binding protein (PTB) and coronavirus N protein could help the formation and stabilization of such a complex, since they have been shown to bind MHV genomic RNA (117, 160, 161). However, many basic questions still remain unanswered. Which signal is responsible for the RTC to slow down or stop and which signal stimulates a strand transfer to the leader region? TRS-flanking regions have been proposed to be involved in this step (235), however comparative sequence analyses did so far not yield a common signature for such an RNA element. To which extend does the proposed stem loop structure (261) at the leader TRS impact on template strand transfer? Furthermore, are there particular nsps that act as "transcription factors" to guide coronavirus discontinuous minus strand synthesis? How, in structural terms, is the relocation of the 3' end of the nascent minus strand RNA to the 5' end of the genomic template being mediated? And finally, why did coronaviruses evolve such a complex mechanism of discontinuous extension of minus strand RNAs to produce their characteristic nested set of sg mRNAs?

4.5.3 *Cis*-acting elements regulating genome RNA replication

Originally, systematic analysis of elements required for coronavirus genome replication was enabled by the discovery of defective interfering (DI) RNAs, which are remnants of viral genomic RNAs bearing multiple extensive deletions. These RNA constructs are not independently viable, but they can propagate by using the RNA synthesis machinery provided by a helper virus. Thus, DIs must have retained precisely those *cis*-acting elements required for replication. The first coronavirus DI to be discovered was from the JHM strain of MHV (170, 172) and subsequently DIs from other strains and species of coronaviruses have been described (53, 114, 180, 201, 265). All coronavirus DI RNAs are comprised of sequences derived from the 5' and 3' genomic termini, and furthermore, often carry internal genome sequences that may harbor a packaging signal involved in selective packaging of an RNA into progeny virions (139).

Studies carried out in various coronavirus species revealed that the first 467 – 649 nts of the genomic 5' end are indispensable for replication (53, 59, 82, 126, 140, 164, 168). In most cases, probably with the only exception of IBV, the minimal 5' *cis*-acting elements extend into the coding region of the replicase gene product nsp1. The well described BCoV 5' *cis*-acting element contains at least five stem-loop structures numbered I-V in 5' to 3' direction (26). The structure of stem loop I and II have been confirmed biochemically and were found to be essential (52). Stem loop III is well conserved amongst group II coronaviruses and has also been shown to be essential for DI RNA replication. A short intra-5′ UTR open reading frame (ORF) of unknown function is associated with stem loop III. Integrity of the small ORF, but not the conservation of the peptide sequence seems to be critical (209). Stem loop IV and V extend into the ORF1a-coding region and both have been shown to be essential (34, 210). Whether these described 5' *cis*-acting elements are necessary only in the context of DI replication or also play a role in virus replication still remains to be elucidated. For MHV the secondary structure of the 5'-most 140 nts in the 5' UTR has been predicted and structural support has been provided by NMR studies. Additionaly a mutational analysis revealed the essential role of stem loop 2 in MHV replication (162).

At the 3' end of the coronavirus genome is a 3' UTR, ranging in size from 273 nts-505 nts followed by a polyA tail. The demarcation of essential regions at the 3' end

began also with DI RNA studies. As for the 5' UTR, the required region not only encompassed the entire 3' UTR, but also parts of the adjacent N ORF (140, 164, 166, 168). However, this statement is only valid for group II coronaviruses. Mapping of group I and group III coronaviruses 3' *cis*-acting replication signals showed that no fragment of N was implemented (59, 126). Controversially, mutations engineered in MHV genome support the notion that the 3' genomic element required for viral RNA replication lies entirely within the 3' UTR. Rearrangements of the MHV genome that translocated the N gene had no effect on viral replication (62).

The secondary structure of the group II coronavirus 3'UTR is rather well characterized. Using recombinant MHV it has been shown that a functionally essential bulged stem-loop (BSL) followed by an essential pseudoknot reside at the upstream end of the 3'UTR (276). The basal part of the BSL can also bind with one strand of the first stem of the pseudoknot (PK) and thus, both structures cannot form simultaneously. Therefore it has been proposed that they constitute a molecular switch, with one component regulating the folding of the other, and possibly regulating different steps of viral replication (90). Downstream of the PK is a region which is less well conserved. This hypervariable region (HVR) can be mutated or entirely removed from the viral genome with little effect on virus replication in tissue culture (91). The nonessential nature of the HVR is surprising, since the region harbors the octanucleotide 5'-GGAAGAGC-3', which is almost universally conserved among coronaviruses and is always situated some 70 to 80 nt from the 3' end of the genome. The refinement of the complete structure of the MHV 3' UTR indicates that the minimal 3' *cis*-acting element required for MHV RNA synthesis is limited to no more than 160 nts of the 3' UTR. This means that nearly half of the 3' UTR, bases 30 through 170, can be discarded without affecting the basic mechanism of viral RNA synthesis. The non-essential region encompasses *in vitro* binding sites for a number of host cell proteins, including PTB, hnRNP, a complex of mitochondrial aconitase, and the chaperones mtHSP70, HSP60, and HSP40. It follows that these binding sites cannot be strictly required for RNA synthesis, although they may play ancillary roles yet to be defined (see chapter 6) (301).

4.6 Coronavirus reverse genetics

The extreme large size of coronavirus genome and the instability of specific coronavirus sequences in conventional cloning vectors (e.g. plasmid DNAs) are regarded as major obstacles to the generation of recombinant viruses by traditional reverse genetic techniques. Therefore, reverse genetic systems for coronavirus are exclusively based on non-traditional approaches. First, Masters and colleagues (141, 175, 177) reported a method termed “targeted RNA recombination” that is based on recombination of MHV with a synthetic donor RNA. This approach is benefitting from the high rate of recombination in MHV (9, 12, 137, 138, 148) probably occurring via a template switching mechanism (171). Initially, a temperature-sensitive MHV mutant has been recombined with a synthetic donor RNA containing the mutation of choice in the N gene. Recombinant viruses have been selected at the restrictive temperature against the temperature sensitive parental virus. However, a more sophisticated and stringent method based on a switch of target-cell specificity has been reported recently (144, 177). Targeted RNA recombination has been successfully used for the manipulation of the 3’ third of coronavirus genomes including all structural genes, accessory proteins and 3’ UTR (177), and its application to two other coronaviruses has been reported (103, 219). However this technique is limited to the modification of the 3’-third of a coronavirus genome. Hence manipulation of the 5’ UTR and replicase genes had to await the development of systems based on the construction of full-length cDNA coronavirus clones. In 2000 Enjuanes and collaborators reported the development of the first reverse genetic system based on full-length cDNA. They used a bacterial artificial chromosome (BAC) that harbors a full-length TGEV cDNA (4). Soon after, Baric and colleagues reported a system based on the systematic assembly of a full-length TGEV cDNA by *in vitro* ligation of six adjoining plasmid-derived cDNA subclones spanning the entire TGEV genome (285). Finally, Siddell and colleagues showed an alternative to the cDNA cloning in bacterial systems. They used vaccinia virus as an eukaryotic cloning vector and stably inserted a full-length cDNA of HCoV-229E (253, 256). Regardless of the different cloning strategies and protocols established for recovery of the recombinant viruses, full-length cDNA-based systems enable the modification of all regions within coronavirus genomes.

The number of coronaviruses which can be studied by reverse genetic systems is constantly increasing, and currently includes a number of human (HCoV-229E,

HCoV-OC43, SARS-CoV) and animal coronaviruses (MHV, TGEV, IBV, FIPV). (2, 4, 13, 37, 45, 79, 92, 103, 144, 175, 177, 219, 239, 248, 253, 256, 285-287). Reverse genetic analyses have extended our knowledge on virtually all aspects of coronavirus infections, including tropism, pathogenesis, packaging and mechanisms and requirements for viral RNA synthesis. This knowledge together with the ability to modify in principle any base in the genome will help to develop novel coronavirus vaccines and vectors.

4.7 Innate immunity and coronavirus

Efficient and rapid antiviral host responses consist predominantly of the production of type I interferons (IFNs), an essential part of the innate immune system (251). Approximately 13 different IFN-α, and one IFN β are known as type I IFNs. They can be secreted by all mammalian nucleated cells however the signaling molecules involved in viral recognition, the amounts of type I IFNs produced and secreted can differ among cell types. These soluble factors induce an array of intracellular effectors including protein kinase R (PKR), 2'-5'oligoadenylate synthetases (2'-5 OAS) and Mx proteins which halt viral replication (241). Besides their direct antiviral role, IFNs also inhibit cell proliferation, regulate apoptosis and most importantly modulate the immune response, such as activation of the adaptive immune response via IFNγ (111, 195).

A hallmark of coronavirus infections is the strongly limited ability to induce type I IFN production. It has been shown that several cells lines, fibroblasts, or conventional dendritic cells are not able to produce type I IFN after infection with MHV. Also that neither macrophages nor monocyte-derived DC are able to produce type I IFN after SARS-CoV infection (130, 212, 289). Nevertheless, coronavirus replication can be reduced *in vitro* and *in vivo* by treatment with IFN-α. For example type I IFN treatment is able to diminish severity of SARS-like symptoms in SARS-CoV infected macaques and can reduce replication of MHV in mice (43, 101, 291). Strikingly, mice lacking the type I IFN-receptor (IFNAR$^{-/-}$) rapidly succumb to MHV infection (42). These findings reflect the importance of type I IFNs in the defense against coronaviral infections. Plasmacytoid dendritic cells (pDC) have been identified as a major source of type I IFNs in human and mice (8, 41, 187, 231). In particular during

MHV infection they play an important role in producing IFNα to protect mice from lethal liver disease (42).

Although coronaviruses are sensitive to IFN, the early production of these cytokines is highly restricted to pDCs which have been shown to recognize MHV infection through TLR7 (42). This strongly suggests that coronaviruses have evolved strategies to evade antiviral innate host responses either by avoiding or inhibiting the production of IFN. One possible mechanism may be the replication of coronaviruses in a double membrane vesicle, probably protecting viral RNA and replication intermediates from the recognition by pathogen recognition receptors (97, 204, 234, 242, 257). It has been proposed that MHV can inhibit IFNα production, at the level of translation, since IFNα mRNA can be found in MHV infected cells, but almost no IFNα protein can be detected in supernatants from these cells (216). Furthermore various SARS-CoV and MHV gene products have been proposed to either directly inhibit IFN production or interfere with downstream signaling events (88, 133, 142, 143, 300). For example, IRF3 signaling is affected during SARS-CoV infection (238). However, the mechanisms by which coronaviral proteins could inhibit type I IFN production, participate in the avoidance of coronavirus recognition, or block downstream events of host cell innate immune responses (e.g. IFN signaling, antiviral effector molecules) remain to be further characterized.

5 Aim of the thesis

Coronaviruses are positive stranded RNA viruses mainly associated with respiratory and enteric diseases. They can cause severe diseases in livestock and companion animals. In humans, coronavirus infections manifest usually as mild respiratory tract disease (common cold). However, the severe acute respiratory syndrome (SARS), caused by a formerly unknown coronavirus (SARS-CoV), exemplified the potential of coronaviruses to also seriously impact on human health.

The major aim of this thesis was to investigate the role of replicase-encoded gene products in the context of viral RNA replication and host interactions. Furthermore, we aimed to define the importance of host innate immune responses to combat coronavirus infections.

6 Original research articles

"Genetic Interactions between an Essential 3' *cis*-Acting RNA Pseudoknot, Replicase Gene Products, and the Extreme 3' End of the Mouse Coronavirus Genome"

Roland Züst, Timothy B. Miller, Scott J. Goebel, Volker Thiel, and Paul S. Masters

Own contribution to this article: Recombinant MHV viruses containing either a 6 nt insertion alone or in combination with suppressor mutations in nsp8 or nsp9 or supressor mutations in nsp8/nsp9 alone have been generated and analyzed by plaque size, growth kinetics and sequencing.

JOURNAL OF VIROLOGY, Feb. 2008, p. 1214–1228 Vol. 82, No. 3
0022-538X/08/$08.00+0 doi:10.1128/JVI.01690-07

Genetic Interactions between an Essential 3′ *cis*-Acting RNA Pseudoknot, Replicase Gene Products, and the Extreme 3′ End of the Mouse Coronavirus Genome▽

Roland Züst,[1] Timothy B. Miller,[2] Scott J. Goebel,[2] Volker Thiel,[1] and Paul S. Masters[2]*

Research Department, Kantonal Hospital St. Gallen, St. Gallen, Switzerland,[1] and Wadsworth Center, New York State Department of Health, Albany, New York 12201[2]

Received 3 August 2007/Accepted 11 November 2007

The upstream end of the 3′ untranslated region (UTR) of the mouse hepatitis virus genome contains two essential and overlapping RNA secondary structures, a bulged stem-loop and a pseudoknot, which have been proposed to be elements of a molecular switch that is critical for viral RNA synthesis. It has previously been shown that a particular six-base insertion in loop 1 of the pseudoknot is extremely deleterious to the virus. We have now isolated multiple independent second-site revertants of the loop 1 insertion mutant, and we used reverse-genetics methods to confirm the identities of suppressor mutations that could compensate for the original insertion. The suppressors were localized to two separate regions of the genome. Members of one class of suppressor were mapped to the portions of gene 1 that encode nsp8 and nsp9, thereby providing the first evidence for specific interactions between coronavirus replicase gene products and a *cis*-acting genomic RNA element. The second class of suppressor was mapped to the extreme 3′ end of the genome, a result which pointed to the existence of a direct base-pairing interaction between loop 1 of the pseudoknot and the genomic terminus. The latter finding was strongly supported by phylogenetic evidence and by the construction of a deletion mutant that reduced the 3′ UTR to its minimal essential elements. Taken together, the interactions revealed by the two classes of suppressors suggest a model for the initiation of coronavirus negative-strand RNA synthesis.

RNA virus genomes contain *cis*-acting sequences and structures that interact with viral and cellular components to initiate a variety of essential functions. Such interactions can mediate RNA replication and transcription, the selective translation of viral transcripts, and the specific packaging of progeny genomic RNA (gRNA) into assembling virions. Initiation of RNA virus genome replication occurs at the extreme 3′ end of gRNA in order to produce a strand of complementary polarity. For positive-strand RNA viruses, the initiation of negative-strand RNA synthesis requires the specific recognition of the viral gRNA template and the juxtaposition of replicative proteins and the 3′ genomic terminus. *cis*-acting sequences are believed to play pivotal roles in these processes. An intriguing example of how *cis*-acting sequences can coordinate the assembly and targeting of a replication complex to the initiation site of negative-strand RNA synthesis has been provided by studies of poliovirus replication (4, 23, 57). A crucial initial event in this system is the formation of a ribonucleoprotein complex around a cloverleaf RNA structure at the 5′ end of the poliovirus genome. This complex consists of the poliovirus protease-polymerase precursor 3CD and the cellular poly(rC) binding protein, both of which bind to the 5′ cloverleaf (1, 2, 7, 17). In order to target poliovirus 3CD to the initiation site of negative-strand RNA synthesis, another cellular protein, poly(A) binding protein, becomes involved. Poly(A) binding protein is associated with the poly(A) tail of the poliovirus genomic RNA (which also serves as a *cis*-acting replication element) and bridges the 5′ and 3′ genomic termini by binding to the poly(rC) binding protein and 3CD (4, 23). Thus, in this example, *cis*-acting elements provide not only the basis for the discrimination between viral and cellular RNA but also a platform for the assembly of a negative-strand replication initiation complex.

Coronaviruses are a family of positive-strand RNA viruses possessing a complex, multicomponent RNA synthetic machinery and a sophisticated program of gene expression that is characterized by the transcription of a 3′-nested set of subgenomic RNAs (sgRNAs), in addition to gRNA replication (41). These features are shared with other members of the nidovirus order, which also includes arteriviruses, toroviruses, and roniviruses. For these viruses, the synthesis of both gRNA and sgRNA begins with the initiation of negative-strand RNA at the 3′ end of the genome (49). A prerequisite for this event is the translation of the replicase gene from the positive-strand RNA genome, resulting in two large polyproteins. Extensive self-processing by viral proteinases residing within the polyproteins eventually generates a number of processing intermediates and 15 to 16 mature end products, termed nonstructural proteins (nsp's) 1 to 16 (nsp1 to nsp16) (67). Many nsp's colocalize, together with the structural nucleocapsid (N) protein, at double-membrane vesicles to form the membrane-associated replication complex (8, 10, 14, 22, 53). Although this complex is believed to interact with *cis*-acting elements in order to replicate and transcribe viral RNAs (9), our knowledge about specific interactions that may be involved in the various

* Corresponding author. Mailing address: David Axelrod Institute, Wadsworth Center, NYSDOH, New Scotland Avenue, P.O. Box 22002, Albany, New York 12201-2002. Phone: (518) 474-1283. Fax: (518) 473-1326. E-mail: masters@wadsworth.org.

▽ Published ahead of print on 21 November 2007.

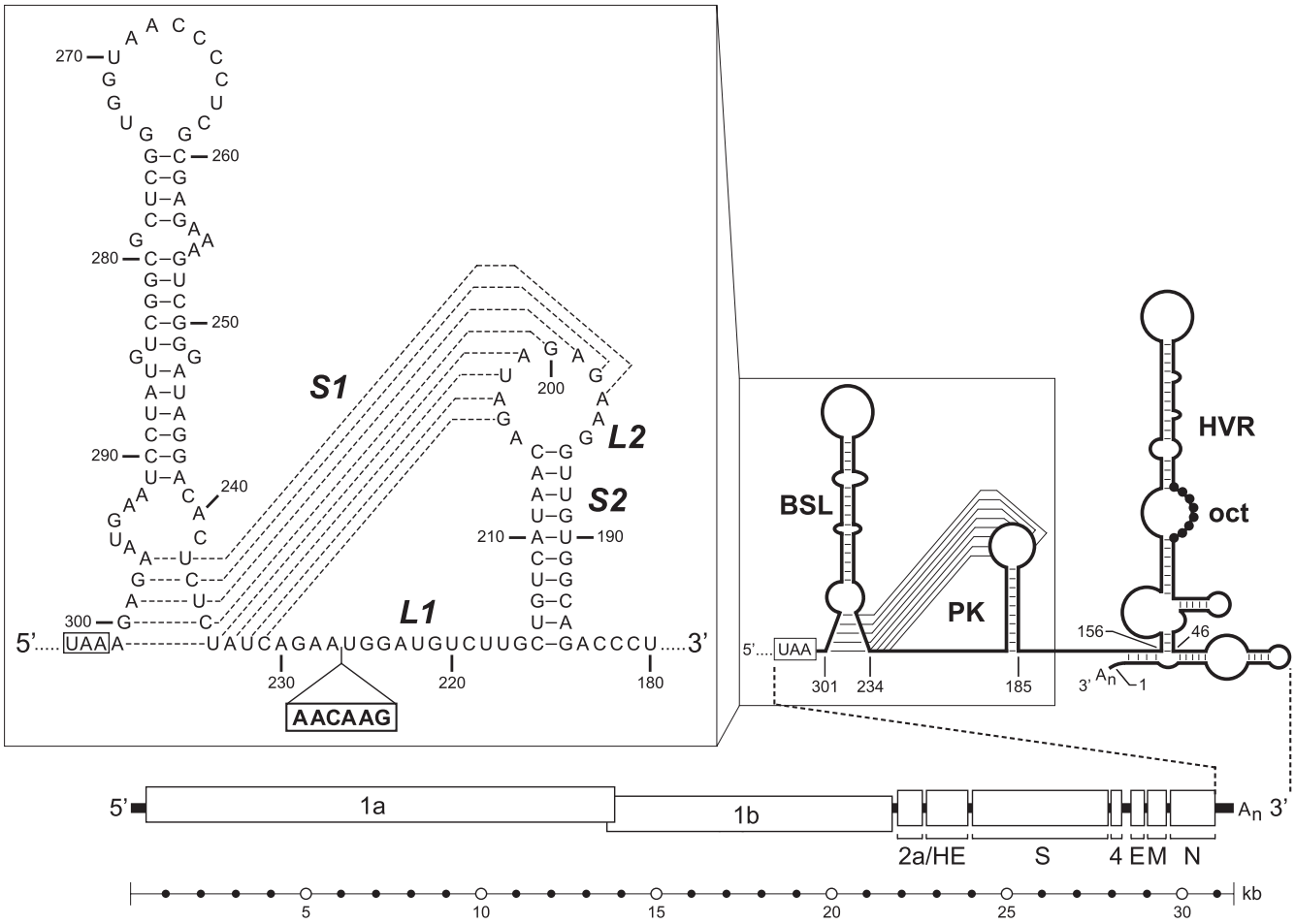

FIG. 1. Structure of the MHV 3′ UTR. The organization of the 31.3-kb MHV genome is shown at the bottom. Above this, at the right, is a schematic of the current model of the RNA secondary structure of the entire 301-nt 3′ UTR. The 3′ UTR comprises an essential bulged stem-loop (BSL; nt 234 through 301) (18, 26, 27) and overlapping pseudoknot (PK; nt 185 through 238) (18, 60, 63). Downstream of these structures is a nonessential HVR (nt 46 through 156), which contains the highly conserved coronavirus octanucleotide motif (oct), 5′-GGAAGAGC-3′ (19, 39). The arrangements shown for the segment downstream of the HVR (nt 1 through 67) and for part of the segment between the HVR and the pseudoknot (nt 143 through 160) are those proposed by Liu and coworkers (38) but are modified in the work reported herein. At the upper left is a detailed view of the upstream end of the 3′ UTR, denoting the pseudoknot stems (S1 and S2) and loops (L1 and L2). Broken lines represent alternative base pairings either for the bottom stem segment of the bulged stem-loop or for pseudoknot stem 1. Also indicated is the 6-nt insertion (AACAAG) in pseudoknot loop 1 that was constructed in the mutant Alb391 (18). All nucleotide numbering is from the first base at the 3′ end of the genome, excluding poly(A), and the N-gene stop codon is boxed.

steps of coronavirus RNA synthesis is extremely limited. RNA-binding activity has been ascribed to a number of replicase gene products (16, 32, 55, 56, 66) and to the N protein (41). However, currently available structural and biochemical data do not yet allow the assignment of any of these RNA-binding proteins to defined interactions with *cis*-acting elements. Additionally, it is not known whether cellular proteins that have been shown to bind to viral RNA, such as PTB (28), hnRNP A1 (29), and a complex of mitochondrial aconitase and chaperones (45, 46, 64, 65), are critically involved in coronavirus RNA synthesis.

A fairly comprehensive view of *cis*-acting elements located at the 3′ end of the coronavirus genome has come from studies of mouse hepatitis virus (MHV) and its close relative, bovine coronavirus (BCoV) (9, 42). Both MHV and BCoV are members of the second of the three phylogenetic groups into which coronaviruses are sorted. For MHV, work with viral mutants has demonstrated that the 3′ genomic *cis*-acting elements essential for RNA synthesis lie entirely within the 301-nucleotide (nt) 3′ untranslated region (3′ UTR) (13, 18), even though earlier studies with defective interfering (DI) RNAs had suggested a potential role for a portion of the adjacent N gene (33, 36, 40). The current picture of the MHV 3′ UTR, shown in Fig. 1, began with the definition of structures at its upstream end. Immediately following the N-gene stop codon is a bulged stem-loop (27). Adjacent to this is a classical hairpin-type pseudoknot (60), first discovered in BCoV. Exhaustive genetic analyses, in addition to chemical and enzymatic probing, have confirmed the existence and the essential nature of these two structures both in DI RNAs and in the intact viral genome (18, 26, 27, 60). Most significantly, the bottommost stem of the bulged stem-loop and stem 1 of the pseudoknot overlap, and thus, the two cannot simultaneously fold to completion. Consequently, we have previously proposed that these alternative

structures are components of a molecular switch regulating a transition between individual steps of viral RNA synthesis (18, 26).

Overlapping bulged stem-loops and pseudoknots are maintained in the upstream 3′ UTRs of all group 2 coronaviruses, including severe acute respiratory syndrome coronavirus (SARS-CoV) (18, 20), human coronavirus HKU1 (61), and the recently discovered bat coronaviruses HKU4, HKU5, and HKU9 (62). (Although it is stated otherwise in reference 62, HKU9 clearly harbors a pseudoknot, running from nucleotide 28898 through 28947, and two candidate overlapping bulged stem-loops can be found upstream of it.) This structural conservation, despite considerable primary sequence divergence, strongly implies functional conservation. More to the point, it has been shown that the entire 3′ UTR of either BCoV (27) or SARS-CoV (20) can functionally replace the MHV 3′ UTR. Similarly, multiple group 2 coronaviruses closely related to MHV and BCoV are competent to serve as helper viruses for the replication of a BCoV DI RNA (63).

Most of the downstream remainder of the MHV 3′ UTR is composed of a hypervariable region (HVR) (Fig. 1); the HVR is highly divergent in both sequence and structure, even among closely related coronaviruses like MHV and BCoV. The structure of the MHV HVR has been confirmed by enzymatic probing (38). Detailed genetic analysis has shown that unlike the RNA elements in the upstream portion of the 3′ UTR, the HVR can be mutated or entirely removed from the viral genome with little effect on virus replication in tissue culture (19). The nonessential nature of the HVR is surprising, since the region harbors the octanucleotide 5′-GGAAGAGC-3′, which is almost universally conserved among coronaviruses and is always situated some 70 to 80 nt from the 3′ end of the genome. Although deletion of the HVR greatly attenuates MHV virulence in the mouse host, the HVR's dispensability with respect to in vitro replication greatly simplifies consideration of the basic mechanism of RNA synthesis.

In our previous mutational analysis of the bulged stem-loop and pseudoknot, we observed that loop 1 of the pseudoknot is extremely sensitive to insertions of various sizes (18). A threshold of viability was seen to occur at an insertion size of six nucleotides: an insertion one base smaller, AACAA, was fully tolerated, whereas an insertion one base larger, AACAACA, was lethal. One particular 6-nt insertion, AACAAA, had only a minimal effect on the viral phenotype. By contrast, a mutant designated Alb391, with a 6-nt insertion of AACAAG, was extremely unstable. Alb391 formed very small plaques compared to those of the wild type, and it gave rise to large-plaque revertants within a single passage. In the work described here, we carried out an analysis of multiple revertants of Alb391. The results of this study provide the first indication of an interaction between a 3′ *cis*-acting element required for viral RNA synthesis and components of the coronavirus replicase. In addition, our results point to an interaction between stem 1 of the pseudoknot and the extreme 3′ terminus of the MHV genome. These two sets of interactions suggest a model for the initiation of viral negative-strand RNA synthesis.

MATERIALS AND METHODS

Cells and viruses. Wild-type MHV-A59, MHV mutants, and revertants were propagated in mouse 17 clone 1 (17Cl1) cells. MHV plaque assays and plaque purifications were carried out in mouse L2 or L929 cells, which were overlaid with 1% Noble agar and stained with neutral red at 48 h postinfection. The interspecies chimeric virus fMHV.v2 (18) was grown in feline FCWF cells. Vaccinia viruses were propagated in CV-1 and BHK-21 cells, and plaque purifications were performed on CV-1 and D980R cells (11).

Vaccinia virus-based MHV reverse genetics. The recombinant MHV mutants rAlb391, rN8-Alb391, rN9-Alb391, rN8, and rN9 were derived from vaccinia virus vMHV-inf-1, which contains a cloned full-length MHV-A59 cDNA (GenBank accession number AY700211). Mutagenesis was done using the reverse-genetics system described previously (11, 24). Briefly, two rounds of vaccinia virus-mediated homologous recombination were performed using the *Escherichia coli* guanine-phosphoribosyltransferase (GPT) gene as a selection marker. First, the target region within the MHV cDNA was replaced by the GPT gene, and second, the GPT gene was replaced by a mutated version of the target region. To construct recombinant vaccinia viruses encoding the Alb391-specific AACAAG insertion in the MHV 3′ UTR, we used the plasmid pRec5 for recombination with vaccinia virus vMHV-inf-1. The GPT gene in pRec5 is flanked on its left by MHV-A59 nt 28510 to 29024 and on its right by 500 bp of vaccinia DNA that is encoded downstream of the MHV-A59 3′ terminus in vMHV-inf-1. The resulting recombinant vaccinia virus, vRec5, was used for recombination with the plasmid pRec7 to insert the Alb391-specific 3′ terminus. The plasmid pRec7 contains MHV Alb391 nt 28510 to 31335, followed by a synthetic poly(A) sequence and 500 bp of vaccinia virus DNA. The resulting recombinant vaccinia virus clone was designated vMHV-rAlb391. To mutagenize nsp8 and nsp9, the region encoding MHV nsp7 to nsp11 was replaced by GPT, using vaccinia virus-mediated homologous recombination of vMHV-inf-1 or vMHV-rAlb391 with plasmid pRec3. The plasmid pRec3 encodes the GPT gene flanked on its left by MHV-A59 nt 11464 to 11956 and on its right by MHV-A59 nt 13594 to 14151. The resulting recombinant vaccinia viruses were then recombined with reverse transcription (RT)-PCR-derived DNA fragments obtained from RNA isolated from the Alb391 revertant Rev2 or Rev3. The resulting recombinant vaccinia viruses thus produced were designated vMHV-rN8 (carrying the Rev2 mutations in nsp8 and the wild-type MHV 3′ UTR), vMHV-rN9 (carrying the Rev3 mutation in nsp9 and the wild-type MHV 3′ UTR), vMHV-rN8-Alb391 (carrying the Rev2 mutations in nsp8 and the Alb391 3′ UTR), and vMHV-rN9-Alb391 (carrying the Rev3 mutation in nsp9 and the Alb391 3′ UTR). The identities of plasmids and recombinant vaccinia viruses were confirmed by sequencing analysis of the mutated regions. Further cloning details, plasmid maps, and sequences are available from the authors upon request.

Recombinant coronaviruses were rescued from cloned cDNA using purified, EagI-cleaved vaccinia virus DNA as a template for the in vitro transcription of recombinant full-length MHV genomic RNA, which was electroporated into BHK-MHV-N cells as described previously (11). Following electroporation, the transfected BHK-MHV-N cells were mixed with a fourfold excess of murine 17Cl1 cells and cultured at 37°C. At days 1 and 2 postelectroporation, tissue culture supernatants were taken for further analysis.

Targeted RNA recombination. For the construction of the ΔHVR3 mutant and the reconstruction of the 3′ UTR A2G mutation, targeted RNA recombination with host range-based selection was used, as described in detail previously (13, 18, 19, 20, 34, 35, 43). In brief, monolayers of feline FCWF cells were infected with fMHV.v2 and were then transfected by electroporation with capped, T7 polymerase-transcribed donor RNAs (mMessage mMachine transcription kit; Ambion). Templates for donor RNAs were derived from pSG6 (18) via PCR-based mutagenesis methods, which replaced plasmid segments between unique restriction sites in the 3′ UTR or the downstream polylinker. pSG6 contains a cDNA segment of the 5′-most 0.5 kb of the MHV genome linked to the 3′-most 8.6 kb of the MHV genome. Progeny virus from infected and transfected feline cells were selected on the basis of having regained the ability to form plaques on murine L2 cell monolayers, and the resulting recombinant candidates were purified through two rounds of plaque titration. For mutants constructed by targeted RNA recombination, the wild-type virus used for comparisons was Alb240, a well-characterized isogenic recombinant that was previously reconstructed from fMHV and pMH54 donor RNA (35).

Characterization of mutants and revertants. For analysis of the sequences of constructed mutants and isolated revertants, total cellular RNA was extracted from infected monolayers and reverse transcribed with avian myeloblastosis virus (Life Sciences) or Superscript II (Invitrogen) reverse transcriptase using random hexanucleotide (Boehringer Mannheim) or MHV sequence-specific primers. Regions of the genome were then amplified by PCR under standard conditions using AmpliTaq polymerase (Roche), and PCR products were purified with Quantum-prep columns (Bio-Rad) prior to automated sequencing. For viruses for which the entire genome was sequenced (Rev2, Rev5, and Rev6), the extreme 5′-end sequence was obtained through rapid amplification of cDNA ends (5′/3′

RACE kit; Roche). In order to resolve the mixed sequence obtained for the mutant rAlb391 isolate S3, we cloned RT-PCR products using the pGEM-T Easy Vector System (Promega), and individual plasmids were subsequently sequenced.

For the measurement of growth kinetics, confluent monolayers of 17Cl1 cells were inoculated at a multiplicity of 0.01 or 5.0 PFU per cell (for the ΔHVR3 mutant) or at a multiplicity of 1.0 PFU per cell (for all other mutants) for 2 h at 37°C. Inocula were removed, monolayers were washed three times, and incubation was continued in fresh medium at 37°C. Sample aliquots of medium were then withdrawn at various times from 2 to 32 h postinfection, and infectious titers were subsequently determined on mouse L2 cells.

RNA structural predictions were carried out with the *mfold* software (44, 68), available at http://www.bioinfo.rpi.edu/applications/mfold.

Radiolabeling of viral RNA. Intracellular viral RNA was metabolically labeled in 17Cl1 cells as described previously (18–20, 27). In brief, 20-cm^2 confluent monolayers were infected with the ΔHVR3 mutant or wild-type MHV at a multiplicity of 5.0 PFU per cell at 37°C. Infected cells were starved from 2 h through 8 h postinfection in Eagle's minimal essential medium containing 5% dialyzed fetal bovine serum with 1/10 of the normal concentration of phosphate. Cells were then labeled from 8 h through 10 h postinfection in 1 ml phosphate-free medium containing 100 μCi per ml [^{33}P]orthophosphate (MP Biomedicals), 5% dialyzed fetal bovine serum, and 20 μg of actinomycin D (Sigma) per ml. Total cytoplasmic RNA was purified, and samples were analyzed by electrophoresis through 1% agarose containing formaldehyde and were visualized by fluorography.

TABLE 1. Sequence analysis of initial set of candidate reverting mutations of Alb391[a]

Mutant	Gene or region	Nucleotide change(s)[b]	Amino acid change(s)[c]
Rev1	3′ UTR	Deletion of nt 1 through 5 of the 6-nt insertion between bases 226 and 227	None
Rev2	nsp8	G12439A, C12452U	D62N, T66I
Rev3	nsp9	U13017G	N60K
Rev4	nsp8	A12344G	Q30R
Rev5	3′ UTR	A2G	None
Rev6	3′ UTR	A2G	None

[a] For Rev2, Rev5, and Rev6, the entire genomes were sequenced. For Rev1, Rev3, and Rev4, the genomic regions sequenced were as follows: the 5′-most 510 bases, the segment of gene 1a encoding nsp7 through nsp10, and the entire 3′ UTR.

[b] Nucleotide numbering is from the 5′ end of the genome for replicase (gene 1) mutations and from the 3′ end of the genome, excluding poly(A), for 3′ UTR mutations. All mutants, except Rev1, retained the 6-nt insertion (AACAAG) between bases 226 and 227 of the 3′ UTR.

[c] Amino acid numbering indicates the residue position in each processed replicase protein product.

RESULTS

Initial revertant analysis of a 3′ UTR pseudoknot mutant. In a previous study, we used targeted RNA recombination to construct a number of mutants of the MHV 3′ UTR bulged stem-loop and pseudoknot in order to obtain an understanding of the structural requirements of these two elements and their interrelationship (18). An additional goal was to generate severely impaired viral mutants that might direct us to genetic interactions between the 3′ UTR and other regions of the genome. A mutant that met the latter criterion was Alb391, in which an insertion of 6 nt, AACAAG, was made between bases 226 and 227 of pseudoknot loop 1 (Fig. 1). Alb391 had a markedly defective phenotype, exhibiting slow growth and forming much smaller plaques than did wild-type virus at 33°C, 37°C, and 39°C. Revertants of this mutant were rapidly selected in as few as one or two passages. Six independent revertants (Rev1 to Rev6), which formed plaques identical to or slightly smaller than those of the wild type, were isolated and analyzed by partial or total genomic sequencing (Table 1). One of these, Rev1, had lost the first five bases of the insertion, retaining a footprint of only the final G residue. This finding constituted strong evidence that the 6-nt insertion, rather than some extraneous mutation, was indeed responsible for the Alb391 phenotype.

All of the other revertants retained the complete 6-nt insertion, indicating that second-site suppressor mutations had to account for their observed reversion. For one of these, Rev2, we determined the sequence of the entire viral genome and compared it to the particular database reference sequence (GenBank accession number NC001846) that is closest to the laboratory strain from which Alb391 had been derived. A total of nine mutations, two synonymous and seven nonsynonymous, were found relative to the reference sequence. However, all except two of these base changes also occurred in the corresponding wild-type virus or in the immediate fMHV precursor to Alb391, and they were therefore not associated with reversion. The two remaining mutations produced a pair of closely spaced coding changes in nsp8 (Table 1), which is one of a group of four small processed polypeptide products encoded by the downstream-most end of replicase gene 1a. Similarly, sequencing of the nsp7-through-nsp10 region of both Rev3 and Rev4 revealed single coding mutations in nsp9 and in nsp8, respectively (Table 1). Notably, both nsp8 and nsp9 have been described as RNA-binding proteins, and nsp8 has been shown to possess an RNA-dependent RNA polymerase (RdRp) activity (16, 30, 56, 66). By contrast, Rev5 and Rev6 were found to have no mutations in the nsp7-through-nsp10 region, but each had the same A-to-G transition at the penultimate nucleotide preceding the poly(A) tail (denoted A2G in the numbering system used for the 3′ UTR) (Table 1). Initially we did not consider this mutation to be significant, since A2G is distant from the pseudoknot and since the same base change occurs naturally in MHV strain 3 (47). Accordingly, we sequenced the entire genomes of Rev5 and Rev6 and found no other base changes. Thus, our initial revertant analysis detected three classes of candidate reverting mutations for the 3′ UTR pseudoknot insertion in Alb391: one mapping to the original site of the insertion, a second falling within the replicase gene, and the last near the 3′ genomic terminus.

Reconstruction of Alb391 by full-length cDNA cloning. To test whether replicase gene mutations, mapping some 20 kb distant from the original lesion, were responsible for reversion of the Alb391 mutation, we aimed to reconstruct a subset of the revertants. To accomplish this, we decided to use the vaccinia virus-based complete reverse genetics system for MHV (11, 58), which, unlike targeted RNA recombination (43), allows access to the huge coronavirus replicase gene. However, we first needed to clarify whether the Alb391-specific 6-nt insertion would confer the same phenotype in the genetic background of the recombinant MHV-inf-1 molecular clone. Therefore, we generated the 6-nt pseudoknot insertion mutation in the MHV-inf-1 genome and analyzed the rescued mutant, designated rAlb391. In accord with previous results, the reengineered mutant was found to be extremely unstable, even at the earliest stages of recovery. As shown in Fig. 2A, rAlb391 virus obtained from N protein-expressing cells that had been

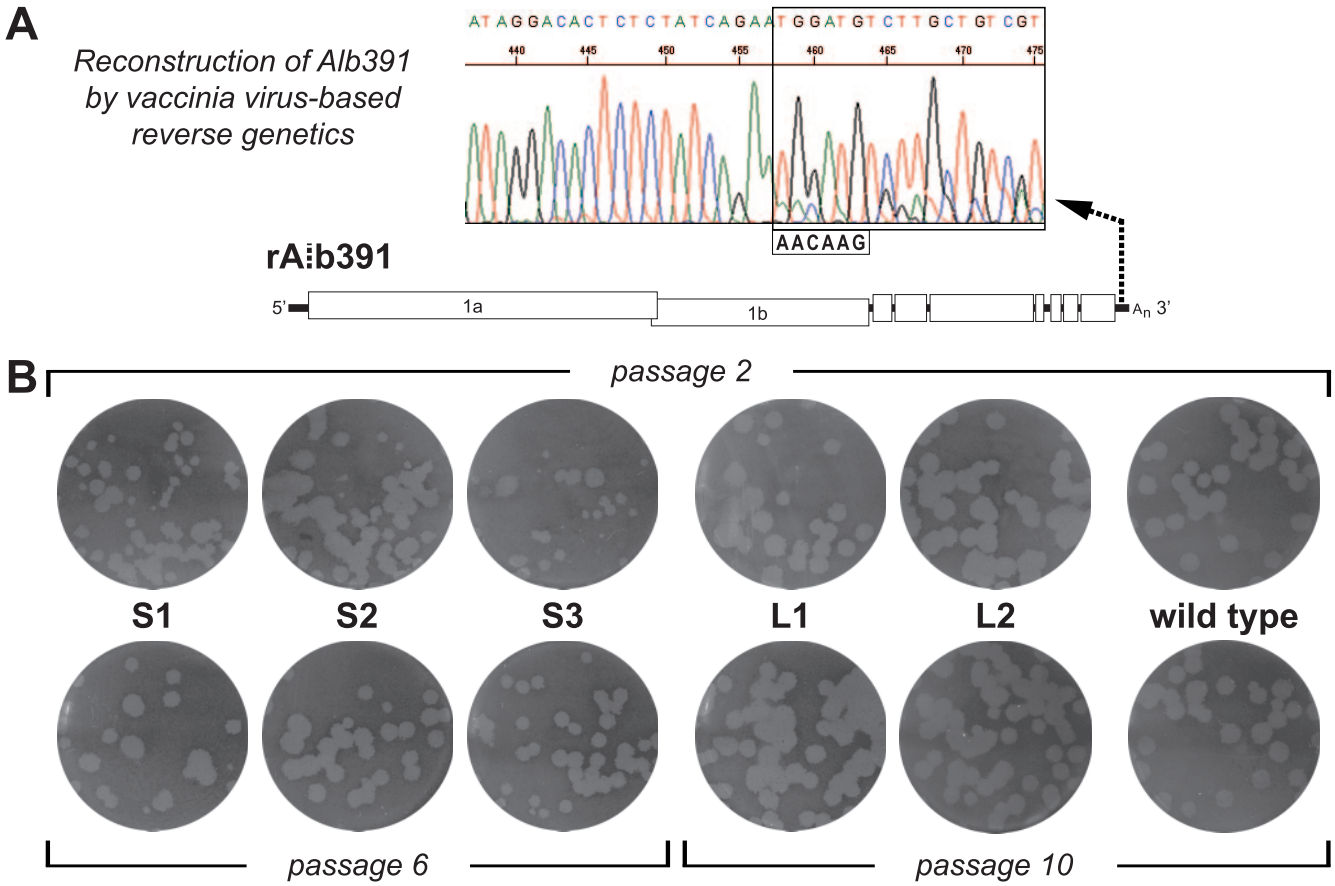
A
Reconstruction of Alb391 by vaccinia virus-based reverse genetics
AACAAG
rAlb391
5'
1a
1b
An 3'
B
passage 2
S1
S2
S3
L1
L2
wild type
passage 6
passage 10
C
3' PK
nsp9
S1
passage 2
passage 6
passage 2
passage 6
D
3' PK
S2
passage 2
passage 6
E
3' PK
3' end
3' PK
3' end
S3a
S3b
5/9
4/9

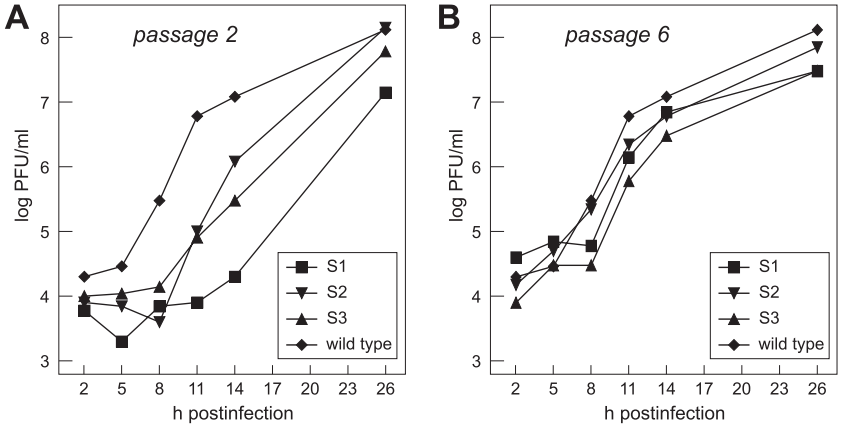

FIG. 3. Growth kinetics for small-plaque isolates S1 to S3 of rAlb391, compared with a wild-type control. Cultures were inoculated with passage-2 virus (A) or passage-6 virus (B) at a multiplicity of 1.0 PFU per cell. Data shown are a set from one representative of duplicate experiments, which gave highly similar results.

transfected with synthetic mutant genomic RNA had a mixture of mutant and wild-type sequence at the position of the insertion (and consequently at all points downstream in a positive-strand sequence). Plaques of rAlb391 exhibited considerable heterogeneity, ranging from very small to wild-type size (data not shown). To analyze this in more detail, we picked 3 of the smallest plaques (S1 through S3) and 2 of the largest plaques (L1 and L2) and propagated them for 6 and 10 passages, respectively. Isolates L1 and L2 formed uniformly large plaques at passages 2 and 10 (Fig. 2B), and sequence analysis revealed that they had exactly lost the 6-nt insertion (data not shown); this identified them as precise primary-site revertants.

By contrast, isolates S1 through S3 had a variety of plaque sizes by passage 2. By passage 6, they formed fairly uniform plaques that were the same size, or nearly the same size, as those of the wild type (Fig. 2B). Sequencing showed that this stability had been achieved through the acquisition of one of a number of new mutations. In the stock of isolate S1, the 6-nt 3′ UTR pseudoknot insertion was retained. However, by passage 6, a previously unseen nsp9 mutation had been selected (A13010G), resulting in the amino acid change D58G (Fig. 2C). For isolate S2, the passage-6 stock was composed of a new type of primary site footprint mutant, in which the last three bases of the 6-nt insertion (AAG), as well as the next downstream base (U), were deleted (Fig. 2D). There were no additional changes in either the nsp7-through-nsp10 region or the remainder of the 3′ UTR of S2 passage 6. Finally, bulk sequencing of the passage-6 stock of isolate S3 gave a mixture of sequences, which were resolved through TA cloning of RT-PCR products from the 3′ UTR. Five out of nine TA clones were found to have the same 3-nt footprint of the original insertion that had been found in the S2 isolate by passage 6 (Fig. 2E, left), with no other mutations in the 3′ UTR. On the other hand, the remaining four TA clones showed an intact 6-nt insertion, accompanied by the same A2G mutation that had been found in Rev5 and Rev6 (Fig. 2E, right). The S3 passage-6 stock had no additional changes in the nsp7-through-nsp10 region of the genome. In accord with the apparently strong selective pressure against the original Alb391 mutation, the growth of passage-2 stocks of the S1 through S3 isolates was greatly impaired relative to that of the wild type for at least the first 11 h of infection (Fig. 3A). Later, by 26 h postinfection, S1 through S3 mutant titers appeared to approach that of the wild type, but this may have reflected the emergence and overrunning of the cultures by revertants. By passage 6, the small-plaque isolates replicated with kinetics comparable to that of the wild type (Fig. 3B). As expected, the growth kinetics for either the passage-2 or passage-10 stocks of the L1 and L2 isolates were indistinguishable from the kinetics for the wild type (data not shown).

Taken together, these results showed that the AACAAG insertion mutation in pseudoknot loop 1 conferred the same phenotype in the MHV-inf-1 genetic background as had been seen in the initial Alb391 mutant (18). Furthermore, the analyses of the Alb391 and rAlb391 revertants revealed the same three classes of compensatory mutations, as summarized in Fig. 4A. First, there were primary-site revertants, in which there occurred loss of the entirety or a portion of the AACAAG insertion, as in rAlb391 isolates L1 and L2 or in the two types of footprint mutations in Rev1 and rAlb391 isolates

FIG. 2. Reconstruction of the Alb391 3′ UTR insertion mutant by using the vaccinia virus-based reverse-genetics system for MHV. (A) Sequence of RT-PCR product from the 3′ UTR of the initially recovered mutant, rAlb391. The position of the AACAAG insertion is denoted, and mixed sequence downstream of the site of the insertion is boxed. (B) Plaques from passages 2 and 6 of three small-plaque isolates of rAlb391 (S1 to S3), compared with plaques from passages 2 and 10 of two large-plaque isolates of rAlb391 (L1 and L2) and a wild-type control. (C) Sequences of RT-PCR products from the pseudoknot region (3′ PK) of the 3′ UTR and nsp9 from passages 2 and 6 of the S1 isolate; note that the nsp9 sequence is the negative sense. (D) Sequences of RT-PCR products from the pseudoknot region of the 3′ UTR from passages 2 and 6 of the S2 isolate. (E) Sequences of the pseudoknot region and the downstream terminus (3′ end) of the 3′ UTR of representative TA clones from passage 6 of the S3 isolate. In C to E, the insertion or its remnant is boxed, and mutant nucleotides or their wild-type counterparts are circled.

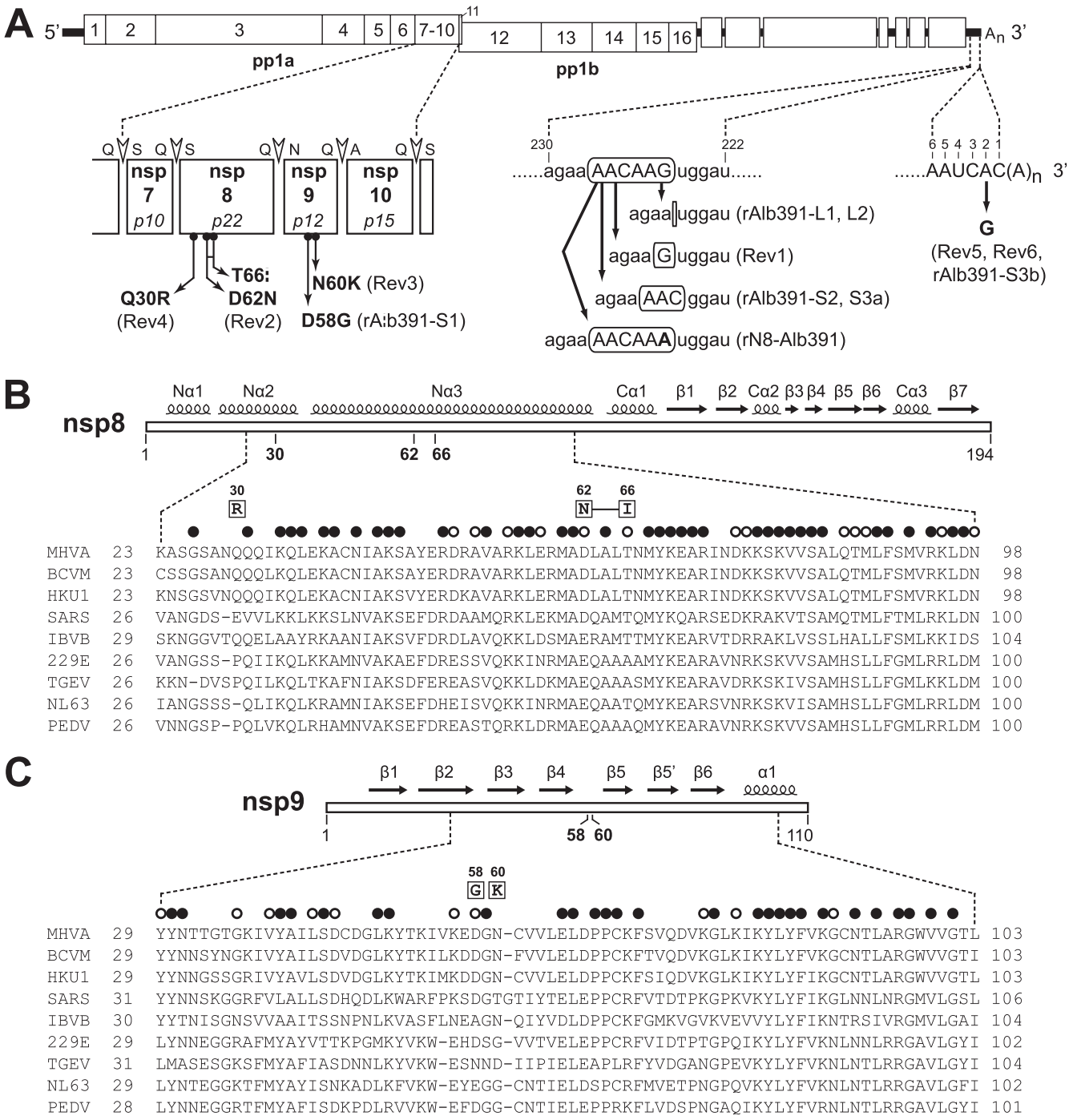

FIG. 4. Genetic cross talk between loop 1 of the 3′ UTR pseudoknot and both gene 1a and the 3′ end of the MHV genome. (A) Summary of all types of reverting mutations from the original Alb391 mutant and the reconstructed mutant rAlb391. In the expansion of the region of the genome encoding nsp7 to nsp10, main protease cleavage sites (8, 52) are denoted by open arrowheads and the flanking amino acid residues are indicated; alternate names for the MHV nsp7-to-nsp10 polypeptides are given in italics. In the expansions of regions of the 3′ UTR, nucleotide numbering is from the first base at the 3′ end of the genome, excluding poly(A). The original 6-nt insertion and remnants thereof are boxed; mutated nucleotides are shown in bold. For each type of reverting mutation, the designations of independently obtained isolates are given in parentheses. (B) Loci of the reverting mutations in nsp8. The schematic of the secondary structure of nsp8 of SARS-CoV corresponds to the crystal structure reported by Zhai and coworkers (66). (C) Loci of the reverting mutations in nsp9. The schematic of the secondary structure of nsp9 of SARS-CoV corresponds to the crystal structure reported by Egloff and coworkers (16), but it is also substantially the same as that reported by Sutton and coworkers (56). Beneath the schematics in panels B and C are alignments for portions of nsp8 and nsp9 of coronaviruses spanning all three phylogenetic groups. GenBank accession numbers for the sequences shown are as follows: MHVA, MHV strain A59, AY700211; BCVM, bovine coronavirus strain Mebus, U00735; HKU1, human coronavirus strain HKU1, AY597011; SARS, SARS coronavirus strain Urbani, AY278741; IBVB, infectious bronchitis virus strain Beaudette, M94356; 229E, human coronavirus strain 229E, AF304460; TGEV, transmissible gastroenteritis virus strain Purdue, AJ271965; NL63, human coronavirus strain NL63, AY567487; and PEDV, porcine epidemic diarrhea virus strain CV777, AF353511. MHV mutant Alb391 reverting mutations are boxed above each alignment. Filled circles mark residues that are identical among at least seven of the nine sequences; open circles mark additional residues that are identical among all group 2 coronaviruses. Amino acid numbering indicates the residue position in each processed replicase protein product.

S2 and S3. Second, four independent reverting mutations, Rev2 through Rev4 and rAlb391 isolate S1, mapped to three loci in nsp8 and nsp9, altering moderately conserved residues in these RNA-binding proteins. Finally, three independent revertants, Rev5, Rev6, and rAlb391 isolate S3, each had a single point mutation, changing the second residue of the 3′ UTR from A to G.

Interactions between the 3′ UTR pseudoknot and replicase gene products. Having shown that Alb391 and the reconstructed rAlb391 mutants displayed the same phenotype, we next examined the effects of reconstruction of two of the gene 1a candidate reverting mutations in both the presence and the absence of the 3′ UTR pseudoknot AACAAG insertion. For this purpose, we chose the pair of nsp8 mutations from Rev2 (G12439A and C12452U) and the single nsp9 mutation from Rev3 (U13017G) (Table 1). We analyzed three independent isolates bearing the nsp8 mutations in the presence of the 3′ UTR insertion (mutant rN8-Alb391) and two isolates bearing the nsp8 mutations alone (mutant rN8). Likewise, two isolates each were analyzed for the nsp9 mutation in the presence (mutant rN9-Alb391) or the absence (mutant rN9) of the 3′ UTR insertion (Fig. 5A). The rN8-Alb391 and rN9-Alb391 reconstructed revertants produced plaques that were only slightly smaller than those of the wild type (Fig. 5B), demonstrating that the nsp8 and nsp9 mutations were indeed responsible for the suppression of the Alb391 phenotype in Rev2 and Rev3. In general, the rN8-Alb391 and rN9-Alb391 mutants were stable for up to 10 passages: the nsp8 or nsp9 mutation remained unchanged, and the 6-nt insertion in the 3′ UTR was retained. However, an exception to this trend was that for 2 of the rN8-Alb391 isolates, the 6th residue of the 3′ UTR insertion (G) was gradually replaced by A over the course of 10 passages. An example of this replacement is shown in Fig. 5C. This suggested that the nsp8 mutations could not optimally compensate for the distortion of the 3′ UTR pseudoknot and that there was some residual selective pressure to mitigate the effect of the AACAAG insertion. The suppression of the Alb391 phenotype was also evident in the growth kinetics for the rN8-Alb391 and rN9-Alb391 mutants, which closely resembled the kinetics for the wild type at both passage 2 and passage 10 (Fig. 5D and E). At early times postinfection, both mutants lagged slightly behind the wild type, but they were far more robust than the passage-2 small-plaque isolates of rAlb391 (Fig. 3).

Somewhat differently, plaques of the rN8 and rN9 mutants were of fully wild-type size, indicating that the suppressor mutations, in isolation, were not noticeably deleterious to the virus (Fig. 5B). Sequence analysis confirmed this inference. The nsp8 and nsp9 mutations were stable over 10 passages, and their presence did not select for any compensating changes in the 3′ UTRs of these viruses. In addition, the growth kinetics for the rN8 and rN9 mutants were highly similar to that for the wild type (data not shown).

Collectively, these data demonstrated that the mutated replicase gene products nsp8 and nsp9 are still functional in the context of both the wild-type 3′ UTR and the Alb391 3′ UTR. More importantly, it was directly proven, by reconstruction of the Alb391 revertants Rev2 and Rev3, that the replicase gene mutations mapping to nsp8 and nsp9 could compensate for the markedly defective phenotype of Alb391, thus making it very likely that the other two replicase gene mutations, found in revertants Rev4 and rAlb391 isolate S1, were also genuine suppressors of the severe growth defect mediated by the 6-nt pseudoknot insertion. These data were indicative of an interaction of two replicase gene products, the RNA-binding proteins nsp8 and nsp9, with an essential *cis*-acting RNA pseudoknot located at the MHV 3′ UTR.

Interactions between the pseudoknot and the 3′ end of the genome. The last class of revertant, the A2G mutation, was very surprising, because the poly(A)-adjacent end of the genome was not obviously connected with the 3′ UTR pseudoknot in previous RNA structural analyses. To confirm whether A2G was truly a reverting mutation, we reconstructed this base change in both the presence and absence of the 6-nt pseudoknot insertion, using targeted RNA recombination. As we had observed for the replicase gene mutations, the A2G mutation, on its own, produced no detectable phenotype (as is also the case for MHV strain 3 [47]). Similarly, recombinants containing A2G together with the pseudoknot insertion formed plaques that were only slightly smaller than plaques of the wild type and were rescued at a much higher frequency than Alb391 (data not shown). This proved conclusively that the apparently simple A2G mutation could also suppress the severe impairment caused by the AACAAG pseudoknot insertion.

This result also provided the first indication of the existence of a direct interaction between pseudoknot loop 1 and the 3′ genomic terminus. The folding of these regions that is shown in Fig. 1 is derived from a study (38) in which a structure running from nt 166 to the 3′ end of the genome was predicted with the *mfold* software (44, 68). At the outset, the chosen 5′ upper limit of nt 166 would have excluded potential interactions with further-upstream portions of the 3′ UTR, including the pseudoknot. Indeed, we found that the lowest-free-energy *mfold* predictions obtained for the distal end of the 3′ UTR, running instead from the start of pseudoknot loop 1 (nt 230) through the 3′ terminus, support a different RNA secondary structure, which is shown in Fig. 6A. In this case, the 3′-most 29 nt of the genome are seen to form two helices with further upstream regions, one with pseudoknot loop 1 and one with the segment immediately distal to pseudoknot stem 2. The likelihood of this alternative structure is further supported by its absolute phylogenetic conservation among all other known group 2 coronaviruses, including the closely related BCoV and human coronavirus OC43 as well as the more divergent SARS-CoV, human coronavirus HKU1, and bat coronaviruses HKU4, HKU5, and HKU9 (Fig. 6B). Thus, not only do members of this coronavirus subfamily strictly maintain the 3′ UTR bulged stem-loop and pseudoknot but they also appear to be required to preserve base pairing between loop 1 of the pseudoknot and the 3′ end of the genome. Similar loop 1–3′-end structures potentially occur in the genomes of the group 1 and group 3 coronaviruses, but as yet no experimental evidence supports their existence.

To further test the loop 1–3′-end interaction in MHV, we designed a mutant harboring a large deletion within the 3′ UTR that would retain the two putative helices of the new model while eliminating the entire HVR and all of the adjacent region that was formerly thought to base pair with the 3′ end of the genome. We had previously constructed a deletion mu-

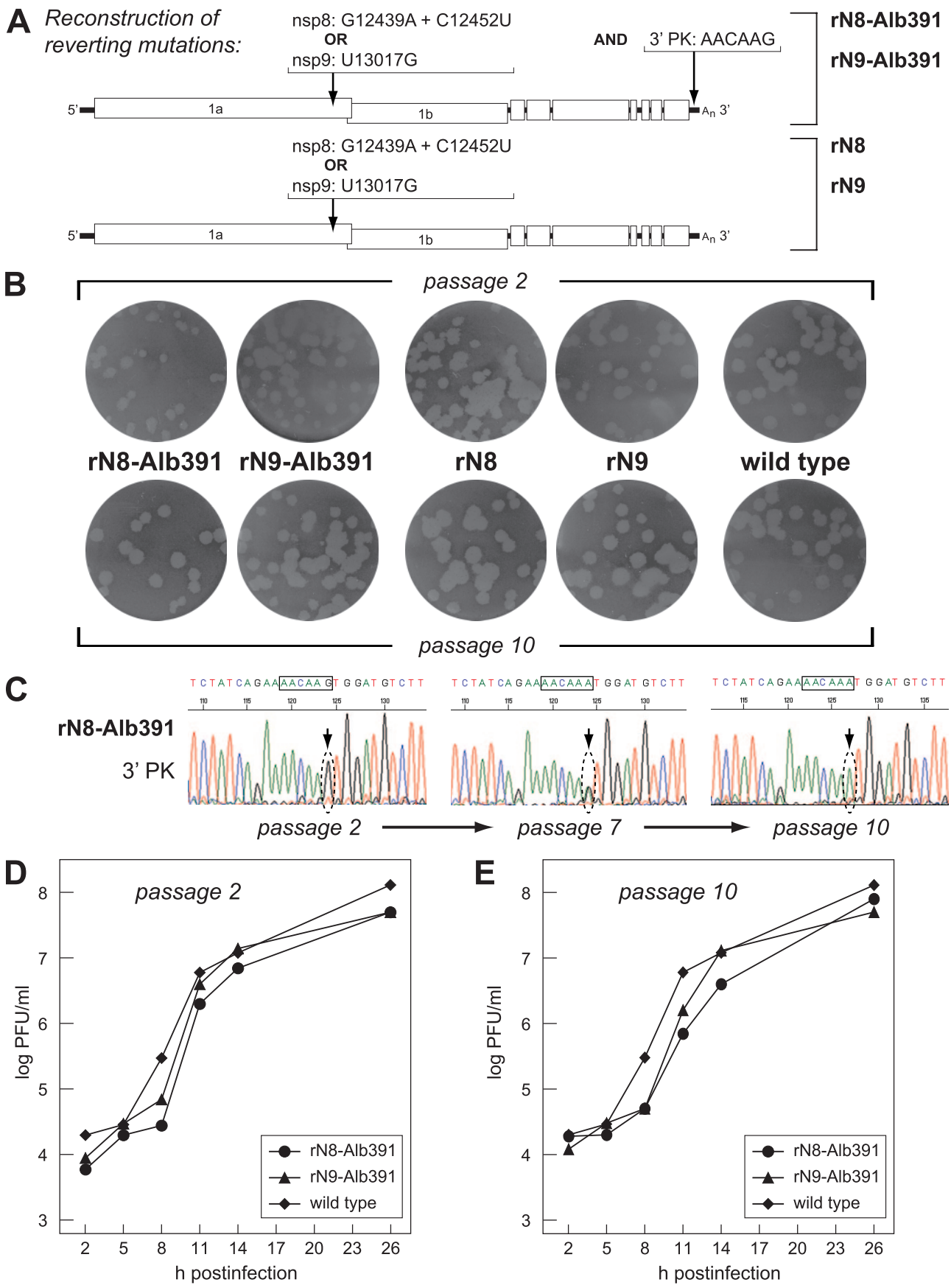
A
Reconstruction of reverting mutations:
nsp8: G12439A + C12452U
OR
nsp9: U13017G
AND
3' PK: AACAAG
rN8-Alb391
rN9-Alb391
5'
1a
1b
An 3'
nsp8: G12439A + C12452U
OR
nsp9: U13017G
rN8
rN9
B
passage 2
rN8-Alb391
rN9-Alb391
rN8
rN9
wild type
passage 10
C
rN8-Alb391
3' PK
passage 2
passage 7
passage 10
D
passage 2
log PFU/ml
h postinfection
rN8-Alb391
rN9-Alb391
wild type
E
passage 10
log PFU/ml
h postinfection
rN8-Alb391
rN9-Alb391
wild type

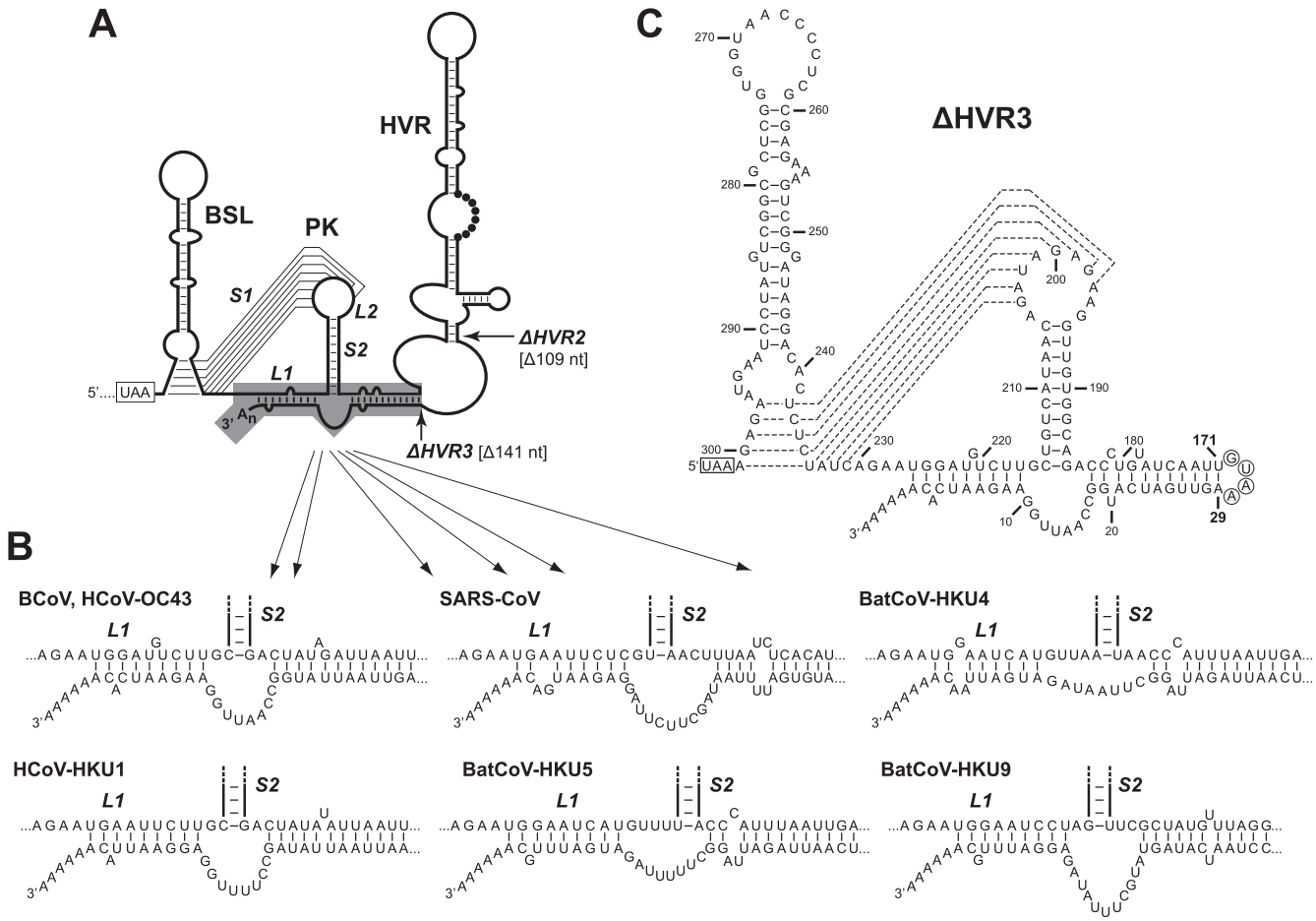

FIG. 6. Interaction between loop 1 (L1) of the 3′ UTR pseudoknot (PK) and the 3′ end of the genome. (A) Refinement of the complete structure of the MHV 3′ UTR, incorporating base pairing of the 3′ end of the genome with both pseudoknot loop 1 and the region downstream of pseudoknot stem 2 (S2); other abbreviations are the same as those used in Fig. 1. Arrows indicate points at which truncations were introduced in the previously characterized ΔHVR2 deletion mutant (19) and in a new mutant, the ΔHVR3 mutant. (B) Phylogenetic conservation of the loop 1–3′-end interaction among all group 2 coronaviruses. GenBank accession numbers for the sequences shown, other than those given in the legend to Fig. 4, are as follows: HCoV-OC43, human coronavirus strain OC43, AF523847; and bat coronavirus (BatCoV) strains HKU4, HKU5, and HKU9, respectively, EF065505, EF065509, and EF065513. (C) Detailed view of the complete 164-nt 3′ UTR of the ΔHVR3 mutant. Broken lines represent alternative base pairings either for the bottom stem segment of the bulged stem-loop or for pseudoknot stem 1. Nucleotides of the tetraloop introduced between positions 29 and 171 are circled. Nucleotide numbering is from the first base at the 3′ end of the genome, excluding poly(A), and the N-gene stop codon is boxed.

tant, the ΔHVR2 mutant (Fig. 6A), in which 109 nt of the 3′ UTR were excised with little consequence to the in vitro growth of the virus (19). In the new mutant, designated the ΔHVR3 mutant, we created an even more extensive deletion, of 141 nucleotides, in which all sequence between bases 29 and 171 was replaced by a tetraloop capping the helix downstream of pseudoknot stem 2 (Fig. 6C). The ΔHVR3 mutant was not only viable but formed plaques that were 80% of the size of wild-type plaques and were larger than those of the previously characterized ΔHVR2 virus. Moreover, the ΔHVR3 mutant exhibited growth kinetics comparable to those of the wild type in single-step, high-multiplicity infections (Fig. 7A) and in multicycle, low-multiplicity infections (Fig. 7B). Under both conditions, growth of the ΔHVR3 mutant lagged behind that of

FIG. 5. Reconstruction of viruses harboring candidate gene 1a reverting mutations of Alb391. (A) Recombinants rN8-Alb391 and rN9-Alb391, respectively, contain the nsp8 and nsp9 mutations from revertants Rev2 and Rev3 in the presence of the original Alb391 3′ UTR insertion mutation. Recombinants rN8 and rN9, respectively, contain the Rev2 and Rev3 mutations in the presence of the wild-type 3′ UTR. (B) Plaques from passages 2 and 10 of rN8-Alb391, rN9-Alb391, rN8, and rN9, compared with a wild-type control; the wild-type control plaques are the same as those shown in Fig. 2. (C) Sequences of RT-PCR products from the pseudoknot region (3′ PK) of the 3′ UTR from passages 2, 7, and 10 of one rN8-Alb391 isolate. The variable base of the AACAAG insertion is denoted. (D and E) Growth kinetics for reconstructed revertants rN8-Alb391 and rN9-Alb391, compared with a wild-type control. Cultures were inoculated with passage-2 virus (D) or passage 10 virus (E) at a multiplicity of 1.0 PFU per cell. Data shown for each mutant are a set from one representative of duplicate experiments, which gave highly similar results. Also, duplicate sets from two additional independent isolates of rN8-Alb391 were essentially identical to the data shown.

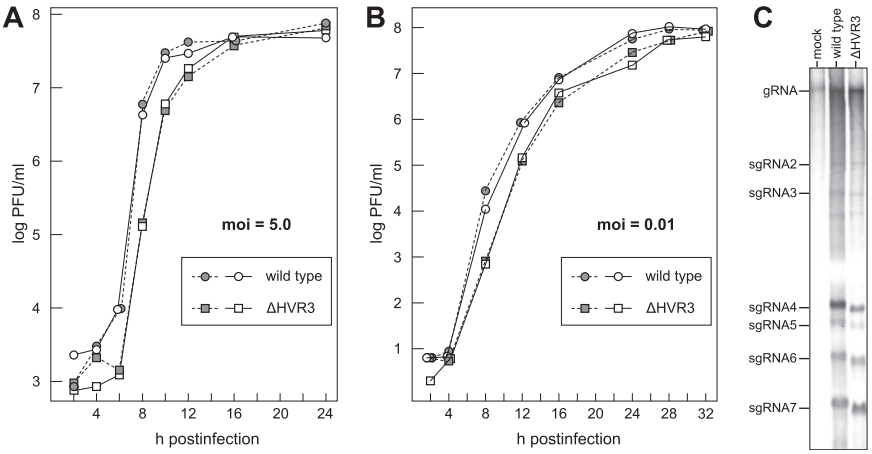

FIG. 7. Replicational competence of the ΔHVR3 mutant. Growth kinetics of the ΔHVR3 mutant relative to that of the wild type at a high multiplicity of infection (5.0 PFU per cell) (A) or a low multiplicity of infection (0.01 PFU per cell) (B). Open and solid symbols represent results from two independent experiments. (C) RNA synthesis by the ΔHVR3 mutant and the wild type. Infected or mock-infected 17Cl1 cells were metabolically labeled with [^{33}P]orthophosphate in the presence of actinomycin D, and RNA was isolated and electrophoretically separated in 1% agarose containing formaldehyde as described in Materials and Methods.

the wild type by 2 h but ultimately reached the same maximal titers. Additionally, metabolic labeling of infected cells revealed no significant difference in gRNA or sgRNA synthesis between the mutant and the wild type (Fig. 7C). Taken together, these results showed that the 3′ genomic *cis*-acting elements essential for MHV RNA synthesis are restricted to two separate segments of the 3′ UTR, nucleotides 1 through 29 and nucleotides 171 through 301. Surprisingly, therefore, almost half of the 3′ UTR is dispensable with respect to functions required for growth in tissue culture.

DISCUSSION

All RNA viruses harbor *cis*-acting sequences and structures in their genomes that are critical for replication. Within the order *Nidovirales*, 3′ *cis*-acting elements are currently best characterized for the group 2 coronaviruses, in which an overlapping bulged stem-loop and pseudoknot in the 3′ UTR have been found to be essential for RNA synthesis (Fig. 1) (9, 42). In the group 3 coronaviruses, a functionally essential stem-loop is located at the upstream end of the 3′ UTR (12), but the status of different nearby candidate pseudoknots is unresolved (20, 60). Conversely, the group 1 coronaviruses all contain a very highly conserved pseudoknot, but a neighboring potential counterpart of the bulged stem-loop (15) is not clearly identifiable in every member of this group. Over a greater phylogenetic distance, in the arteriviruses, which have much smaller 3′ UTRs, certain required *cis*-acting RNA structures have been described that extend into the upstream N gene (5, 6, 59). It is not obvious at present how closely analogous to coronavirus 3′ elements these RNA structures will turn out to be, but the genomes of members of the two virus families might be expected to interact in similar ways with their respective replicases, which are highly homologous (21).

Interactions between the pseudoknot and the 3′ end of the genome. In the work presented here, we analyzed revertants of a highly defective MHV mutant containing a particular insertion, AACAAG, in loop 1 of the 3′ UTR pseudoknot (summarized in Fig. 4A). Our finding of six independent primary-site reverting mutations that deleted or altered part or all of the insertion confirmed that the insertion was, in actuality, the basis of the deleterious and unstable genotype of the original mutant. More informative, however, were two groups of second-site reverting mutations that were obtained in both the original mutant, Alb391, which had been constructed by targeted RNA recombination, and rAlb391, which was reconstructed by vaccinia virus-based reverse genetics. These two classes of suppressors mapped to distinct regions of the genome, thereby revealing two types of previously unsuspected interactions. One class, independently isolated three times, was represented by a single type of revertant, in which the second 3′ UTR residue upstream of the poly(A) tail was changed from an A to a G. That this single base change could rescue the Alb391 insertion mutant suggested that the 3′ end of the genome must somehow communicate with loop 1 of the pseudoknot. This conclusion led us to identify a longer-range secondary structure in which the 3′ end of the genome folds into two helices through base pairing with pseudoknot loop 1 and with the region downstream of pseudoknot stem 2 (Fig. 6). Additional evidence in support of this interaction came from the following: (i) *mfold*-based structural predictions; (ii) the total conservation of the interaction among all known group 2 coronaviruses (and possibly also among group 1 and group 3 coronaviruses); (iii) our construction of a mutant, the ΔHVR3 mutant, which preserves this base pairing in a drastically minimized version of the 3′ UTR; and (iv) our previous finding of the lethality of a more extensive deletion in the 5′-ward direction, ΔHVR1, which suggested that at least some subset of nucleotides 157 through 184 must be essential (19).

It is noteworthy that in our redefined folding of the 3′ end of the genome, base A2 does not participate in a Watson-Crick base pair (Fig. 6). Thus, it is not immediately obvious how the A2G mutation relieves the problem caused by the AACAAG insertion. We favor the explanation that the insertion in loop 1 forces an alternative folding of the pseudoknot-3′ end interac-

tion and that the A2G mutation destabilizes this alternative structure, thereby allowing the wild-type fold to predominate. This notion is supported by the fact that the A2G mutation, in the context of an otherwise wild-type 3′ UTR, has no detectable effect on the viral phenotype. A potentially related observation is that the mutation A2U, which is also neutral by itself, is lethal in combination with the AACAAG insertion (data not shown). Further mutational analysis will be needed to more completely define the sequence and structural requirements for the interaction between the extreme 3′ end of the genome and pseudoknot loop 1, as well as the region downstream of pseudoknot stem 2.

The viability and nearly normal phenotype of the ΔHVR3 mutant indicate that the minimal 3′ *cis*-acting element required for MHV RNA synthesis is limited to no more than 160 nt of the 3′ UTR. This means that nearly half of the 3′ UTR, bases 30 through 170, can be discarded without affecting the basic mechanism of viral RNA synthesis. The deleted region in the ΔHVR3 mutant encompasses in vitro binding sites for a number of host cell proteins, including PTB (27), hnRNP A1 (28), and a complex of mitochondrial aconitase and the chaperones mtHSP70, HSP60, and HSP40 (45, 46, 64, 65). It follows that these binding sites cannot be strictly required for RNA synthesis, although they may play ancillary roles yet to be defined. Additionally, the region of the 3′ UTR that was eliminated in the ΔHVR3 mutant encompasses some RNA segments that were previously proposed to base pair with the 3′ end of the genome (38) (Fig. 1). Our redefined folding of the 3′ UTR is also at variance with an alternative *mfold*-predicted structure proposed for solely the 3′-terminal 42 nt of the genome (31). Notably, our results prompt reconsideration of the conclusions reached by a previous study, which mapped the promoter for negative-strand RNA synthesis based on RNase protection assays specific for the negative strand of a heterologous RNA that was connected to progressively decreasing lengths of the MHV 3′ UTR (37). That work concluded that the promoter for negative-strand initiation constitutes the last 45 to 55 nt of the genome. However, it is now clear that the essential sequence at the 3′ end of the genome is no more than 29 nt, together with a poly(A) tail of at least 5 to 10 residues (54). Moreover, we suggest that nt 1 to 29, on its own, is not sufficient for the initiation of negative-strand RNA synthesis, but it likely acts in association with the pseudoknot. Such an association would normally occur in *cis*, but in the promoter mapping experiments (37), it must have occurred in *trans*, between the heterologous RNA and the helper virus genome.

Interactions between the pseudoknot and gene 1a replicase products. The second class of suppressor mutations found in our genetic analysis was represented by four independently isolated revertants that mapped to nsp8 or nsp9. These replicase components fall within a group of small proteins, nsp7 through nsp10 (each 10 to 22 kDa), that are encoded at the downstream end of gene 1a (Fig. 4A) (8, 52). All four are processed from the replicase polyproteins 1a and 1ab by the main viral proteinase (nsp5), and they localize in discrete perinuclear and cytoplasmic foci in infected cells as parts of the membrane-associated replication complex (8, 10, 14, 22, 53).

Structural studies of each of the highly conserved SARS-CoV homologs of nsp7 through nsp10 have recently been reported. SARS-CoV nsp9, the crystal structure of which was separately solved by two groups, has been shown to have nonspecific RNA-binding activity and a fold not previously seen in any RNA-binding protein (16, 56). Nsp9 crystallizes in two dimeric forms, and biophysical evidence has also been presented for the existence of an interaction between nsp9 and nsp8 (56). A hexadecameric complex of SARS-CoV nsp8 and nsp7 has been found to bind to double-stranded RNA. The crystal structure of this complex (66), partially confirmed by the nuclear magnetic resonance solution structure of nsp7 (48), is a hollow cylinder potentially able to encircle double-stranded nucleic acid. Within this ring, which resembles a processivity clamp, nsp8 monomers are folded in two different conformations. Finally, there are two independently solved structures of SARS-CoV nsp10, which reveal that it represents a novel class of zinc finger protein which assembles into a dodecameric complex having a weak affinity for single- and double-stranded RNA (32, 55). A classical MHV mutant, *ts*LA6, which has the phenotype of shutoff of negative-strand RNA synthesis at the nonpermissive temperature (3, 51), has been mapped to nsp10 (50), and reverse-genetics analysis of MHV nsp10 has also indicated that this protein plays an essential role in viral RNA synthesis (14).

In the absence of further information, such as would be provided by RNA cocrystals, we cannot yet use the abundance of available structural data to draw strong conclusions about the nature of the reverting mutations that suppress the Alb391 pseudoknot insertion mutation. Each of the four nsp8 or nsp9 reverting mutations introduces a more basic charge into its respective molecule (Fig. 4B and C). The exact loci of the nsp8 mutations Q30R and D62N-T66I suggest that the mutations are most likely to affect the packing between monomers at the interface of the two nsp8 molecules in different conformations in the asymmetric unit of the nsp7-nsp8 hexadecamer. Likewise, the nsp9 mutations D58G and N60K may affect intersubunit beta-sheet interactions that stabilize one type of dimer formation (56). In both cases, these alterations could indirectly influence the RNA-binding specificity or affinity of nsp8 or nsp9. Alternatively, the conformations of the nsp's in a polyprotein precursor or in an RNA-bound form may differ from that revealed in the crystal structure, and thus, the increased positive charge caused by the reverting mutations might then directly enhance the affinity of nsp8 or nsp9. We are currently seeking in vitro biochemical data to corroborate these ideas.

Very surprisingly, purified SARS-CoV nsp8 has recently been found to possess RdRp activity, and it has been proposed to function as a primase for the canonical coronavirus RdRp, nsp12 (30). The in vitro enzymatic activity of SARS-CoV nsp8 has a dependence on manganese ion, and it exhibits a strong preference for cytidine-rich RNA templates, synthesizing small oligoribonucleotides of six or fewer residues. We have confirmed these same properties for the MHV homolog of nsp8 (S. J. Goebel and P. S. Masters, unpublished data). Imbert and coworkers (30), who discovered the RdRp activity of nsp8, have suggested that nsp8 could act at multiple points throughout the genomic template, although it must be noted that the characteristics of this enzyme may be substantially altered in the company of nsp7, nsp9, nsp10, and the authentic viral RNA substrate. In view of our suppressor results, we favor the idea that nsp8 acts as a primase during the initiation of negative-

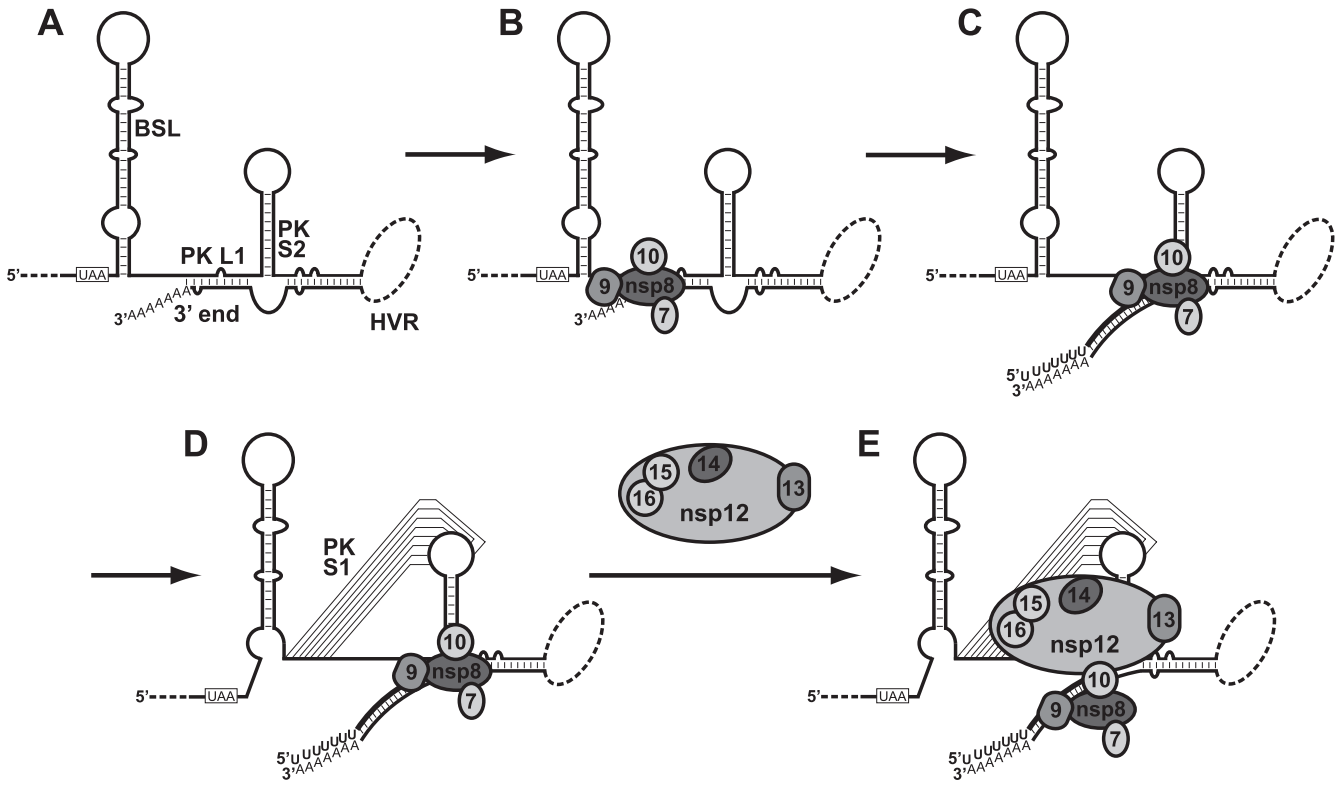

FIG. 8. Hypothetical model of initiation of coronavirus negative-strand RNA synthesis. (A) At the outset, formation of the pseudoknot is precluded by (i) closure of the bottom segment of the bulged stem-loop (BSL) and (ii) the interaction between pseudoknot (PK) loop 1 (L1) and the 3′ end of the genome. (B) The nsp8 primase, in conjunction with nsp7, nsp9, and nsp10, binds to the stem formed by loop 1 and the 3′ end. (C) Synthesis of the 5′ end of negative-strand RNA by the nsp8 primase separates the 3′ end of the genome from loop 1, thereby allowing the pseudoknot to form (D). The nsp12 RdRp then binds to the pseudoknot, together with nsp13 (helicase), nsp14 (ExoN nuclease), nsp15 (NendoU nuclease), and nsp16 (methyltransferase). (E) The nsp12 complex carries out elongation of the negative-strand primer. Not shown are possible roles played by other nsp's, the poly(A) binding protein, and the viral N protein.

strand synthesis. The interactions of the MHV 3′ pseudoknot loop 1 with the extreme 3′ genomic terminus and with nsp8 and nsp9 would position a template RNA secondary structure and particular replicase components very close to the start site of negative-strand RNA synthesis, which initiates with production of a tract of oligo(U) some 9 to 26 residues into the poly(A) tail (25). It is thus conceivable that the primase activity of nsp8 is involved in the initiation of coronavirus negative-strand RNA synthesis before the canonical RdRp activity, encoded by the nsp12 gene, can resume negative-strand RNA synthesis by elongating the nsp8-derived primer molecules. This idea is supported by the fact that nsp12 can be targeted to replication complexes when expressed in *trans* as a fusion protein with green fluorescent protein in MHV-infected cells; moreover, nsp12 can be coimmunoprecipitated with nsp8 and nsp9 from infected cell lysates (10).

Model for initiation of MHV negative-strand RNA synthesis. Our suppressor results, integrated with the finding of primase activity of nsp8, thus lead us to propose a model for initiation of MHV negative-strand RNA synthesis, which is shown in Fig. 8. We speculate that the most stable conformation of the 3′ UTR RNA is one in which the bulged stem-loop is fully folded and the 3′ end of the genome is annealed to pseudoknot loop 1. These two folding alternatives would preclude formation of stem 1 of the pseudoknot. The stem formed by loop 1 and the 3′ end of the genome is postulated to serve as the site of assembly of a complex that includes at least nsp8 and nsp9 and probably also nsp7 and nsp10. These replicase constituents may act as processed monomers, as shown. Alternatively, they may be part of a much larger nsp4-nsp11 precursor, which has been suggested to be the relevant species for negative-strand RNA synthesis (50). Thus, the MHV 3′ pseudoknot in conjunction with the 3′ end of the genome may constitute a *cis*-acting element that allows the specific recognition of the gRNA as the template for initiation of minus-strand RNA synthesis. Following substrate recognition, initiation of negative-strand RNA synthesis by the nsp8 primase complex leads to separation of the 3′ end of the genome from loop 1, thereby allowing formation of stem 1 of the pseudoknot. Finally, the completely folded pseudoknot, in conjunction with nsp8 and nsp9, then recruits the nsp12 RdRp and the associated activities contained in nsp13 through nsp16, and the resulting complex resumes the elongation of negative-strand RNA.

We are aware that many mechanistic details of this process remain to be elucidated. The proposed role of the MHV pseudoknot in association with the 3′ genomic end bears some resemblance to the function of the 5′ *cis*-acting element required for the assembly and positioning of the poliovirus preinitiation RNA synthesis complex discussed above (4, 23).

However, it remains to be established whether *cis*-acting elements located at the 5′ end of the coronavirus genome also participate in this process. Although the notion of genome circularization has been previously invoked (29, 69), there is currently no clear evidence that coronavirus 5′ and 3′ genomic ends are bridged by viral or cellular proteins or by heretofore-unidentified RNA-RNA interactions. Congruent with the analogy to the poliovirus system, however, it has been demonstrated that the length of the poly(A) tail of coronavirus DI RNA affects the efficiency of replication (54). Finally, the exact composition of the coronavirus preinitiation complex remains to be determined; the complex conceivably assembles cotranslationally and involves more nsp's than are pictured in our model. We hope that our discovery of an interaction between an essential 3′ *cis*-acting pseudoknot, specific replicase gene products, and the extreme 3′ end of the MHV genome will provide a starting point for further genetic, structural, and biochemical analyses aimed at establishing a more detailed understanding of the earliest events of coronavirus RNA synthesis.

ACKNOWLEDGMENTS

We are grateful to Joachim Jaeger for providing valuable help in localizing the nsp8 and nsp9 mutations in the reported X-ray crystal structures. We thank the Molecular Genetics Core Facility of the Wadsworth Center for some of the DNA sequencing reported here.

This work was supported by the Swiss National Science Foundation (V.T.) and by Public Health Service grants AI 45695 and AI 060755 from the National Institutes of Health (P.S.M.).

REFERENCES

1. **Andino, R., G. E. Rieckhof, and D. Baltimore.** 1990. A functional ribonucleoprotein complex forms around the 5′ end of poliovirus RNA. Cell **63:**369–380.
2. **Andino, R., G. E. Rieckhof, P. L. Achacoso, and D. Baltimore.** 1993. Poliovirus RNA synthesis utilizes an RNP complex formed around the 5′-end of viral RNA. EMBO J. **12:**3587–3598.
3. **Baric, R. S., and B. Yount.** 2000. Subgenomic negative-strand RNA function during mouse hepatitis virus infection. J. Virol. **74:**4039–4046.
4. **Barton, D. J., B. J. O'Donnell, and J. B. Flanegan.** 2001. 5′ cloverleaf in poliovirus RNA is a cis-acting replication element required for negative-strand synthesis. EMBO J. **20:**1439–1448.
5. **Beerens, N., and E. J. Snijder.** 2006. RNA signals in the 3′ terminus of the genome of Equine arteritis virus are required for viral RNA synthesis. J. Gen. Virol. **87:**1977–1983.
6. **Beerens, N., and E. J. Snijder.** 20 June 2007. An RNA pseudoknot in the 3′ end of the arterivirus genome has a critical role in regulating viral RNA synthesis. J. Virol. doi:10.1128/JVI.00747-07.
7. **Blyn, L. B., K. M. Swiderek, O. Richards, D. C. Stahl, B. L. Semler, and E. Ehrenfeld.** 1996. Poly(rC) binding protein 2 binds to stem-loop IV of the poliovirus RNA 5′ noncoding region: identification by automated liquid chromatography-tandem mass spectrometry. Proc. Natl. Acad. Sci. USA **93:**11115–11120.
8. **Bost, A. G., R. H. Carnahan, X. T. Lu, and M. R. Denison.** 2000. Four proteins processed from the replicase gene polyprotein of mouse hepatitis virus colocalize in the cell periphery and adjacent to sites of virion assembly. J. Virol. **74:**3379–3387.
9. **Brian, D. A., and R. S. Baric.** 2005. Coronavirus genome structure and replication. Curr. Top. Microbiol. Immunol. **287:**1–30.
10. **Brockway, S. M., C. T. Clay, X. T. Lu, and M. R. Denison.** 2003. Characterization of the expression, intracellular localization, and replication complex association of the putative mouse hepatitis virus RNA-dependent RNA polymerase. J. Virol. **77:**10515–10527.
11. **Coley, S. E., E. Lavi, S. G. Sawicki, L. Fu, B. Schelle, N. Karl, S. G. Siddell, and V. Thiel.** 2005. Recombinant mouse hepatitis virus strain A59 from cloned, full-length cDNA replicates to high titers in vitro and is fully pathogenic in vivo. J. Virol. **79:**3097–3106.
12. **Dalton, K., R. Casais, K. Shaw, K. Stirrups, S. Evans, P. Britton, T. D. K. Brown, and D. Cavanagh.** 2001. *cis*-acting sequences required for coronavirus infectious bronchitis virus defective-RNA replication and packaging. J. Virol. **75:**125–133.
13. **de Haan, C. A. M., H. Volders, C. A. Koetzner, P. S. Masters, and P. J. M. Rottier.** 2002. Coronaviruses maintain viability despite dramatic rearrangements of the strictly conserved genome organization. J. Virol. **76:**12491–12493.
14. **Donaldson, E. F., A. C. Sims, R. L. Graham, M. R. Denison, and R. S. Baric.** 2007. Murine hepatitis virus replicase protein nsp10 is a critical regulator of viral RNA synthesis. J. Virol. **81:**6356–6368.
15. **Dye, C., and S. G. Siddell.** 2005. Genomic RNA sequence of feline coronavirus strain FIPV WSU-79/1146. J. Gen. Virol. **86:**2249–2253.
16. **Egloff, M. P., F. Ferron, V. Campanacci, S. Longhi, C. Rancurel, H. Dutartre, E. J. Snijder, A. E. Gorbalenya, C. Cambillau, and B. Canard.** 2004. The severe acute respiratory syndrome-coronavirus replicative protein nsp9 is a single-stranded RNA-binding subunit unique in the RNA virus world. Proc. Natl. Acad. Sci. USA **101:**3792–3796.
17. **Gamarnik, A. V., and R. Andino.** 1997. Two functional complexes formed by KH domain containing proteins with the 5′ noncoding region of poliovirus RNA. RNA **3:**882–892.
18. **Goebel, S. J., B. Hsue, T. F. Dombrowski, and P. S. Masters.** 2004. Characterization of the RNA components of a putative molecular switch in the 3′ untranslated region of the murine coronavirus genome. J. Virol. **78:**669–682.
19. **Goebel, S. J., T. B. Miller, C. J. Bennett, K. A. Bernard, and P. S. Masters.** 2007. A hypervariable region within the 3′ *cis*-acting element of the murine coronavirus genome is nonessential for RNA synthesis but affects pathogenesis. J. Virol. **81:**1274–1287.
20. **Goebel, S. J., J. Taylor, and P. S. Masters.** 2004. The 3′ *cis*-acting genomic replication element of the severe acute respiratory syndrome coronavirus can function in the murine coronavirus genome. J. Virol. **78:**7846–7851.
21. **Gorbalenya, A. E., L. Enjuanes, J. Ziebuhr, and E. J. Snijder.** 2006. *Nidovirales*: evolving the largest RNA virus genome. Virus Res. **117:**17–37.
22. **Gosert, R., A. Kanjanahaluethai, D. Egger, K. Bienz, and S. C. Baker.** 2002. RNA replication of mouse hepatitis virus takes place at double-membrane vesicles. J. Virol. **76:**3697–3708.
23. **Herold, J., and R. Andino.** 2001. Poliovirus RNA replication requires genome circularization through a protein-protein bridge. Mol. Cell **7:**581–591.
24. **Hertzig, T., E. Scandella, B. Schelle, J. Ziebuhr, S. G. Siddell, B. Ludewig, and V. Thiel.** 2004. Rapid identification of coronavirus replicase inhibitors using a selectable replicon RNA. J. Gen. Virol. **85:**1717–1725.
25. **Hofmann, M. A., and D. A. Brian.** 1991. The 5′ end of coronavirus minus-strand RNAs contain a short poly(U) tract. J. Virol. **65:**6331–6333.
26. **Hsue, B., T. Hartshorne, and P. S. Masters.** 2000. Characterization of an essential RNA secondary structure in the 3′ untranslated region of the murine coronavirus genome. J. Virol. **74:**6911–6921.
27. **Hsue, B., and P. S. Masters.** 1997. A bulged stem-loop structure in the 3′ untranslated region of the genome of the coronavirus mouse hepatitis virus is essential for replication. J. Virol. **71:**7567–7578.
28. **Huang, P., and M. M. C. Lai.** 1999. Polypyrimidine tract-binding protein binds to the complementary strand of the mouse hepatitis virus 3′ untranslated region, thereby altering conformation. J. Virol. **73:**9110–9116.
29. **Huang, P., and M. M. C. Lai.** 2001. Heterogeneous nuclear ribonucleoprotein A1 binds to the 3′ untranslated region and mediates potential 5′-3′-end cross talks of mouse hepatitis virus RNA. J. Virol. **75:**5009–5017.
30. **Imbert, I., J. C. Guillemot, J. M. Bourhis, C. Bussetta, B. Coutard, M. P. Egloff, F. Ferron, A. E. Gorbalenya, and B. Canard.** 2006. A second, non-canonical RNA-dependent RNA polymerase in SARS coronavirus. EMBO J. **25:**4933–4942.
31. **Johnson, R. F., M. Feng, P. Liu, J. J. Millership, B. Yount, R. S. Baric, and J. L. Leibowitz.** 2005. Effect of mutations in the mouse hepatitis virus 3′(+)42 protein binding element on RNA replication. J. Virol. **79:**14570–14585.
32. **Joseph, J. S., K. S. Saikatendu, V. Subramanian, B. W. Neuman, A. Brooun, M. Griffith, K. Moy, M. K. Yadav, J. Velasquez, M. J. Buchmeier, R. C. Stevens, and P. Kuhn.** 2006. Crystal structure of nonstructural protein 10 from the severe acute respiratory syndrome coronavirus reveals a novel fold with two zinc-binding motifs. J. Virol. **80:**7894–7901.
33. **Kim, Y.-N., Y. S. Jeong, and S. Makino.** 1993. Analysis of *cis*-acting sequences essential for coronavirus defective interfering RNA replication. Virology **197:**53–63.
34. **Kuo, L., G.-J. Godeke, M. J. B. Raamsman, P. S. Masters, and P. J. M. Rottier.** 2000. Retargeting of coronavirus by substitution of the spike glycoprotein ectodomain: crossing the host cell species barrier. J. Virol. **74:**1393–1406.
35. **Kuo, L., and P. S. Masters.** 2003. The small envelope protein E is not essential for murine coronavirus replication. J. Virol. **77:**4597–4608.
36. **Lin, Y.-J., and M. M. C. Lai.** 1993. Deletion mapping of a mouse hepatitis virus defective interfering RNA reveals the requirement of an internal and discontiguous sequence for replication. J. Virol. **67:**6110–6118.
37. **Lin, Y.-J., C.-L. Liao, and M. M. C. Lai.** 1994. Identification of the *cis*-acting signal for minus-strand RNA synthesis of a murine coronavirus: implications for the role of minus-strand RNA in RNA replication and transcription. J. Virol. **68:**8131–8140.
38. **Liu, Q., R. F. Johnson, and J. L. Leibowitz.** 2001. Secondary structural elements within the 3′ untranslated region of mouse hepatitis virus strain JHM genomic RNA. J. Virol. **75:**12105–12113.

39. **Liu, Q., W. Yu, and J. L. Leibowitz.** 1997. A specific host cellular protein binding element near the 3′ end of mouse hepatitis virus genomic RNA. Virology **232:**74–85.
40. **Luytjes, W., H. Gerritsma, and W. J. M. Spaan.** 1996. Replication of synthetic interfering RNAs derived from coronavirus mouse hepatitis virus-A59. Virology **216:**174–183.
41. **Masters, P. S.** 2006. The molecular biology of coronaviruses. Adv. Virus Res. **66:**193–292.
42. **Masters, P. S.** 2007. Genomic *cis*-acting elements in coronavirus RNA replication, p. 63–78. *In* V. Thiel (ed.), Coronaviruses: molecular and cellular biology. Caister Academic Press, Norwich, United Kingdom.
43. **Masters, P. S., and P. J. M. Rottier.** 2005. Coronavirus reverse genetics by targeted RNA recombination. Curr. Top. Microbiol. Immunol. **287:**133–159.
44. **Mathews, D. H., J. Sabina, M. Zuker, and D. H. Turner.** 1999. Expanded sequence dependence of thermodynamic parameters improves prediction of RNA secondary structure. J. Mol. Biol. **288:**911–940.
45. **Nanda, S. K., R. F. Johnson, Q. Liu, and J. L. Leibowitz.** 2004. Mitochondrial HSP70, HSP40, and HSP60 bind to the 3′ untranslated region of the Murine hepatitis virus genome. Arch. Virol. **149:**93–111.
46. **Nanda, S. K., and J. L. Leibowitz.** 2001. Mitochondrial aconitase binds to the 3′ untranslated region of the mouse hepatitis virus genome. J. Virol. **75:** 3352–3362.
47. **Parker, M. M., and P. S. Masters.** 1990. Sequence comparison of the N genes of five strains of the coronavirus mouse hepatitis virus suggests a three domain structure for the nucleocapsid protein. Virology **179:**463–468.
48. **Peti, W., M. A. Johnson, T. Herrmann, B. W. Neuman, M. J. Buchmeier, M. Nelson, J. Joseph, R. Page, R. C. Stevens, P. Kuhn, and K. Wuthrich.** 2005. Structural genomics of the severe acute respiratory syndrome coronavirus: nuclear magnetic resonance structure of the protein nsP7. J. Virol. **79:**12905–12913.
49. **Sawicki, S. G., D. L. Sawicki, and S. G. Siddell.** 2007. A contemporary view of coronavirus transcription. J. Virol. **81:**20–29.
50. **Sawicki, S. G., D. L. Sawicki, D. Younker, Y. Meyer, V. Thiel, H. Stokes, and S. G. Siddell.** 2005. Functional and genetic analysis of coronavirus replicase-transcriptase proteins. PLoS Pathog. **1:**e39.
51. **Schaad, M. C., and R. S. Baric.** 1994. Genetics of mouse hepatitis virus transcription: evidence that subgenomic negative strands are functional templates. J. Virol. **68:**8169–8179.
52. **Schiller, J. J., A. Kanjanahaluethai, and S. C. Baker.** 1998. Processing of the coronavirus MHV-JHM polymerase polyprotein: identification of precursors and proteolytic products spanning 400 kilodaltons of ORF1a. Virology **242:** 288–302.
53. **Sims, A. C., J. Ostermann, and M. R. Denison.** 2000. Mouse hepatitis virus replicase proteins associate with two distinct populations of intracellular membranes. J. Virol. **74:**5647–5654.
54. **Spagnolo, J. F., and B. G. Hogue.** 2000. Host protein interactions with the 3′ end of bovine coronavirus RNA and the requirement of the poly(A) tail for coronavirus defective genome replication. J. Virol. **74:**5053–5065.
55. **Su, D., Z. Lou, F. Sun, Y. Zhai, H. Yang, R. Zhang, A. Joachimiak, X. C. Zhang, M. Bartlam, and Z. Rao.** 2006. Dodecamer structure of severe acute respiratory syndrome coronavirus nonstructural protein nsp10. J. Virol. **80:** 7902–7908.
56. **Sutton, G., E. Fry, L. Carter, S. Sainsbury, T. Walter, J. Nettleship, N. Berrow, R. Owens, R. Gilbert, A. Davidson, S. Siddell, L. L. Poon, J. Diprose, D. Alderton, M. Walsh, J. M. Grimes, and D. I. Stuart.** 2004. The nsp9 replicase protein of SARS-coronavirus, structure and functional insights. Structure **12:**341–353.
57. **Teterina, N. L., D. Egger, K. Bienz, D. M. Brown, B. L. Semler, and E. Ehrenfeld.** 2001. Requirements for assembly of poliovirus replication complexes and negative-strand RNA synthesis. J. Virol. **75:**3841–3850.
58. **Thiel, V., and S. G. Siddell.** 2005. Reverse genetics of coronaviruses using vaccinia virus vectors. Curr. Top. Microbiol. Immunol. **287:**199–227.
59. **Verheije, M. H., R. C. Olsthoorn, M. V. Kroese, P. J. M. Rottier, and J. J. Meulenberg.** 2002. Kissing interaction between 3′ noncoding and coding sequences is essential for porcine arterivirus RNA replication. J. Virol. **76:**1521–1526.
60. **Williams, G. D., R. Y. Chang, and D. A. Brian.** 1999. A phylogenetically conserved hairpin-type 3′ untranslated region pseudoknot functions in coronavirus RNA replication. J. Virol. **73:**8349–8355.
61. **Woo, P. C. Y., S. K. P. Lau, C.-M. Chu, K.-H. Chan, H.-W. Tsoi, Y. Huang, B. H. L. Wong, R. W. S. Poon, J. J. Cai, W.-K. Luk, L. L. M. Poon, S. S. Y. Wong, Y. Guan, J. S. M. Peiris, and K.-Y. Yuen.** 2005. Characterization and complete genome sequence of a novel coronavirus, coronavirus HKU1, from patients with pneumonia. J. Virol. **79:**884–895.
62. **Woo, P. C. Y., M. Wang, S. K. P. Lau, H. Xu, R. W. S. Poon, R. Guo, B. H. L. Wong, K. Gao, H.-W. Tsoi, Y. Huang, K. S. M. Li, C. S. F. Lam, K.-H. Chan, B.-J. Zheng, and K.-Y. Yuen.** 2007. Comparative analysis of twelve genomes of three novel group 2c and group 2d coronaviruses reveals unique group and subgroup features. J. Virol. **81:**1574–1585.
63. **Wu, H.-Y., J. S. Guy, D. Yoo, R. Vlasak, E. Urbach, and D. A. Brian.** 2003. Common RNA replication signals exist among group 2 coronaviruses: evidence for in vivo recombination between animal and human coronavirus molecules. Virology **315:**174–183.
64. **Yu, W., and J. L. Leibowitz.** 1995. Specific binding of host cellular proteins to multiple sites within the 3′ end of mouse hepatitis virus genomic RNA. J. Virol. **69:**2016–2023.
65. **Yu, W., and J. L. Leibowitz.** 1995. A conserved motif at the 3′ end of mouse hepatitis virus genomic RNA required for host protein binding and viral RNA replication. Virology **214:**128–138.
66. **Zhai, Y., F. Sun, X. Li, H. Pang, X. Xu, M. Bartlam, and Z. Rao.** 2005. Insights into SARS-CoV transcription and replication from the structure of the nsp7-nsp8 hexadecamer. Nat. Struct. Mol. Biol. **12:**980–986.
67. **Ziebuhr, J.** 2005. The coronavirus replicase. Curr. Top. Microbiol. Immunol. **287:**57–94.
68. **Zuker, M.** 2003. Mfold web server for nucleic acid folding and hybridization prediction. Nucleic Acids Res. **31:**3406–3415.
69. **Zuniga, S., I. Sola, S. Alonso, and L. Enjuanes.** 2004. Sequence motifs involved in the regulation of discontinuous coronavirus subgenomic RNA synthesis. J. Virol. **78:**980–994.

6 Original Research Articles

“Control of coronavirus infection through plasmacytoid dendritic-cell-derived type I interferon”

Luisa Cervantes-Barragan, Roland Züst, Friedemann Weber, Martin Spiegel, Karl Lang, Shizuo Akira, Volker Thiel, and Burkhard Ludewig

Own contribution to this article: Expression of IFN-β, IP-10, IFN-α4, IFN-α after infection with MHV is substantially different in bone marrow-derived cDCs as compared to pDCS. Performed by RT-PCR using total RNA.

Control of coronavirus infection through plasmacytoid dendritic-cell–derived type I interferon

Luisa Cervantes-Barragan,[1,2] Roland Züst,[1] Friedemann Weber,[3] Martin Spiegel,[3] Karl S. Lang,[4] Shizuo Akira,[5] Volker Thiel,[1] and Burkhard Ludewig[1]

[1]Research Department, Kantonal Hospital St Gallen, St Gallen, Switzerland; [2]Unidad de Investigación Médica en Inmunoquímica, Hospital de Especialidades, Mexico City, Mexico; [3]Abteilung Virologie, Institut fur Medizinische Mikrobiologie und Hygiene, Universitat Freiburg, Freiburg, Germany; [4]Institute of Experimental Immunology, University Hospital, Zurich, Switzerland; [5]Department of Host Defense, Osaka University, Osaka, Japan

This study demonstrates a unique and crucial role of plasmacytoid dendritic cells (pDCs) and pDC-derived type I interferons (IFNs) in the pathogenesis of mouse coronavirus infection. pDCs controlled the fast replicating mouse hepatitis virus (MHV) through the immediate production of type I IFNs. Recognition of MHV by pDCs was mediated via TLR7 ensuring a swift IFN-α production following encounter with this cytopathic RNA virus. Furthermore, the particular type I IFN response pattern was not restricted to the murine coronavirus, but was also found in infection with the highly cytopathic human severe acute respiratory syndrome (SARS) coronavirus. Taken together, our results suggest that rapid production of type I IFNs by pDCs is essential for the control of potentially lethal coronavirus infections. (Blood. 2007;109:1131-1137)

Introduction

Type I IFNs (IFNα/β) play a decisive role in shaping antiviral immune responses.[1] Signaling through the type I IFN receptor leads to the activation of a particular set of genes, including protein kinase R, and Mx proteins,[2] which exert potent direct antiviral effects. Other type I IFN–stimulated gene products, such as IFN-γ, activate downstream elements of the innate immune system that further promote rapid clearance of the viral pathogen.[3] Although almost all hematopoietic and nonhematopoietic cells are able to produce IFN-α/β after viral infections, plasmacytoid dendritic cells (pDCs) are the major source of IFN-α, both in humans and mice.[4-7] One key feature of pDCs is the expression of receptors for single-stranded RNA or DNA such as Toll-like receptor 7 (TLR7)[8,9] and TLR9,[10,11] respectively, which are essential to sense the viral pathogen and to trigger the innate immune response. In mouse cytomegalovirus (MCMV) infection, pDCs respond quickly and generate the first wave of IFN-α.[12,13] These previous studies have clearly established an important role of pDCs for the rapid production of type I IFNs in antiviral immune responses.

Coronaviruses are positive-stranded RNA viruses that are able to infect a broad range of vertebrates and are associated mainly with respiratory, enteric, and, sometimes, systemic diseases.[14] Human coronaviruses are known to generally cause mild upper-respiratory tract disease, including common cold, and occasional enteric infections. The emergence of a novel coronavirus (COV) causing severe acute respiratory syndrome (SARS) highlighted the potential of coronaviruses to seriously impact on human health.[14] Phylogenetic analyses revealed a close relationship of SARS-CoV to group II coronaviruses,[15] which is prototyped by the mouse hepatitis virus (MHV). MHV causes enteritis, pneumonia, hepatitis, and demyelinating encephalomyelitis in mice and is one of the most extensively studied coronaviruses in vitro and in vivo.[16] Both SARS-CoV and MHV have a similar genome organization and share common mechanisms and enzymes involved in genome expression.[15,17] Because of these similarities, it is conceivable that the pathogenesis of and the immune response against systemic MHV infection in mice recapitulates some of the essential features of SARS-CoV infection.

The immune response against MHV is characterized by a strong cytotoxic T-cell (CTL) response that mediates initial clearance of the virus,[18,19] whereas neutralizing antibodies appear to be required to prevent re-emergence of the persistent infection.[20,21] In contrast to the well-characterized defense mechanisms of the adaptive immune response against MHV, the innate immune response has not been sufficiently characterized. Similarly, the importance of innate immune mechanisms triggered by SARS-CoV has remained enigmatic. Several studies have shown that peripheral-blood mononuclear cells (PBMCs) from SARS-CoV–infected individuals produce high amounts of inflammatory cytokines and chemokines, but not type I IFNs.[22-24] Furthermore, in vitro studies have shown that neither macrophages nor monocyte-derived DCs respond to SARS-CoV infection with significant IFN-α production.[25-28] Nonetheless, there is clear evidence that treatment with recombinant IFN-β or IFN-α can inhibit SARS-CoV replication in vitro,[29-31] and, most importantly, diminish the severity of SARS-CoV infection in vivo.[32,33] Thus, although the antiviral activity of type I IFNs in SARS-CoV infections has been clearly demonstrated, it remains to be established whether a significant production of type I IFNs can be achieved upon coronavirus infection and how this may impact on virus replication and disease. The present study addressed this issue and identified pDCs as the major source of type I IFNs during cytopathic coronaviral replication. We show furthermore that pDCs are crucial during the initial phase of MHV

Submitted May 17, 2006; accepted September 5, 2006. Prepublished online as *Blood* First Edition Paper, September 19, 2006; DOI 10.1182/blood-2006-05-023770.

The publication costs of this article were defrayed in part by page charge payment. Therefore, and solely to indicate this fact, this article is hereby marked "advertisement" in accordance with 18 USC section 1734.

infection since widespread replication in various nonlymphoid organs, and the associated organ damage, is efficiently kept in check through pDC-derived type I IFNs.

Materials and methods

Mice and viruses

C57BL/6 (B6) mice were obtained from Charles River Laboratories (Sulzfeld, Germany). TLR3$^{-/-}$,[34] TLR7$^{-/-}$,[35] TLR3$^{-/-}$/TLR7$^{-/-}$, and MyD88$^{-/-}$[36] mice were bred in the Institut für Labortierkunde (University of Zurich, Switzerland). 129Sv and type I IFN receptor–deficient (IFNAR$^{-/-}$) mice[37] were obtained from the Institut für Labortierkunde (University of Zurich) and bred in our facilities. All mice were maintained in individually ventilated cages and were used between 6 and 9 weeks of age. All animal experiments were performed in accordance with the Swiss federal legislation on animal protection.

MHV A59 was generated from a molecularly cloned cDNA[38] based on the Albany strain of MHV A59 and propagated on L929 cells. SARS-CoV (isolate Frankfurt-1) was kindly provided by Stephan Becker (University of Marburg, Germany) and propagated on Vero cells. The Newcastle disease virus (NDV; strain H53) stock was grown on 10-day-old embryonated chicken eggs.

Isolation of dendritic cells and flow cytometry

Murine conventional DCs (cDCs) and pDCs were obtained from spleens of 129Sv or IFNAR$^{-/-}$ mice following digestion with collagenase type II (Invitrogen, Basel, Switzerland) for 20 minutes at 37°C. Cells were resuspended in PBS supplemented with 2% FCS and 2 mM EDTA and overlaid on 20% Optiprep density gradient medium (Sigma-Aldrich, Basel, Switzerland). After centrifugation at 700*g* for 15 minutes, low-density cells were depleted of CD3$^+$ and CD19$^+$ cells using DYNAL magnetic beads according to the instructions of the manufacturer (Invitrogen). The DC-enriched preparations were stained with α–PDCA-1, α-CD11b, and α-CD11c, and the distinct pDC and cDC populations were sorted using a fluorescence-activated cell sorter (FACS) ARIA (BD Biosciences, Allschwil, Switzerland). Purity of both cell preparations was always more than 98%.

Murine bone marrow–derived cDCs or pDCs were generated by 6 to 7 days of culture with either granulocyte-monocyte colony-stimulating factor (GM-CSF)–containing supernatant from the cell line X63-GM-CSF (kindly provided by Dr Antonius Rolink, University of Basel) or Flt3-L (R&D systems, Oxford, United Kingdom) at 20 ng/mL, respectively. Bone marrow–derived cDCs were further purified using Optiprep density gradient centrifugation. Bone marrow–derived pDCs were purified using the mouse pDC isolation kit (Miltenyi Biotec, Bergisch Gladbach, Germany) adapted for the isolation of in vitro–derived pDCs by adding CD11b-biotin to the negative selection cocktail.

Human circulating conventional dendritic cells and plasmacytoid dendritic cells were isolated from healthy donors (obtained from the Blood Bank of the University Hospital Freiburg, Germany). PBMCs were obtained by Ficoll-Hypaque density gradient centrifugation. Human pDCs or cDCs were further purified by magnetic sorting with human plasmacytoid dendritic-cell isolation kit (Miltenyi Biotec) or human BDCA-1 dendritic-cell isolation kit (Miltenyi Biotec), respectively. Purity of both cell preparation was for all donors more than 90% (with B cells being the major contaminating cell type).

Cells were analyzed with a FACSCalibur flow cytometer using CellQuest software (BD Biosciences). The antibodies CD123 biotin, CD11c PE, B220 APC, and CD11b FITC were purchased from Biolegend (San Diego, CA); and CD303 (BDCA-2)–PE, mPDCA-1-FITC, mPDCA-1-PE, and CD11c-APC, from Miltenyi Biotec.

Virus infections, determination of virus titers, and liver enzyme values

Human pDCs and cDCs were exposed to SARS-CoV or NDV for 1 hour at 37°C, washed, and plated at 1.5×10^5/mL. Murine pDCs or cDCs were infected with MHV A59 for 1 hour at 37°C, washed, and plated at 1 to 2×10^5/mL. CpG ODN 2216 was used as a positive control for IFN-α production as described previously.[39]

Mice were injected intraperitoneally with 5 pfu MHV A59 and killed at the indicated time points. For depletion of pDCs, mice were injected intraperitoneally with 0.5 mg α–mPDCA-1 (Miltenyi Biotec) or 0.5 mg rat IgG2b isotype control antibody (Biolegend) 12 hours prior to infection. Organs were stored at −70°C until further analysis. Blood was incubated at room temperature to coagulate and was then centrifuged, and serum was used for alanine 2-oxoglutarate-aminotransferase (ALT) measurements using a Hitachi 747 autoanalyzer (Tokyo, Japan). Virus titers in organs were determined from frozen organs after weighing and homogenization. Viral titers were determined by standard plaque assay using L929 cells.

Histology, IFN-α ELISA, and reverse-transcription–polymerase chain reaction (RT-PCR)

Organs were fixed in 4% formalin and embedded in paraffin. Sections were stained with hematoxylin and eosin. Human IFN-α and mouse IFN-α concentration in cell-culture supernatants or serum was measured by enzyme-linked immunosorbent assay (ELISA; PBL Biomedical Laboratories, Piscataway, NJ) according to the manufacturer's instructions. To detect cellular and viral mRNAs in pDCs and cDCs, total cellular RNA was prepared using the RNeasy Kit for murine DCs (Qiagen, Basel, Switzerland) or Trifast (PEQLAB, Erlangen, Germany) for human DCs. Reverse transcription was done with 100 ng total RNA using the SuperScript II First-Strand Synthesis System (Invitrogen). PCR was performed with Red Taq Polymerase (Sigma-Aldrich) using standard protocols. The following primers were used for amplification: *mIFN-β* forward, 5′-CATCAACTATAAGCAGCTCCA-3′; *mIFN-β* reverse, 5′TTCAAGTGGAGAGCAGTTGAG3′; *mIFN-α4* forward, 5′CTGGTCAGCCTGTTCTCTAGGATGT3′; *mIFN-α4* reverse, 5′TCAGAGGAGGTTCCTGCATCAC3′; *mIFN-α total* forward, 5′ATGGCTAGRCTC TGTGCTTTCCT3′; *mIFN-α total* reverse, 5′AGGGCTCTCCAGAYTTCTGCTCTG3′; *mGAPDH* forward, 5′CATCAAGAAGGTGGTGAAGC3′; *mGAPDH* reverse, 5′CCTGTTGCTGTAGCCGTATT3′; *MHV-N* forward, 5′TCCTGGTTTTCTGGCATTACCCAG3′; and *MHV-N* reverse, 5′CTGAGGCAATACCGTGCCGGGCGC3′. Primer sequences for amplifying human IFN-β were 5′CATACCCACGGAGAAAGGACATT3′ and 5′TGATAGACATTAGCCAGGAGGTTC3′; for ISG56, 5′AAGTGGACCCTGAAAACCCTGAAT3′ and 5′TGCCCTTTTGTAGCCTCCTTGAT3′; for MxA, 5′GTTGTTTCCGAAGTGGACATCGCAAAA3′ and 5′CGGGCATCTGGTCACGAT3′; and for γ-actin, 5′GCCGGTCGCAATGGAAGAAGA3′ and 5′CATGGCCGGGGTGTTGAAGGTC3′. SARS-CoV transcription was detected by using primer 5′TGTCTAGCAGCAATAGCGCGAGGGC3′ for reverse transcription and primers 5′GGAAAAGCCAACCAACCTCGATCTCT3′ and 5′AAGTTGTAGCACGGTGGCAGC3′ for PCR.

Results

Rapid type I IFN production in pDCs following MHV infection

In a first set of experiments, the type I IFN response of pDCs and cDCs following encounter with MHV was determined. To this end, CD11c^{low}B220$^+$PDCA-1$^+$ pDCs and CD11c$^+$B220$^-$ cDCs were sorted from spleen-cell suspensions (Figure 1A-B) and infected with MHV. Primary pDCs but not cDCs responded with rapid and significant production of IFN-α (Figure 1C). The high IFN-α production in pDCs correlated well with the control of the virus infection (Figure 1D). Bone marrow–derived pDCs and cDCs that were differentiated with the growth factors Flt-3L or GM-CSF, respectively, responded in a similar pattern: rapid and high production of IFN-α in pDCs but not in cDCs (Figure 2A-B) and a good containment of the viral replication by pDCs (Figure 2C-D). A time-course RT-PCR analysis confirmed that the type I IFN response is considerably slower in cDCs (Figure 2E) compared

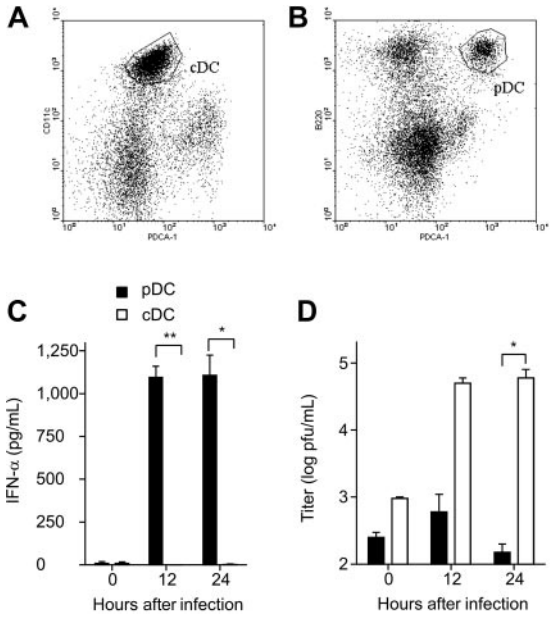

Figure 1. Type I IFN production and viral replication in MHV-infected splenic cDCs and pDCs. (A) Flow cytometric analysis of splenic cDCs ($CD11c^+PDCA\text{-}1^-$) and (B) splenic pDCs $CD11c^{low}$ $B220^+$ $PDCA\text{-}1^-$ before FACS sorting. Gates for sorting are indicated. (C) Primary FACS-purified murine splenic cDCs or pDCs were infected with MHV at a multiplicity of infection (moi) of 1. IFN-α secretion to culture supernatants was determined by ELISA at the indicated time points. (D) Virus titers in culture supernatants were determined by plaque assay. (C-D) Data represent mean values ± SD pooled from 2 experiments. Statistical analysis was performed using Student *t* test (*$P < .05$; **$P < .01$).

with pDCs (Figure 2F). Furthermore, pDCs lacking the type I IFN receptor were more susceptible to MHV infection than wild-type pDCs (Figure 2G-H). It appears therefore that pDCs are well equipped to respond efficiently against MHV with a strong type I IFN production, and that this early reaction exerts a potent protective effect against this cytopathic virus.

Type I IFN signaling is essential for the control of MHV infection

Signaling through the type I IFN receptor (IFNAR) is essential for the control of several viral infections.[40] To assess the importance of type I IFN signaling in the course of an MHV infection, IFNAR-deficient ($IFNAR^{-/-}$) and 129Sv wild-type (wt) mice were infected with 5 pfu MHV. MHV infection in $IFNAR^{-/-}$ mice was lethal within only 48 hours, while wt mice survived without showing signs of MHV infection–associated clinical disease (Figure 3A). Furthermore, $IFNAR^{-/-}$ but not wt mice showed rapidly rising liver enzyme values in serum (Figure 3B) and an acute hemorrhagic liver disease with massive hepatocyte necrosis (Figure 3C). The detailed time-course analysis of viral spread in both $IFNAR^{-/-}$ and wt mice indicated that a functional type I IFN system is essential to restrict the initial viral replication to the spleen and to prevent spread to nonhematopoietic organs such as the lung and the central nervous system (Figure 3D). Notably, the replication of the strongly hepatotropic MHV in the liver was efficiently reduced in the presence of a functional type I IFN system with a reduction of viral titers of 3 to 4 orders of magnitude (Figure 3D). It is thus most likely that the rapidly lethal disease in $IFNAR^{-/-}$ mice following MHV infection is a consequence of an insufficient initial control of the cytopathic virus in the spleen and the subsequent high-level replication in various organs, eventually causing an acute multiorgan failure.

Early control of MHV infection through pDC-derived type I IFN

The above results suggested that the initial control of MHV requires an efficient type I IFN response that might be generated by pDCs. It has been shown that pDCs use the TLR pathway rather than the RNA helicase RIG-I for recognition of RNA viruses and to produce type I IFN.[41] Therefore, to investigate how pDCs recognize MHV, bone marrow–derived pDCs from TLR3-deficient ($TLR3^{-/-}$), TLR3 and TLR7 double knock-out ($TLR3^{-/-}$/$TLR7^{-/-}$), TLR7-deficient ($TLR7^{-/-}$), and MyD88-deficient ($MyD88^{-/-}$) mice were infected with a low dose of MHV (moi = 1), and the production of IFN-α was determined after 24

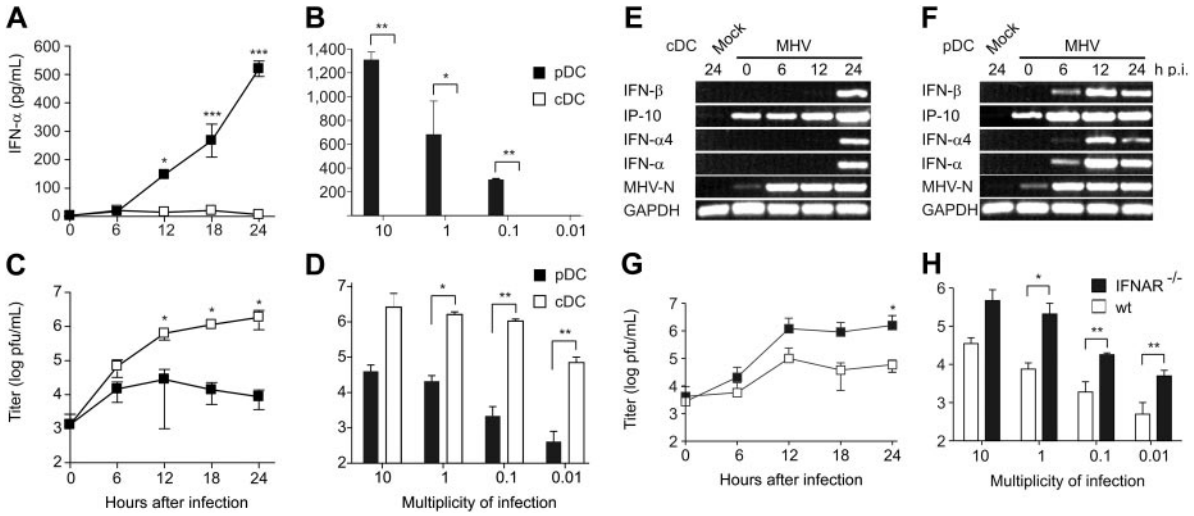

Figure 2. Type I IFN production and viral replication in MHV-infected in vitro–derived cDCs and pDCs. Infection of bone marrow–derived pDCs and cDCs with MHV. (A,C) IFN-α and virus titers in tissue culture supernatants were determined at the indicated times after MHV infection (moi = 1), or (B,D) at 24 hours after MHV infection with different moi as indicated. Values in panels A-D represent means ± SD from triplicate measurements. Experiments in panels A-D were repeated 3 times with comparable results. Expression of IFN-β, IP-10, IFN-α4, IFN-α , GAPDH, or MHV nucleoprotein (MHV-N) mRNAs was determined by RT-PCR using total RNA from bone marrow–derived (E) cDCs or (F) pDCs infected with MHV (moi = 1) or treated with PBS (mock). (G-H) Viral replication in MHV-infected wt or $IFNAR^{-/-}$ pDCs. Cells were infected with MHV A59 at (G) an moi of 1 or (H) at different moi as indicated. Virus titers in culture supernatants were determined by plaque assay at (G) the indicated times after MHV A59 infection (moi = 1) or (H) 24 hours after MHV infection. (A-D,G-H) Data represent mean values ± SD pooled from 2 experiments. Statistical analysis was performed using Student *t* test (*$P < .05$; **$P < .01$, ***$P < .001$).

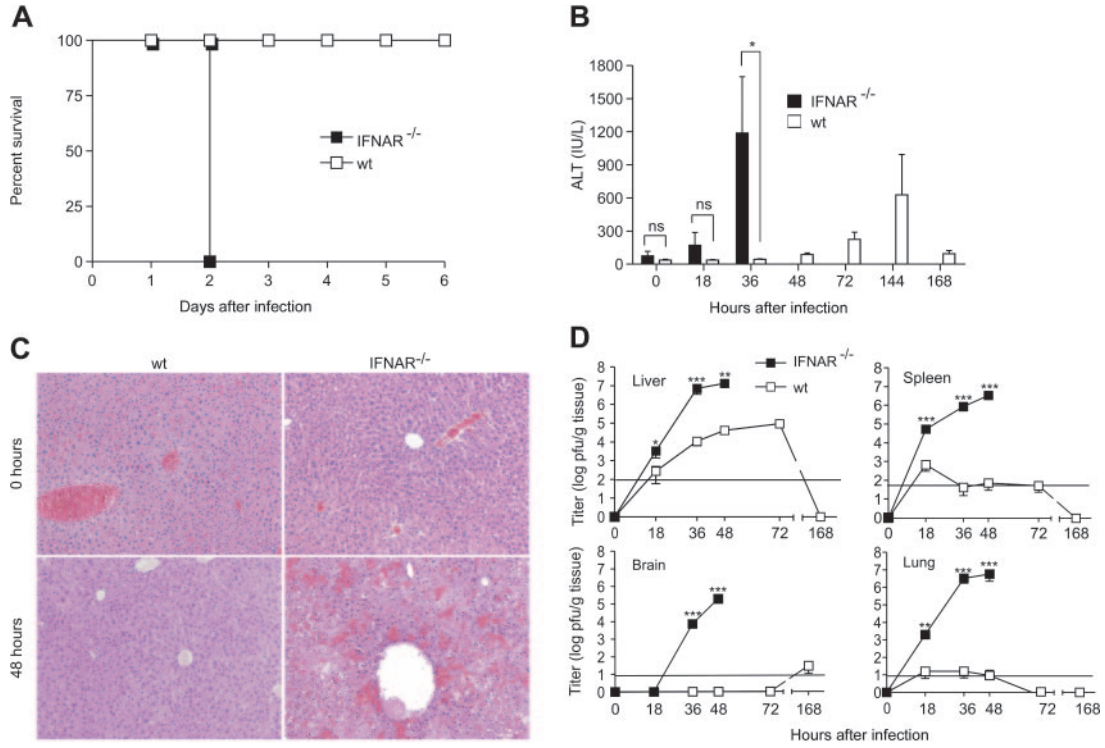

Figure 3. Impact of type I IFN signaling during MHV infection. IFNAR$^{-/-}$ or wt mice were injected intraperitoneally with 5 pfu MHV A59. (A) Health status of IFNAR$^{-/-}$ and wt mice was monitored twice daily after infection (n = 6). (B) ALT values were measured at the indicated time points after infection. (C) Liver pathology in IFNAR$^{-/-}$ and wt mice before or 48 hours after MHV A59 infection. Hematoxylin-eosin staining of 4% formaldehyde-fixed sections. Images were acquired using a Leica DMRA microscope (Leica, Heerbrugg, Switzerland) with a 25×/0.65 NA objective (total magnification, ×162). Images were processed using Adobe Photoshop (Adobe Systems, San Jose, CA). (D) Viral titers in liver, spleen, brain, and lung of MHV A59–infected IFNAR$^{-/-}$ or wt mice were determined at different time points after infection. Results represent the mean of 6 individual mice per time point. Solid horizontal lines in panel D represent limit of detection in the plaque assay. Data in panels B and D represent means ± SD from 2 experiments with a total of 3 or 6 mice evaluated per time point. Statistical analysis was performed using Student *t* test (ns, $P > .05$; $^{*}P < .05$; $^{**}P < .01$; $^{***}P < .001$).

hours. Comparable amounts of IFN-α were found in the supernatants of TLR3$^{-/-}$ and wt control pDC cultures (Figure 4). In contrast, pDCs from neither TLR7$^{-/-}$, TLR3$^{-/-}$/TLR7$^{-/-}$, nor MyD88$^{-/-}$ mice responded with a significant IFN-α production to MHV infection (Figure 4), clearly indicating that MHV recognition by pDCs is triggered exclusively via the TLR7/MyD88 pathway.

To assess the importance of pDC-derived IFN-α during MHV infection in vivo, pDCs were ablated by the depleting antibody PDCA-1. As described for MCMV by Krug et al,[11] pDC depletion was accompanied by severely diminished IFN-α levels in serum following MHV infection (Figure 5A). The treatment with PDCA-1 resulted in an 80% depletion of splenic pDCs for roughly 48 hours (not shown). Although profound effects on viral titers could be observed (Figure 5B), transient pDC depletion did not lead to lethality following low-dose MHV infection. Nevertheless, initial viral titers in spleens were more than 1000-fold increased in pDC-depleted compared with isotype control antibody–treated mice, and virus was found in other organs such as lung or brain (Figure 5B). To exclude complement-mediated global changes in the status of the immune system, we evaluated the effect of natural killer (NK) cell depletion via anti–asialo GM1. Depletion of NK cells altered neither initial viral replication and distribution nor IFN-α levels in serum (not shown). Finally, ALT values in PDCA-1–depleted mice were elevated compared with control animals (Figure 5C), indicating significant liver damage. These data clearly show that pDCs are important for the early control of MHV infection and that the lack of pDCs not only leads to uncontrolled viral replication and spread to different organs but also impacts on the severity of viral disease.

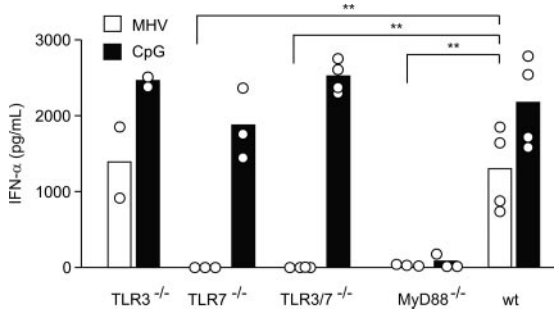

Figure 4. pDCs sense MHV via TLR7. Bone marrow–derived pDCs from TLR3$^{-/-}$, TLR7$^{-/-}$, TLR3$^{-/-}$/TLR7$^{-/-}$, MyD88$^{-/-}$, or wt mice were infected with MHV A59 (moi = 1) or treated with CpG oligonucleotides. IFN-α in tissue culture supernatants was determined 24 hours after infection by ELISA. Bars represent means with values from individual mice shown as open circles. Statistical analysis was performed using Student *t* test ($^{**}P < .01$).

Rapid induction of type I IFNs in pDCs following SARS-CoV infection

In order to relate the above findings to a pathogenic and potentially lethal human coronavirus infection, the ability of pDCs to produce IFN-α following encounter with SARS-CoV was assessed. Primary pDCs and cDCs were isolated from peripheral blood of healthy donors and infected with SARS-CoV. As described for monocyte-derived cDCs,[28] primary cDCs from healthy donors were also not able to produce significant amounts of IFN-α (Figure 6A) and did not up-regulate transcripts of IFN-β and IFN-stimulated genes such as ISG56 and MxA, located downstream in the type I IFN signaling pathway

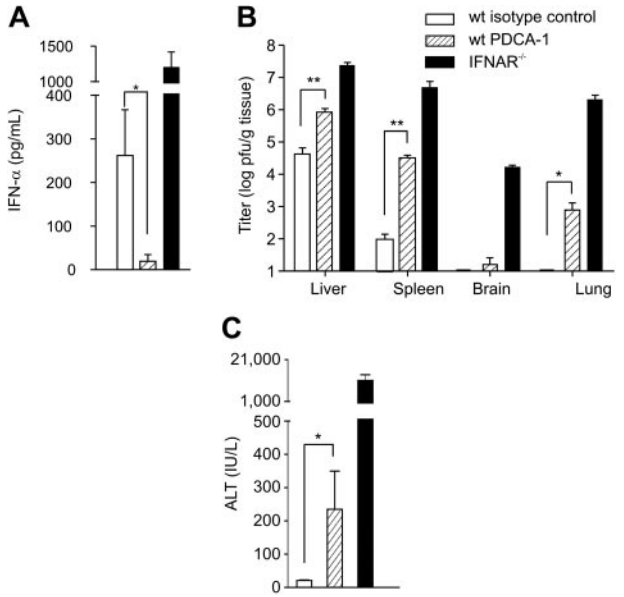

Figure 5. Effect of antibody-mediated pDC depletion on MHV infection. 129Sv mice were treated with rat IgG2b (wt isotype control) or α–mPDCA-1 (wt PDCA-1) and infected intraperitoneally with 5 pfu MHV A59 (n = 6). IFNAR$^{-/-}$ mice (n = 3) were used to demonstrate uncontrolled MHV spread in the absence of a functional IFN system. (A) IFN-α concentration in serum (means ± SD), (B) viral titers (means ± SD) in liver, spleen, brain, and lung, and (C) serum ALT values (means ± SD) were assessed at 48 hours after infection. (A-C) Statistical analysis was performed using Student *t* test (*$P < .05$; **$P < .01$).

(Figure 6B). In contrast and as expected from the MHV experiments, pDCs were able to produce IFN-α early after SARS-CoV infection (Figure 6A). Furthermore, IFN-β, MxA, or ISG56 mRNA expression was found in infected pDCs (Figure 6C). Based on this evidence and the unsuccessful efforts from previous studies to determine a cell type that produces IFN-α in response to SARS-CoV,[25-28] we conclude that pDCs are most likely the major source of type I IFNs in SARS-CoV infection.

Discussion

In this study, we demonstrate a unique and essential function for type I IFN–producing pDCs: protection against the rapidly replicating and cytopathic murine coronavirus. Furthermore, we have identified pDCs as the source of type I IFN in response to human SARS-CoV, suggesting an important biologic role of pDC-derived type I IFNs for highly pathogenic coronavirus infections in humans.

The expression of TLRs that recognize viral products such as CpG oligonucleotides[10,11] or ssRNA[9] has indicated that pDCs represent a highly specialized cell type that provides an early response against a particular set of infectious agents. A further characteristic of pDCs is the constitutively high expression of IFN regulatory factor-7 (IRF-7),[42,43] which directly stimulates IFN-α expression, independently of an IFN-β–mediated feedback loop.[44] In MHV infection, this efficient direct IFN-α induction appears to be not only essential for the regulation of the magnitude of the type I IFN response, but also important to restrict replication of this cytopathic virus within pDCs. Furthermore, pDC-derived type I IFNs provide an efficient "bystander" protection because the initial replication of MHV in lymphoid organs such as the spleen was diminished in the presence of pDCs. Notably, in MHV infection this function of pDCs cannot be substituted by other cells as demonstrated, for example, in MCMV infection.[11,13] It is possible that viruses that replicate rather slowly, such as MCMV, cannot reveal the full importance of pDCs in the control of cytopathic viruses that require a swift type I IFN response.

Within secondary lymphoid organs, macrophages are the major target cell of MHV,[14] and recent studies indicate that cDCs can also be readily infected with MHV A59[45] or MHV JHM.[46] It is important to note that the uncontrolled infection of cDCs by MHV is detrimental for the initiation of the adaptive antiviral immune response.[46] The rapid control of MHV through pDC-derived type I IFN in secondary lymphoid organs ensures therefore the subsequent induction of adaptive immune responses. Likewise, a recent study by Smit et al[47] indicates that pDCs not only help to minimize respiratory syncytial virus infection–associated immunopathologic damage, but also facilitate establishment of antiviral T-cell responses in the lung.

Fatal SARS-CoV infection–associated clinical disease is characterized by respiratory insufficiency and, eventually, respiratory failure. One of the reasons for this outcome may be the down-regulation of angiotensin-converting enzyme 2 by the viral spike protein leading to an exacerbation of the pulmonary damage.[48] Furthermore, it is well-documented that SARS-CoV infects macrophages and lymphocytes leading to a pronounced atrophy of lymphoid organs in those patients who succumbed to the infection.[49] Extrapolating from the data obtained in the MHV model, it is likely that these patients may have suffered from an insufficient early control of the virus within lymphoid organs that eventually led to the unrestrained replication in the respiratory tract. Because SARS-CoV is sensitive to type I IFNs both in vitro[30,31,50] and in vivo,[32,33] an early control of SARS-CoV by type I IFNs might have been a decisive advantage for those patients who have survived the

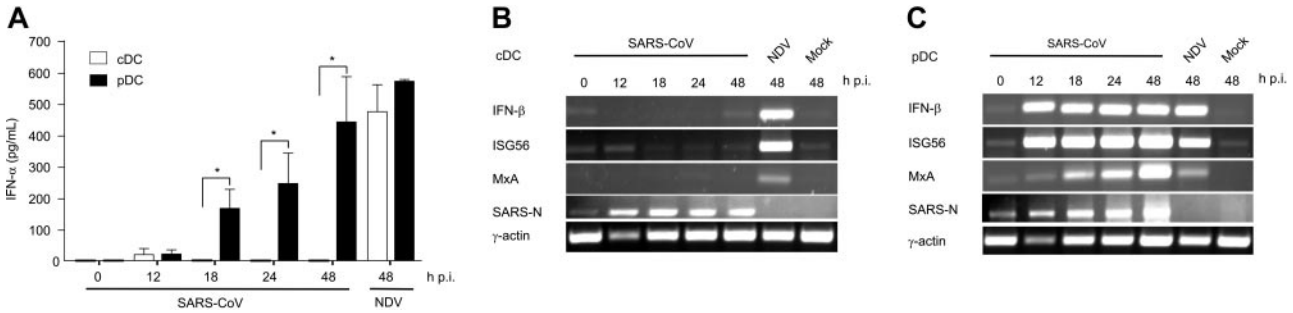

Figure 6. Infection of human pDCs and cDCs with SARS-CoV. Primary pDCs or cDCs were isolated from peripheral blood of healthy donors and infected with either SARS-CoV (moi = 1) or Newcastle disease virus (NDV) as positive control (moi = 5), or were left uninfected (mock). (A) IFN-α in culture supernatants was determined at the indicated time points. Results represent pooled data (means ± SD) using pDCs and cDCs from 4 healthy donors. Statistical analysis was performed using Student *t* test (*$P < .05$). (B-C) Expression of IFN-β, ISG56, MxA, SARS-CoV N protein, and γ-actin mRNAs in (B) cDCs and (C) pDCs was determined by RT-PCR. One representative result of 4 individual experiments is shown.

infection. It is noteworthy that neither macrophages, cDCs, fibroblasts, nor lung epithelial cells[28] are able to mount a significant type I IFN response against SARS-CoV. The lack of a significant type I IFN response in PBMCs of SARS-CoV–infected patients[23] might be due to a partial inhibition of type I IFN signaling not only in nonlymphoid cells,[51,52] but also in pDCs. Therefore, the potential of the various SARS-CoV nonstructural proteins that might inhibit and/or modulate type I IFN responses in pDCs and other important target cells should be addressed in future studies.

Taken together, the results of this study provide insight into the immunopathogenesis of coronavirus-associated diseases by demonstrating an exclusive role of pDC-derived type I IFNs for initial viral control. Triggering of this pathway, for example via specific TLR agonists, might open new avenues for the treatment of coronavirus infections. Indeed, stimulation of TLR3 at the vaginal mucosa can protect mice against herpes simplex virus-2 challenge via the mucosal route.[53] In a clinical setting, systemic administration of a TLR7 agonist elicited potent antiviral effects against hepatitis C virus with significant reduction of plasma viremia.[54] Our data provide the rationale that such a treatment approach might help to reduce initial viral load and eventually favor a mild course of SARS.

Acknowledgments

The authors thank Drs Elke Scandella, Philippe Krebs, and Reinhard Maier for critical reading of the paper. We thank Simone Miller, Beat Ryf, and Valentina Wagner for excellent technical assistance.

This work was supported by the Gebert-Rüf-Stiftung, the UBS Optimus Stiftung, the Swiss National Science Foundation, the European Commission (SARS-DTV), the Deutsche Forschungsgemeinschaft (We 2616/4), and the Sino-German Center for Research promotion (GZ Nr 239 $^{202}/_{12}$).

Abbreviations: MHV indicates mouse hepatitis virus; SARS, severe acute respiratory syndrome; pDCs, plasmacytoid dendritic cells; and cDCs, conventional dendritic cells.

Authorship

Contribution: B.L. and V.T. designed the study and wrote the paper; L.C.-B. performed research and wrote the paper; R.Z., F.W., and M.S. performed research; K.S.L. and S.A. provided mice.

Conflict-of-interest disclosure: The authors declare no competing financial interests.

Correspondence: Burkhard Ludewig, Research Department, Kantonsspital St Gallen, 9007 St Gallen, Switzerland; e-mail: burkhard.ludewig@kssg.ch; Volker Thiel, Research Department, Kantonsspital St Gallen, 9007 St Gallen, Switzerland; e-mail: volker.thiel@kssg.ch.

References

1. Theofilopoulos AN, Baccala R, Beutler B, Kono DH. Type I interferons (alpha/beta) in immunity and autoimmunity. Annu Rev Immunol. 2005;23: 307-336.
2. Der SD, Zhou A, Williams BR, Silverman RH. Identification of genes differentially regulated by interferon alpha, beta, or gamma using oligonucleotide arrays. Proc Natl Acad Sci U S A. 1998; 95:15623-15628.
3. Nguyen KB, Watford WT, Salomon R, et al. Critical role for STAT4 activation by type 1 interferons in the interferon-gamma response to viral infection. Science. 2002;297:2063-2066.
4. Siegal FP, Kadowaki N, Shodell M, et al. The nature of the principal type 1 interferon-producing cells in human blood. Science. 1999;284:1835-1837.
5. Cella M, Jarrossay D, Facchetti F, et al. Plasmacytoid monocytes migrate to inflamed lymph nodes and produce large amounts of type I interferon. Nat Med. 1999;5:919-923.
6. Nakano H, Yanagita M, Gunn MD. CD11c(+) B220(+)Gr-1(+) cells in mouse lymph nodes and spleen display characteristics of plasmacytoid dendritic cells. J Exp Med. 2001;194:1171-1178.
7. Asselin-Paturel C, Boonstra A, Dalod M, et al. Mouse type I IFN-producing cells are immature APCs with plasmacytoid morphology. Nat Immunol. 2001;2:1144-1150.
8. Heil F, Hemmi H, Hochrein H, et al. Species-specific recognition of single-stranded RNA via toll-like receptor 7 and 8. Science. 2004;303:1526-1529.
9. Diebold SS, Kaisho T, Hemmi H, Akira S, Reis e Sousa C. Innate antiviral responses by means of TLR7-mediated recognition of single-stranded RNA. Science. 2004;303:1529-1531.
10. Lund J, Sato A, Akira S, Medzhitov R, Iwasaki A. Toll-like receptor 9-mediated recognition of Herpes simplex virus-2 by plasmacytoid dendritic cells. J Exp Med. 2003;198:513-520.
11. Krug A, French AR, Barchet W, et al. TLR9-dependent recognition of MCMV by IPC and DC generates coordinated cytokine responses that activate antiviral NK cell function. Immunity. 2004; 21:107-119.
12. Dalod M, Salazar-Mather TP, Malmgaard L, et al. Interferon alpha/beta and interleukin 12 responses to viral infections: pathways regulating dendritic cell cytokine expression in vivo. J Exp Med. 2002;195:517-528.
13. Delale T, Paquin A, Asselin-Paturel C, et al. MyD88-dependent and -independent murine cytomegalovirus sensing for IFN-alpha release and initiation of immune responses in vivo. J Immunol. 2005;175:6723-6732.
14. Perlman S, Dandekar AA. Immunopathogenesis of coronavirus infections: implications for SARS. Nat Rev Immunol. 2005;5:917-927.
15. Snijder EJ, Bredenbeek PJ, Dobbe JC, et al. Unique and conserved features of genome and proteome of SARS-coronavirus, an early split-off from the coronavirus group 2 lineage. J Mol Biol. 2003;331:991-1004.
16. Bergmann CC, Lane TE, Stohlman SA. Coronavirus infection of the central nervous system: host-virus stand-off. Nat Rev Microbiol. 2006;4:121-132.
17. Thiel V, Ivanov KA, Putics A, et al. Mechanisms and enzymes involved in SARS coronavirus genome expression. J Gen Virol. 2003;84:2305-2315.
18. Marten NW, Stohlman SA, Zhou J, Bergmann CC. Kinetics of virus-specific CD8+ -T-cell expansion and trafficking following central nervous system infection. J Virol. 2003;77:2775-2778.
19. Bergmann CC, Parra B, Hinton DR, et al. Perforin and gamma interferon-mediated control of coronavirus central nervous system infection by CD8 T cells in the absence of CD4 T cells. J Virol. 2004;78:1739-1750.
20. Lin MT, Hinton DR, Marten NW, Bergmann CC, Stohlman SA. Antibody prevents virus reactivation within the central nervous system. J Immunol. 1999;162:7358-7368.
21. Ramakrishna C, Stohlman SA, Atkinson RD, Shlomchik MJ, Bergmann CC. Mechanisms of central nervous system viral persistence: the critical role of antibody and B cells. J Immunol. 2002; 168:1204-1211.
22. Jones BM, Ma ES, Peiris JS, et al. Prolonged disturbances of in vitro cytokine production in patients with severe acute respiratory syndrome (SARS) treated with ribavirin and steroids. Clin Exp Immunol. 2004;135:467-473.
23. Reghunathan R, Jayapal M, Hsu LY, et al. Expression profile of immune response genes in patients with severe acute respiratory syndrome. BMC Immunol. 2005;6:2.
24. Yu SY, Hu YW, Liu XY, et al. Gene expression profiles in peripheral blood mononuclear cells of SARS patients. World J Gastroenterol. 2005;11: 5037-5043.
25. Yilla M, Harcourt BH, Hickman CJ, et al. SARS-coronavirus replication in human peripheral monocytes/macrophages. Virus Res. 2005;107: 93-101.
26. Law HK, Cheung CY, Ng HY, et al. Chemokine up-regulation in SARS-coronavirus-infected, monocyte-derived human dendritic cells. Blood. 2005;106:2366-2374.
27. Cheung CY, Poon LL, Ng IH, et al. Cytokine responses in severe acute respiratory syndrome coronavirus-infected macrophages in vitro: possible relevance to pathogenesis. J Virol. 2005;79: 7819-7826.
28. Ziegler T, Matikainen S, Ronkko E, et al. Severe acute respiratory syndrome coronavirus fails to activate cytokine-mediated innate immune responses in cultured human monocyte-derived dendritic cells. J Virol. 2005;79:13800-13805.
29. Cinatl J, Morgenstern B, Bauer G, et al. Treatment of SARS with human interferons. Lancet. 2003;362:293-294.
30. Zheng B, He ML, Wong KL, et al. Potent inhibition of SARS-associated coronavirus (SCOV) infection and replication by type I interferons (IFN-alpha/beta) but not by type II interferon (IFN-gamma). J Interferon Cytokine Res. 2004;24: 388-390.

31. Spiegel M, Pichlmair A, Muhlberger E, Haller O, Weber F. The antiviral effect of interferon-beta against SARS-coronavirus is not mediated by MxA protein. J Clin Virol. 2004;30:211-213.
32. Loutfy MR, Blatt LM, Siminovitch KA, et al. Interferon alfacon-1 plus corticosteroids in severe acute respiratory syndrome: a preliminary study. JAMA. 2003;290:3222-3228.
33. Haagmans BL, Kuiken T, Martina BE, et al. Pegylated interferon-alpha protects type 1 pneumocytes against SARS coronavirus infection in macaques. Nat Med. 2004;10:290-293.
34. Honda K, Sakaguchi S, Nakajima C, et al. Selective contribution of IFN-alpha/beta signaling to the maturation of dendritic cells induced by double-stranded RNA or viral infection. Proc Natl Acad Sci U S A. 2003;100:10872-10877.
35. Hemmi H, Kaisho T, Takeuchi O, et al. Small antiviral compounds activate immune cells via the TLR7 MyD88-dependent signaling pathway. Nat Immunol. 2002;3:196-200.
36. Adachi O, Kawai T, Takeda K, et al. Targeted disruption of the MyD88 gene results in loss of IL-1- and IL-18-mediated function. Immunity. 1998;9: 143-150.
37. Muller U, Steinhoff U, Reis LF, et al. Functional role of type I and type II interferons in antiviral defense. Science. 1994;264:1918-1921.
38. Coley SE, Lavi E, Sawicki SG, et al. Recombinant mouse hepatitis virus strain A59 from cloned, full-length cDNA replicates to high titers in vitro and is fully pathogenic in vivo. J Virol. 2005;79:3097-3106.
39. Krug A, Rothenfusser S, Hornung V, et al. Identification of CpG oligonucleotide sequences with high induction of IFN-alpha/beta in plasmacytoid dendritic cells. Eur J Immunol. 2001;31:2154-2163.
40. van den Broek MF, Muller U, Huang S, Zinkernagel RM, Aguet M. Immune defence in mice lacking type I and/or type II interferon receptors. Immunol Rev. 1995;148:5-18.
41. Kato H, Sato S, Yoneyama M, et al. Cell type-specific involvement of RIG-I in antiviral response. Immunity. 2005;23:19-28.
42. Izaguirre A, Barnes BJ, Amrute S, et al. Comparative analysis of IRF and IFN-alpha expression in human plasmacytoid and monocyte-derived dendritic cells. J Leukoc Biol. 2003;74:1125-1138.
43. Honda K, Yanai H, Negishi H, et al. IRF-7 is the master regulator of type-I interferon-dependent immune responses. Nature. 2005;434:772-777.
44. Barchet W, Cella M, Odermatt B, et al. Virus-induced interferon alpha production by a dendritic cell subset in the absence of feedback signaling in vivo. J Exp Med. 2002;195:507-516.
45. Turner BC, Hemmila EM, Beauchemin N, Holmes KV. Receptor-dependent coronavirus infection of dendritic cells. J Virol. 2004;78:5486-5490.
46. Zhou H, Perlman S. Preferential infection of mature dendritic cells by mouse hepatitis virus strain JHM. J Virol. 2006;80:2506-2514.
47. Smit JJ, Rudd BD, Lukacs NW. Plasmacytoid dendritic cells inhibit pulmonary immunopathology and promote clearance of respiratory syncytial virus. J Exp Med. 2006;203:1153-1159.
48. Kuba K, Imai Y, Rao S, et al. A crucial role of angiotensin converting enzyme 2 (ACE2) in SARS coronavirus-induced lung injury. Nat Med. 2005; 11:875-879.
49. Gu J, Gong E, Zhang B, et al. Multiple organ infection and the pathogenesis of SARS. J Exp Med. 2005;202:415-424.
50. Cinatl J Jr, Michaelis M, Scholz M, Doerr HW. Role of interferons in the treatment of severe acute respiratory syndrome. Expert Opin Biol Ther. 2004;4:827-836.
51. Spiegel M, Weber F. Inhibition of cytokine gene expression and induction of chemokine genes in non-lymphatic cells infected with SARS coronavirus. Virol J. 2006;3:17.
52. Spiegel M, Pichlmair A, Martinez-Sobrido L, et al. Inhibition of beta interferon induction by severe acute respiratory syndrome coronavirus suggests a two-step model for activation of interferon regulatory factor 3. J Virol. 2005;79:2079-2086.
53. Ashkar AA, Yao XD, Gill N, et al. Toll-like receptor (TLR)-3, but not TLR4, agonist protects against genital herpes infection in the absence of inflammation seen with CpG DNA. J Infect Dis. 2004; 190:1841-1849.
54. Horsmans Y, Berg T, Desager JP, et al. Isatoribine, an agonist of TLR7, reduces plasma virus concentration in chronic hepatitis C infection. Hepatology. 2005;42:724-731.

6 Original Research Articles

“Coronavirus nsp1 is a major pathogenicity factor: implications for the rational design of coronavirus vaccines”

Roland Züst, Luisa Cervantes-Barragan, Thomas Kuri, Friedemann Weber, Burkhard Ludewig, and Volker Thiel

Own contribution to this article: A recombinant MHV virus containing a 99 nt deletion in nsp1 has been generated and analyzed *in vitro* and *in vivo*. All work except for figure 1 has been done in our lab.

OPEN ACCESS Freely available online PLoS PATHOGENS

Coronavirus Non-Structural Protein 1 Is a Major Pathogenicity Factor: Implications for the Rational Design of Coronavirus Vaccines

Roland Züst[1], Luisa Cervantes-Barragán[1,2], Thomas Kuri[3], Gjon Blakqori[3¤], Friedemann Weber[3], Burkhard Ludewig[1], Volker Thiel[1*]

1 Research Department, Kantonal Hospital St. Gallen, St. Gallen, Switzerland, **2** Unidad de Investigación Médica en Inmunoquímica, Hospital de Especialidades, Centro Médico Nacional Siglo XXI, Instituto Mexicano del Seguro Social, México City, México, **3** Department of Virology, University of Freiburg, Freiburg, Germany

Attenuated viral vaccines can be generated by targeting essential pathogenicity factors. We report here the rational design of an attenuated recombinant coronavirus vaccine based on a deletion in the coding sequence of the non-structural protein 1 (nsp1). In cell culture, nsp1 of mouse hepatitis virus (MHV), like its SARS-coronavirus homolog, strongly reduced cellular gene expression. The effect of nsp1 on MHV replication in vitro and in vivo was analyzed using a recombinant MHV encoding a deletion in the nsp1-coding sequence. The recombinant MHV nsp1 mutant grew normally in tissue culture, but was severely attenuated in vivo. Replication and spread of the nsp1 mutant virus was restored almost to wild-type levels in type I interferon (IFN) receptor-deficient mice, indicating that nsp1 interferes efficiently with the type I IFN system. Importantly, replication of nsp1 mutant virus in professional antigen-presenting cells such as conventional dendritic cells and macrophages, and induction of type I IFN in plasmacytoid dendritic cells, was not impaired. Furthermore, even low doses of nsp1 mutant MHV elicited potent cytotoxic T cell responses and protected mice against homologous and heterologous virus challenge. Taken together, the presented attenuation strategy provides a paradigm for the development of highly efficient coronavirus vaccines.

Citation: Züst R, Cervantes-Barragán L, Kuri T, Blakqori G, Weber F, et al. (2007) Coronavirus non-structural protein 1 is a major pathogenicity factor: Implications for the rational design of coronavirus vaccines. PLoS Pathog 3(8): e109. doi:10.1371/journal.ppat.0030109

Introduction

Coronaviruses are vertebrate pathogens mainly associated with respiratory and enteric diseases [1]. They can cause severe diseases in livestock animals and lead thereby to high economic losses. In humans, coronavirus infections manifest usually as mild respiratory tract disease (common cold) that may cause more severe symptoms in elderly or immune-compromised individuals [2,3]. In 2002–2003, the appearance of severe acute respiratory syndrome (SARS), caused by a formerly unknown coronavirus (SARS-CoV), exemplified the potential of coronaviruses to seriously affect human health [4–7]. The frequent detection of SARS-like coronaviruses in horseshoe bats (*Rhinolophus* sp.) and the broad range of mammalian hosts that are susceptible to SARS-CoV infection may facilitate a potential reintroduction into the human population [8]. Therefore, the development of efficacious coronavirus vaccines is of high medical and veterinary importance.

Effective vaccines controlling virus spread and disease are available for a number of infections, such as smallpox, poliomyelitis, measles, mumps, rubella, influenza, hepatitis A, and hepatitis B [9,10]. Some of these vaccines consist of virus subunits or inactivated virus preparations that mainly induce the production of pathogen-specific antibodies. In contrast, live attenuated vaccines consist of replication-competent viruses that induce broad cellular and humoral immune responses without causing disease [10]. The most prominent live attenuated vaccines are vaccinia virus [11], poliovirus [12], and yellow fever virus (YF-17D) [13]. Despite their documented efficacy, it is still not fully understood why and how successful vaccines work [10,14]. However, recent concepts in immunology provide a link between innate and adaptive immune responses and suggest that the quality, quantity, and longevity of adaptive immune responses is determined very early after infection or vaccination [14]. Of major importance are professional antigen-presenting cells (pAPCs) such as dendritic cells (DCs) and macrophages, which play a major role in (i) sensing pathogen-associated molecular patterns, (ii) inducing innate immune responses, and (iii) shaping the upcoming adaptive immune response. Efficient live attenuated vaccines should therefore not only lack significant pathogenicity, but should also deliver antigens to pAPCs and activate the innate immune system.

Notably, the majority of currently available attenuated vaccines have been derived empirically. Given the recent proceedings in the areas of virus reverse genetics and virus–

Editor: Kanta Subbarao, National Institutes of Health, United States of America

Received February 2, 2007; **Accepted** June 12, 2007; **Published** August 10, 2007

Abbreviations: ALT, alanine 2-oxoglutarate-aminotransferase; cDC, conventional dendritic cell; CTL, cytotoxic T lymphocyte; DC, dendritic cell; IFN, interferon; ISRE, interferon-stimulated response element; LCMV, lymphocytic choriomeningitis virus; MHV, mouse hepatitis virus; nsp1, non-structural protein 1; nt, nucleotide; pAPC, professional antigen-presenting cell; pDC, plasmacytoid dendritic cell; p.i., post infection

* To whom correspondence should be addressed. E-mail: volker.thiel@kssg.ch

¤ Current address: Centre for Biomolecular Sciences, School of Biology, University of St. Andrews, North Haugh, St. Andrews, Scotland, United Kingdom

Author Summary

Prevention of viral diseases by vaccination aims for controlled induction of protective immune responses against viral pathogens. Live viral vaccines consist of attenuated, replication-competent viruses that are believed to be superior in the induction of broad immune responses, including cell-mediated immunity. The recent proceedings in the area of virus reverse genetics allows for the rational design of recombinant vaccines by targeting, i.e., inactivating, viral pathogenicity factors. For coronaviruses, a major pathogenicity factor has now been identified. The effect of coronavirus non-structural protein 1 on pathogenicity has been analyzed in a murine model of coronavirus infection. By deleting a part of this protein, a recombinant virus has been generated that is greatly attenuated in vivo, while retaining immunogenicity. In particular, the mutant virus retained the ability to replicate in professional antigen-presenting cells and fulfilled an important requirement of a promising vaccine candidate: the induction of a protective long-lasting, antigen-specific cellular immune response. This study has implications for the rational design of live attenuated coronavirus vaccines aimed at preventing coronavirus-induced diseases of veterinary and medical importance, including the potentially lethal severe acute respiratory syndrome.

host interactions, the time should be ripe for more rational approaches in vaccine development. An attractive strategy is to target virally encoded pathogenicity factors, such as interferon (IFN) antagonists [15], to attenuate virulence while retaining immunogenicity. This concept has been proposed for the generation of live attenuated influenza virus vaccines encoding altered NS1 proteins [16,17].

Our rudimentary knowledge on coronavirus-encoded pathogenicity factors is reflected by the fact that only a few putative coronaviral pathogenicity factors have been identified and that functional analyses are still limited to the description of in vitro effects [18–20]. For a number of reasons, the non-structural protein 1 (nsp1) is of particular interest in this context. First, coronaviruses are positive-stranded RNA viruses, and the replicase-encoded nsps are expressed from the viral genomic RNA immediately after virus entry by translation of two large polyproteins. nsp1 is encoded at the 5′ end of the replicase gene and is therefore the first mature viral protein expressed in the host cell cytoplasm [21]. Second, a recent in vitro study suggests that SARS-CoV nsp1 may be associated with host cell mRNA degradation and may counteract innate immune responses [18]. Finally, nsp1 is encoded by all mammalian coronaviruses known to date (coronavirus groups 1, 2a, and 2b) [22], and recent structural data on SARS-CoV (group 2b) nsp1 suggest functional similarities to mouse hepatitis virus (MHV; group 2a) nsp1 [23].

Using a reverse genetics approach, we show here that nsp1 is a major pathogenicity factor. Recombinant MHV mutants encoding a deletion in nsp1 replicated as efficiently as wild-type virus in cell culture, but displayed an unprecedented degree of attenuation in mice. Interference with the type I IFN system appears to be the dominant mode of action of murine coronavirus nsp1. Vaccination with the nsp1 mutant virus elicited efficient memory cytotoxic T cell responses and protected against homologous and heterologous virus infections. Our study will pave the way for the generation of novel coronavirus vaccines based on modified coronavirus replicase genes.

Results

Transient nsp1 Expression Affects Cellular Gene Expression

We assessed several replicase-encoded nsps of MHV (strain A59), SARS-CoV, and human coronavirus 229E (HCoV-229E) for their ability to interfere with host cell gene expression. Using transient gene expression studies, we found that MHV-A59, SARS-CoV, and HCoV-229E nsp1 significantly reduced luciferase reporter gene expression under the control of IFN-β, IFN-stimulated response element (ISRE), and SV40 promoters (Figure 1). This is consistent with a recent report suggesting that SARS-CoV nsp1 induces general host cell mRNA degradation [18]. Nevertheless, it should be noted that the nsp1-mediated reduction in reporter protein expression appeared more robust for ISRE and SV40 than for IFN-β promoter-driven expression. Our data also support the hypothesis that MHV encodes a SARS-CoV nsp1 homolog that displays the same function [23]. Although comparative sequence analyses suggest that nsp1 of group 2a/2b coronaviruses (e.g., MHV and SARS-CoV, respectively) and the nsp1 of group 1 coronaviruses (e.g., HCoV-229E) may belong to different protein families [22,23], we also observed reduced reporter gene expression in HCoV-229E nsp1-transfected cells (Figure 1). Whether functional similarities may exist between nsp1 molecules encoded by coronaviruses of different phylogenetic lineages remains to be established in future studies. Importantly, our data also revealed that reporter gene expression from all tested promoters was not affected when C-terminally truncated MHV nsp1 molecules were tested (Figure 1).

Generation of the MHV nsp1 Deletion Mutant

To assess the role of nsp1 in the context of virus replication, we constructed a recombinant MHV encoding a truncated nsp1 protein using our reverse genetic system [24]. Based on the results shown in Figure 1, we decided to delete MHV nucleotides (nts) 829–927 (99 nts). In the resulting mutant virus, MHV-nsp1Δ99, the replicase gene start codon, the translational reading frame, and the residues required for proteolytic release of nsp1 from the replicase polyprotein were maintained (Figure 2A). As reported for a set of similar MHV mutants by Brockway et al. [25], viral growth and peak titers of MHV-nsp1Δ99 in murine 17Clone1 cells were indistinguishable from that of wild-type virus (Figure 2B). To assess the stability of the recombinant MHV-nsp1Δ99, we analyzed the nsp1-coding region by RT-PCR sequencing after seven passages in tissue culture and no nucleotide changes were detected (unpublished data).

Infection of conventional DCs (cDCs) is an early and crucial event for the generation of protective antiviral immunity [26]. MHV productively infects cDCs and activates plasmacytoid DCs (pDCs) to generate a first wave of protective type I IFN [27]. To assess whether the mutant MHV-nsp1Δ99 has retained the ability to infect pAPCs, peritoneal macrophages (Figure 2C), bone marrow–derived $CD11c^+$ cDCs (Figure 2D), and splenic, FACS-sorted $CD11c^+$ cDCs (Figure 2E) were exposed to MHV-nsp1Δ99 and wild-type control virus. Similar to replication kinetics in cell lines (Figure 2B),

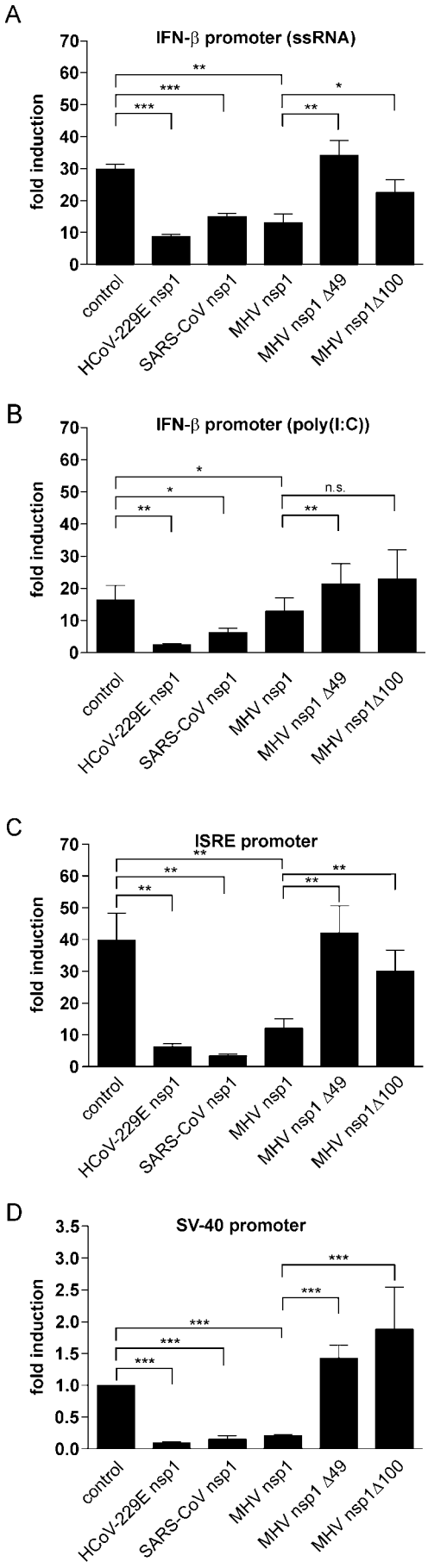

Figure 1. Coronavirus nsp1 Reduces Cellular Gene Expression

(A–C) 293 cells were transfected with p125-Luc reporter plasmid ([A, B]; IFN-β promoter), or p(9–27)4tkD(–39)lucter reporter plasmid ([C]; ISRE promoter) and cotransfected with pRL-SV40, and an expression plasmid encoding a full-length coronavirus nsp1 of HCoV-229E, SARS-CoV, or MHV, or a truncated MHV nsp1 variant (49-nt or 100-nt 3′ end truncations, respectively). At 8 h post transfection, cells were treated with viral single-stranded RNA containing 5′ triphosphates (A) or poly(I:C) (B), or IFN-α (C), and 16 h later luciferase activity was measured. Firefly luciferase activity was normalized to renilla luciferase activity and indicated as fold induction compared to that of control plasmid-transfected cells (control).

(D) 293 cells were transfected with pRL-SV40 and the indicated expression plasmids. Then, 24 h post transfection, luciferase activity was measured. Results represent the mean ± SD of at least four independent experiments. Statistical analysis was performed using paired Student's *t*-test (***, $p < 0.001$; **, $p < 0.01$; *, $p < 0.05$; n.s. (not significant), $p > 0.05$).

doi:10.1371/journal.ppat.0030109.g001

MHV-nsp1Δ99 showed no significant growth defect in primary pAPCs (Figure 2C–2E), indicating that the deletion of nsp1 did not alter the pronounced tropism of MHV for cDCs and macrophages.

Deletion in nsp1 Confers Strong Attenuation In Vivo

MHV-A59 is a hepatotropic and neurotropic virus that can cause acute hepatitis and encephalitis. Following intraperitoneal infection, virus replication is first detectable in spleen and liver, followed by virus spread to other organs, including the central nervous system. Hepatitis is the first clinical sign of disease, accompanied by elevated liver enzyme values in serum. Associated with the appearance of cytotoxic T cell responses approximately at day 5 post infection (p.i.), virus titers usually decline and are no longer detectable after day 7 p.i. Infections with a high dose ($\geq 5 \times 10^6$ pfu, intraperitoneal) may, however, occasionally result in fatality. To evaluate the importance of nsp1 for virus replication and viral pathogenicity in vivo, C57BL/6 mice were infected intraperitoneally with different doses of wild-type MHV or MHV-nsp1Δ99. Both viruses replicated in the spleen, whereby MHV-nsp1Δ99 titers were consistently lower than wild-type virus titers (Figure 3A). Furthermore, MHV-nsp1Δ99 was rapidly cleared and not detectable after day 2 p.i. (Figure 3A). Wild-type, but not mutant virus, was detectable in the liver at low and intermediate dose (50 pfu and 5,000 pfu, respectively) (Figure 3B). When high virus doses (5×10^6 pfu) were applied, MHV-nsp1Δ99 eventually reached the liver at day 2 p.i., but was not detectable at later time points (Figure 3B). MHV-nsp1Δ99 was not detectable in other non-hematopoietic organs, such as lung and central nervous system (unpublished data). Mice infected with wild-type virus showed acute liver disease with elevated liver enzyme values in serum. Furthermore, after high dose infection with wild-type virus (5×10^6 pfu), a significant weight loss that peaked at approximately 10%–15% at day 4 was observed (Figure 3E). In contrast, mice infected with the nsp1 mutant virus remained healthy after low, intermediate, or high dose infections. Even at the highest dose applied (5×10^6 pfu), MHV-nsp1Δ99–infected mice did not lose weight (Figure 3E), and no elevated liver enzyme values were detected in the serum (Figure 3C). This observation correlated well with the absence of hepatocyte necrosis and parenchymal inflammation following MHV-nsp1Δ99 infection (Figure 3D). To further assess the attenuation of the MHV nsp1 mutant, mice were infected intracranially with 200 pfu and 20,000 pfu of MHV-nsp1Δ99

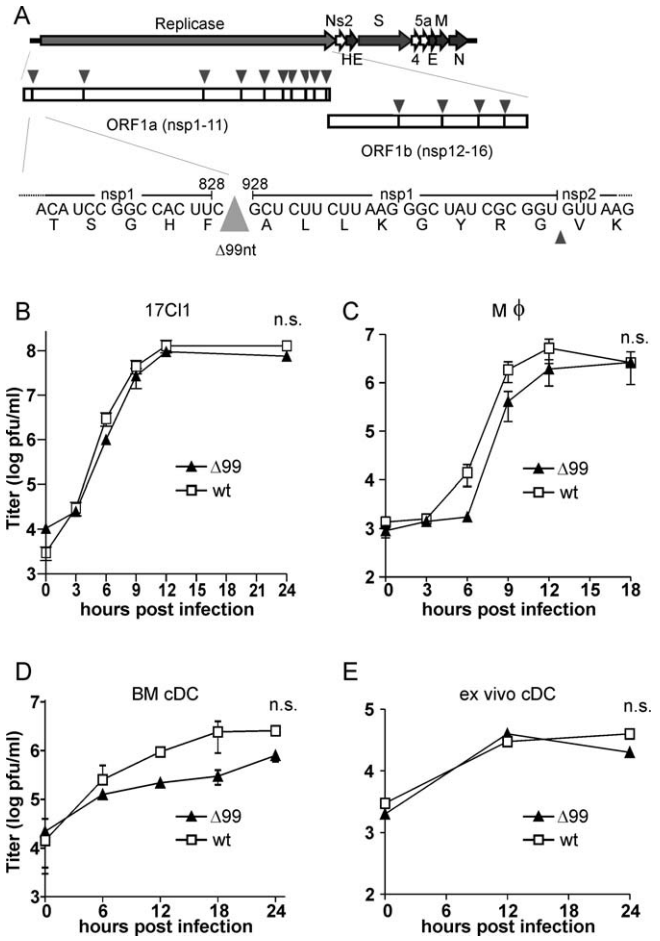

Figure 2. Construction and In Vitro Analysis of MHV-nsp1Δ99

(A) Schematic representation of the MHV-nsp1Δ99 genome organization. The replicase gene, comprised of open reading frames (ORFs) 1a and 1b, is depicted together with viral proteinase cleavage sites (arrowheads) that separate nsps 1–16. The 99-nt deletion within the nsp1-coding region of MHV-nsp1Δ99 is illustrated on the nucleotide and amino acid level. The arrowhead (far right) indicates the nsp1/nsp2 cleavage site.
(B–E) Growth kinetics of MHV-nsp1Δ99– or MHV-A59–infected (MOI = 1) murine 17Clone1 cells (B), inflammatory macrophages (C), bone marrow–derived cDCs (D), and ex vivo cDCs (E). Experiments (C–E) were performed with cells obtained from C57BL/6 mice. Results represent the mean ±SD of two independent experiments. Statistical analysis was performed using Student's *t*-test (n.s., $p > 0.05$).
doi:10.1371/journal.ppat.0030109.g002

or MHV-A59. All mice infected with 200 pfu survived for at least 30 d (unpublished data). Mice infected with 20,000 pfu of MHV-A59 succumbed to the infection, whereas mice infected with 20,000 pfu of MHV-nsp1Δ99 survived and showed no signs of clinical disease (Figure 3F). Collectively, these data demonstrate that MHV-nsp1Δ99 is strongly attenuated in vivo, but has retained the ability to replicate in secondary lymphoid organs, such as the spleen.

Effect of nsp1 on Innate Immune Responses

We have previously shown that pDCs are the major source of IFN-α in the early stages of MHV infection and that type I IFN responses in $CD11c^+$ cDCs are only weakly triggered by MHV [27]. To test whether nsp1 has an influence on the induction of IFN-α, we infected both cDCs and pDCs with MHV-nsp1Δ99 or wild-type MHV. Both viruses elicited rapid and high IFN-α production in Flt3-L–differentiated bone marrow–derived pDCs (Figure 4A) and FACS-sorted primary pDCs (Figure 4B). Furthermore, both wild-type and mutant MHV elicited only a late and weak IFN-α production in cDCs (Figure 4A and 4B). These results suggest that nsp1 does not affect the induction of type I IFN. To assess a potential impact of nsp1 on type I IFN signaling and antiviral effector mechanisms in target cells that efficiently support MHV replication, cDCs and macrophages were pretreated with different dosages of IFN-α and infected with MHV-nsp1Δ99 or wild-type MHV. In cDCs, IFN-α treatment had a comparable effect on the replication of both MHV-nsp1Δ99 and the wild-type control virus (Figure 4C). However, replication of MHV-nsp1Δ99 was, in a dose-dependent manner, more vulnerable to IFN-α treatment in macrophages (Figure 4D), suggesting that nsp1 might counteract IFN signaling and/or the antiviral activities of IFN-induced effector proteins.

Indeed, in vivo experiments in type I IFN receptor-deficient ($IFNAR^{-/-}$) mice [28] strongly support this interpretation. Infection of $IFNAR^{-/-}$ mice with wild-type MHV led to high titers in all tested organs (Figure 5A–5D), indicating that signals transmitted via the IFNAR are crucial for preventing uncontrolled spread of the virus [27]. Surprisingly, the severe attenuation of MHV-nsp1Δ99 in wild-type 129Sv mice was not present in $IFNAR^{-/-}$ mice (Figure 5A–5D). Replication of MHV-nsp1Δ99 in $IFNAR^{-/-}$ mice was largely restored and virus titers reached about 10^4–10^5 pfu/g tissue in several organs after only 36 h (figures 5A–5D). These data strongly suggest that nsp1 has a pivotal role in counteracting type I IFN host responses and provide an explanation for the rapid clearance of MHV-nsp1Δ99 in wild-type mice. Interestingly, liver damage, measured as alanine 2-oxoglutarate-aminotransferase (ALT) levels in serum, was not yet detectable in MHV-nsp1Δ99–infected $IFNAR^{-/-}$ mice at 36 h p.i. (Figure 5E). At 72 h p.i., MHV-nsp1Δ99 reached titers and ALT levels in $IFNAR^{-/-}$ mice comparable to those observed in MHV-A59–infected $IFNAR^{-/-}$ mice at 36 h p.i., demonstrating that MHV-nsp1Δ99 replication in $IFNAR^{-/-}$ is, although with slower kinetics, restored.

Immunization with the MHV nsp1 Deletion Mutant Protects against Homologous and Heterologous Virus Challenge

The phenotypic analysis of MHV-nsp1Δ99 revealed a number of features that are advantageous for live attenuated vaccines. MHV-nsp1Δ99 grows to high titers in cell culture, infects pAPCs, replicates almost exclusively in secondary lymphoid organs, and is strongly attenuated in vivo. To assess the potential of MHV-nsp1Δ99 as an attenuated live vaccine, we replaced accessory gene 4 of MHV-nsp1Δ99 and wild-type MHV-A59 by a gene encoding a fusion protein of the immunodominant cytotoxic T lymphocyte (CTL) epitope (KAVYNFATC) of the lymphocytic choriomeningitis virus (LCMV) and the enhanced green fluorescent protein (GP33-GFP) [29]. The resulting recombinant viruses, MHV-nsp1Δ99-GP33-GFP and MHV-GP33-GFP, were used to infect C57BL/6 mice with different doses (50 and 5,000 pfu, intraperitoneal), and $CD8^+$ T cell responses were assessed using flow cytometry–based detection of intracellular IFN-γ following antigen-specific short-term in vitro restimulation. As shown in Figure 6A and 6B, infection with as few as 50 pfu of MHV-nsp1Δ99-GP33-GFP elicited strong $CD8^+$ T cell responses

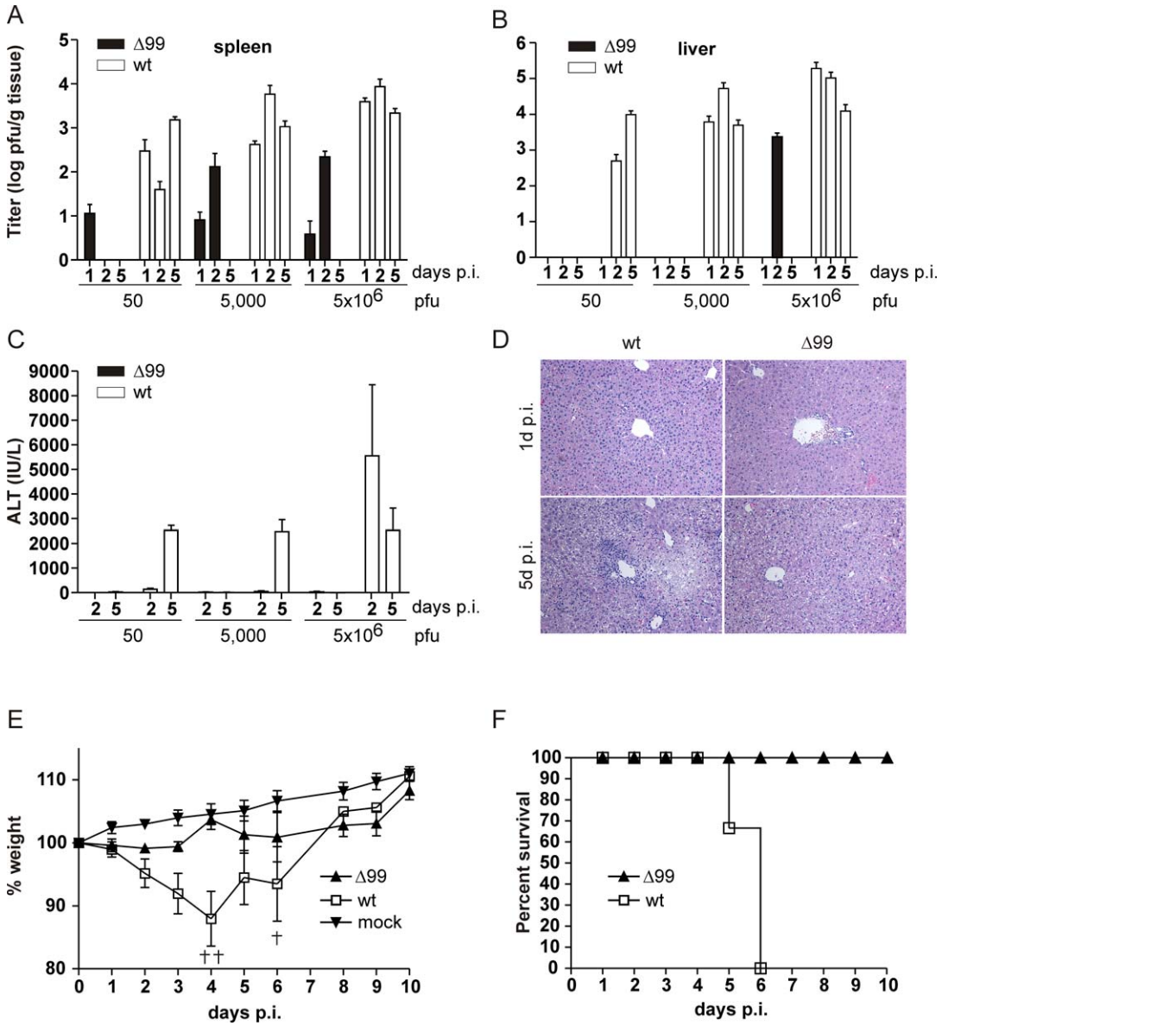

Figure 3. MHV-nsp1Δ99 Is Highly Attenuated In Vivo

C57BL/6 mice were infected intraperitoneally (A–E) or intracranially (F) with the indicated dose of MHV-nsp1Δ99 or MHV-A59. Viral titers in spleens (A) and livers (B) were determined at the indicated time points p.i. (C) Liver enzyme ALT values were measured at the indicated time points p.i. (D) Hematoxylin and eosin–stained liver sections of C57BL/6 mice infected intraperitoneally with 5,000 pfu of MHV-nsp1Δ99 or MHV-A59. The time points of analysis p.i. are indicated. (E) Groups of four mice were either untreated (mock) or infected (intraperitoneally) with 5×10^6 pfu of MHV-nsp1Δ99 or MHV-A59. The weight was monitored daily. † denotes death of mice. (F) Survival of mice (three per group) infected with 20,000 pfu (intracranially) of MHV-nsp1Δ99 or MHV-A59. Mice with severe weight loss (>25%) were defined as moribund and sacrificed. Results (A–C) and (E) represent the mean ±SD of at least three individual mice per time point.

doi:10.1371/journal.ppat.0030109.g003

against both the H2-D^b–restricted GP33 and the H2-K^b–restricted MHV S598 epitope.

To assess the level of protection against homologous MHV-A59 challenge, groups of C57BL/6 mice were immunized (5,000 pfu) with MHV-nsp1Δ99-GP33-GFP, MHV-GP33-GFP, or treated with PBS. Sixteen days p.i., mice were challenged with wild-type MHV (5,000 pfu) and viral titers were determined 5 d post challenge infection. Viral titers were below the limit of detection in MHV-nsp1Δ99-GP33-GFP– and MHV-GP33-GFP–immunized mice (Figure 6C). Together with the absence of elevated liver enzyme values in immunized mice (Figure 6D), these data indicate that vaccination with the attenuated MHV nsp1 mutant provides complete protection against homologous virus challenge.

The reverse genetic system facilitates incorporation of antigens derived from other infectious organisms. In order to determine whether the attenuated nsp1 mutant virus could confer protection against heterologous virus infection, MHV-nsp1Δ99-GP33-GFP–immunized C57BL/6 mice were challenged after 4 wk with LCMV (200 pfu, intravenous). LCMV titers in spleens were significantly reduced both in mice vaccinated with MHV-GP33-GFP and the attenuated MHV-nsp1Δ99-GP33-GFP virus (Figure 6E). Remarkably, only 50 pfu of nsp1 mutant virus expressing the GP33 epitope were

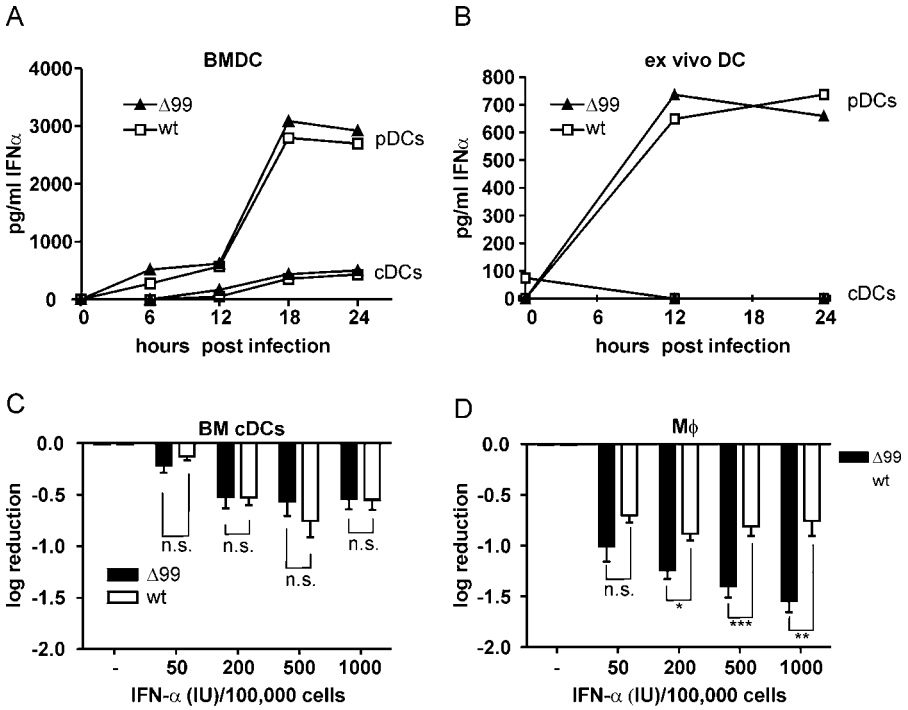

Figure 4. Effect of nsp1 on IFN-α Production and Signaling

C57BL/6 bone marrow–derived (A) or primary (B) splenic cDCs or pDCs were infected with MHV-nsp1Δ99 or MHV-A59 at an MOI of 1. IFN-α secreted into cell culture supernatants was determined by ELISA at the indicated time points. Bone marrow–derived cDCs (C) or inflammatory macrophages (D) from 129Sv mice were treated with 50, 200, 500, or 1,000 U IFN-α/100,000 cells or left untreated. Four hours later, cells were infected with MHV-nsp1Δ99 or MHV-A59 (MOI = 1). Twelve hours p.i., virus titers in culture supernatants were determined by plaque assay. Representative experiments out of two (A, B) or the mean ± SD of two independent experiments (C, D) are shown. Statistical analysis was performed using Student's *t*-test (***, $p < 0.001$; **, $p < 0.01$; *, $p < 0.05$; n.s., $p > 0.05$).

doi:10.1371/journal.ppat.0030109.g004

sufficient to achieve a reduction of LCMV titers by more than 4 orders of magnitude, indicating that nsp1 mutant viruses are well-suited to serve as attenuated recombinant virus vectors against heterologous viral infections.

Discussion

The rational design of live attenuated viral vaccines is greatly facilitated by the identification and targeting of pathogenicity factors. This study demonstrates an unprecedented level of attenuation of a murine coronavirus through a 99-nt deletion in nsp1. The nsp1 mutant virus was rapidly cleared in mice and did not induce clinical signs of disease in immunocompetent mice. These findings in the murine coronavirus model demonstrate that nsp1 is a major pathogenicity factor. In a stepwise approach, we made use of these observations to provide a blueprint for the construction and evaluation of live attenuated coronavirus vaccines encoding a truncated nsp1.

The presented results indicate that nsp1 plays a crucial role in the MHV life cycle by interfering with host innate immune responses. In accordance with the recent report by Kamitani et al. [18], we observed reduced reporter gene expression in transient nsp1 expression studies. The suggestion that SARS-CoV nsp1 may play a role in SARS-CoV pathogenesis by promoting host cell mRNA degradation [18] has now received support through the analysis of a coronavirus nsp1 mutant in a murine model. The MHV nsp1 mutant phenotype led us to conclude that nsp1 mainly affects IFN signaling pathways or other downstream events. The influence on IFN-α induction appears to be limited. These conclusions are based on several observations. First, the analysis of IFN-α production by pDCs and cDCs revealed no significant differences between wild-type and nsp1 mutant virus infections. Second, treatment of macrophages with IFN-α revealed a more efficient reduction of MHV-nsp1Δ99 replication compared with that of wild-type MHV. Finally, and most strikingly, IFNAR$^{-/-}$ mice were highly permissive for the mutant virus, and organ titers almost reached those of wild-type MHV-infected IFNAR$^{-/-}$ mice. Nevertheless, it should be noted that the nsp1 mutant virus replication was still slightly delayed in IFNAR$^{-/-}$ mice. Therefore, further studies are required to define molecular target(s) and the precise function(s) of coronavirus nsp1. Likewise, further studies are required to assess the impact of other coronaviral gene products on coronavirus pathogenicity. Recent reports indicate that coronaviruses most likely express a number of proteins, such as MHV and SARS-CoV nucleocapsid proteins, and SARS-CoV ORF3b and ORF6 proteins, that may interact with innate immune responses [19,20]. Also, the coronavirus replicase gene may harbor additional functions that play a role in virus–host interactions. It has been shown that the MHV and SARS-CoV nsp2 proteins [30], and the highly conserved ADP-ribose-1′′-monophosphatase activity [31] encoded in nsp3, are both dispensable for virus replication in tissue culture, and that a single point mutation in the MHV nsp14 confers a strong attenuation of MHV in mice [32]. Clearly, the murine model, with MHV as a natural mouse pathogen, will be highly

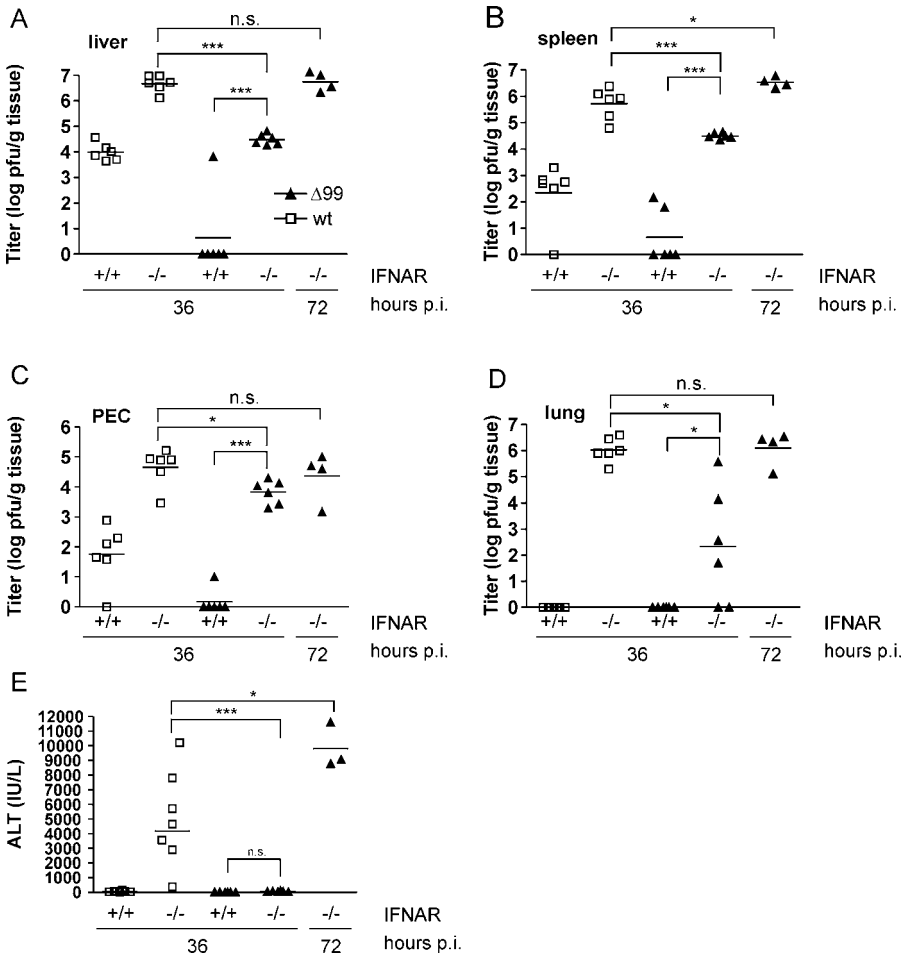

Figure 5. nsp1-Dependent Attenuation Is Reversed in IFNAR$^{-/-}$ Mice

IFNAR$^{-/-}$ or wild-type 129Sv mice were infected intraperitoneally with 500 pfu of MHV-nsp1Δ99 or MHV-A59. At the indicated time points p.i., viral titers in livers (A), spleens (B), peritoneal exudates cells (PEC) (C), and lungs (D) were determined. (E) ALT values in serum were measured at the indicated time points p.i. Horizontal lines represent means with values from individual mice shown as open squares (MHV-A59) or filled triangles (MHV-nsp1Δ99) from two experiments with a total of three to six mice. Statistical analysis was performed using Student's *t*-test (***, $p < 0.001$; *, $p < 0.05$; n.s., $p > 0.05$).
doi:10.1371/journal.ppat.0030109.g005

advantageous in the examination of this issue, because it allows the use of well-characterized inbred and transgenic mice in combination with well-established immunological techniques required to assess the full range of coronavirus–host interactions.

The most remarkable finding of this study is the level of attenuation of the nsp1 mutant virus and its restricted replication in secondary lymphoid organs. It may well be that other coronaviral nsp1 molecules exert similar functions as the MHV nsp1. The coronavirus nsp1 has been suggested as a group-specific marker to differentiate group 1 coronaviruses from group 2a/2b coronaviruses [22]. Our transient nsp1 expression data indeed support the notion that SARS-CoV and MHV may encode evolutionarily conserved nsp1 homologs [22,23]. Nevertheless, further in vivo studies are required to determine whether the group 2b SARS-CoV nsp1 is indeed a functional equivalent to the structurally highly conserved group 2a nsp1 molecules encoded by MHV, bovine coronavirus, porcine hemagglutinating encephalomyocarditis virus, HCoV-OC43, and HCoV-HKU1. Likewise, it will be important to clarify in vivo, whether, despite the apparent lack of any sequence homology [22,23], the nsp1 of group 1 coronaviruses (e.g., HCoV-229E) may represent a functional correlate to the nsp1 of group 2a/2b coronaviruses. Recent progress in the establishment of suitable mouse models for SARS-CoV [33–35] and HCoV-229E [36] will enable researchers to address these questions in future studies.

The chosen attenuation strategy has resulted in the generation of a recombinant virus that fulfills important criteria of a live virus vaccine candidate: (i) growth to high titers in cell culture, which facilitates vaccine production, and (ii) generation of immunological memory that mediates efficient protection against viral challenge. One important aspect of protection against viral infections is the induction of specific cytotoxic T cells by pAPCs in secondary lymphoid organs [14]. A number of coronaviruses, such as MHV, HCoV-229E, feline infectious peritonitis virus, and SARS-CoV, have been shown to infect pAPCs and to replicate in the secondary lymphoid organs [27,37–42]. Because of their pronounced tropism for pAPCs and the induction of strong CTL responses, we propose that coronaviruses represent promising vectors for the expression of heterologous antigens. The identification of nsp1 as a major pathogenicity factor will significantly increase the safety of coronavirus-based vectors

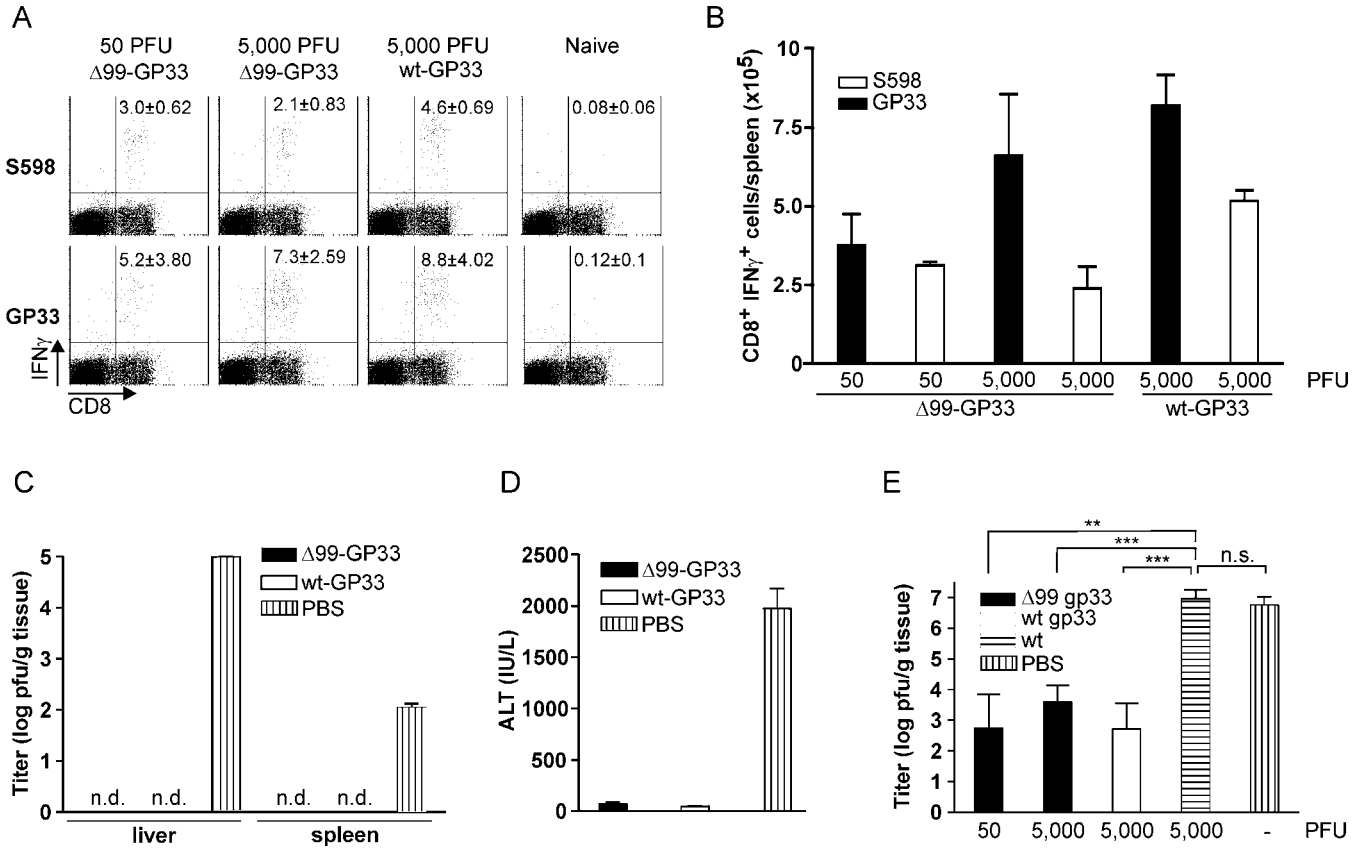

Figure 6. MHV-nsp1Δ99-GP33-GFP and MHV-GP33-GFP Elicit Strong CTL Responses and Protect Mice from Homologous and Heterologous Viral Infections

(A, B) Groups of three C57BL/6 mice were immunized with the indicated doses of MHV-nsp1Δ99-GP33-GFP or MHV-GP33-GFP. IFN-γ–secreting $CD8^+$ splenocytes were determined 8 d post immunization following short-term in vitro restimulation with GP33 or S598 peptide. Values in (A) represent the percentage ±SD of IFN-γ–secreting $CD8^+$ T cells restimulated with GP33 or S598; values in (B) represent the absolute numbers of $CD8^+$ IFN-γ^+ cells ±SD ($n = 6$ for GP33, $n = 3$ for S598). Pooled data from two separate experiments are shown.

(C, D) Groups of three mice were immunized with 5,000 pfu of the indicated virus or PBS-treated and 14 d later challenged with 5,000 pfu of wild-type MHV-A59. At 5 d post challenge, viral titers in liver and spleen were determined (C) and ALT values (D) were measured. Data in graphs (C) and (D) represent means ±SD from one representative experiment. n.d., not detected.

(E) Protection against heterologous viral challenge. Groups of four C57BL/6 mice have been immunized with the indicated viral doses or PBS-treated and 28 d later challenged with 200 pfu of LCMV-WE. At 4 d post challenge, viral titers in spleens were determined. Data in graph represent means ±SD from two pooled experiments with a total of eight mice per group. Statistical analysis was performed using Student's *t*-test (***, $p < 0.001$; **, $p < 0.01$; n.s., $p > 0.05$).

doi:10.1371/journal.ppat.0030109.g006

[43]. For example, the deletion of accessory genes (i.e., not replicase or structural genes) has been described for some coronaviruses to confer attenuation in the natural host [44–46], and the deletion of the structural envelope protein E has resulted in the development of replication-competent, but propagation-deficient, coronavirus vectors [47,48]. Now, with an accompanying deletion in the nsp1-coding sequence, such vectors would be considered "recombination proof", because the deletions are located at opposite genomic regions (i.e., within the replicase gene at the 5′ end and within the structural gene region at the 3′ end of the coronavirus genome), which make the reconstruction of virulent viruses by recombination unlikely. We therefore suggest that accessory gene, E gene, and partial nsp1 gene deletions will result in particular safe vectors with the potential to express multiple heterologous antigens [40,49].

Taken together, our results describe a novel type of coronavirus vaccines based on impaired function of a replicase gene product. We expect that our approach is applicable to most, if not all, mammalian coronaviruses and that it will enable the development of long-desired live attenuated vaccines for important coronavirus-induced diseases in humans and animals.

Materials and Methods

Mice and cells. C57BL/6 mice were obtained from Charles River Laboratories (http://www.criver.com/). 129Sv and type I IFN receptor-deficient mice ($IFNAR^{-/-}$) [28] were obtained from the Institut für Labortierkunde (University of Zürich) and bred in our facilities. All mice were maintained in individually ventilated cages and were used between 6 and 9 wk of age. All animal experiments were performed in accordance with the Swiss Federal legislation on animal protection.

MC57, BHK-21, L929, 293, and CV-1 cells were purchased from the European Collection of Cell Cultures (http://www.ecacc.org.uk/). D980R cells were a kind gift from G. L. Smith, Imperial College, London, United Kingdom. 17Clone1 cells were a kind gift from S. G. Sawicki, Medical University of Ohio, Toledo, Ohio, United States. BHK-MHV-N cells, expressing the MHV-A59 nucleocapsid protein under the control of the TET/ON system (Clontech, http://www.clontech.com/), have been described previously [24]. All cells were

maintained in minimal essential medium supplemented with fetal bovine serum (5%–10%) and antibiotics.

Isolation of dendritic cells and macrophages, flow cytometry, and antibodies. Murine cDCs and pDCs were obtained from spleens of C57BL/6, 129Sv, or IFNAR$^{-/-}$ mice following digestion with collagenase type II (Gibco-BRL, http://www.invitrogen.com/) for 20 min at 37 °C. Cells were resuspended in PBS supplemented with 2% FCS and 2 mM EDTA and overlaid on 20% Optiprep density gradient medium (Sigma-Aldrich, http://www.sigmaaldrich.com/). After centrifugation at 700*g* for 15 min, low density cells were depleted of CD3- and CD19-positive cells using DYNAL magnetic beads according to the instructions of the manufacturer (Invitrogen, http://www.invitrogen.com/). The DC-enriched preparations were stained with α-PDCA-1, α-CD11b, and α-CD11c, and the distinct pDC and cDC populations were sorted using a FACS ARIA (BD Biosciences, http://www.bdbiosciences.com/) sorter. Purity of both cell preparations was always >98%.

Murine bone marrow–derived cDCs or pDCs were generated by 6 to 7 d of culture with either granulocyte-monocyte colony stimulating factor (GM-CSF)-containing supernatant from the cell line X63-GM-CSF (kindly provided by Antonius Rolink, University of Basel, Basel, Switzerland) or Flt3-L (R&D Systems, http://www.rndsystems.com/) at 20 ng/ml, respectively. Bone marrow–derived cDCs were further purified using Optiprep density gradient centrifugation. Bone marrow–derived pDCs were purified using the mouse pDC isolation kit (Miltenyi Biotec, http://www.miltenyibiotec.com/) adapted for the isolation of in vitro–derived pDCs by adding CD11b-biotin to the negative selection cocktail. Antibodies used in this study were purchased from BioLegend (http://www.biolegend.com/): CD11c-PE, B220-APC, CD11b-FITC; or from Miltenyi Biotec: mPDCA-1-FITC and CD11c-APC. Thioglycolate-elicited macrophages were collected from the peritoneal cavity of mice and cultured at 4×10^5 cells per well in DMEM (with 10% FCS, L-glutamine, and penicillin/streptomycin) for 2 h at 37 °C. Non-adherent cells were removed by washing with cold PBS.

Recombinant DNA and viruses. LCMV-WE strain, originally obtained from F. Lehmann-Grube (Hamburg, Germany), was propagated on L929 cells. MHV A59 was generated from a molecularly cloned cDNA [24] based on the Albany strain of MHV A59. Coronaviruses and recombinant vaccinia viruses were propagated, titrated, and purified as described [24,50,51].

Mutant vaccinia viruses are based on the recombinant vaccina virus vMHV-inf-1 (containing the full-length MHV-A59 cDNA) and were generated using our reverse genetic system as described previously [24]. Briefly, the gene to be mutated was replaced by the *Escherichia coli* guanine-phosphoribosyltransferase (GPT) gene through vaccinia virus–mediated homologous recombination, and GPT-positive clones were selected by three rounds of plaque purification on CV-1 cells in the presence of xanthine, hypoxanthine, and mycophenolic acid (GPT-positive selection) [50]. In a second round, the GPT gene was replaced by the mutated gene, and GPT-negative clones, containing the mutated gene, were selected by three rounds of plaque purification on D980R cells in the presence of 6-thioguanine (GPT-negative seletion) [50]. To construct the recombinant vaccinia virus encoding the MHV-nsp1Δ99 cDNA, the 5′ end of the MHV-A59 cDNA in vMHV-inf-1 was replaced by GPT using the plasmid pRec4. This plasmid is based on pGPT-1 [50], and the GPT gene is flanked to its left by 500 bp of vaccinia DNA and to its right by an internal ribosomal entry sequence (IRES) followed by MHV-A59 nts 952-1315. The GPT-negative selection was carried out using the plasmid pRec15. This plasmid contains 250 bp of vaccinia DNA followed by the bacteriophage T7 RNA polymerase promoter, one G nucleotide, and MHV nts 1–828 linked to MHV nts 928-1315. To replace the MHV-A59 accessory gene 4 in vMHV-inf-1 and vMHV-nsp1Δ99 by a gene encoding a fusion protein of EGFP and the LCMV-derived CTL epitope KAVYNFATC (GP33-GFP) [29], the plasmid pRec8 was used for recombination with vaccinia viruses vMHV-inf-1 and vMHV-nsp1Δ99 . This plasmid contains the GPT gene flanked to its left by MHV nts 27500–27967 and to its right by MHV nts 28265–28700. GPT-negative selection was carried out using the plasmid pRec9. This plasmid contains MHV bp 27500–27967, the GP33-GFP gene, and MHV nts 28265–28700. Further cloning details, plasmid maps, and sequences are available from the authors upon request. Recombinant coronaviruses were rescued from cloned cDNA using purified vaccinia virus DNA as template for the in vitro transcription of recombinant MHV genomes as described [51].

The firefly luciferase (FF-Luc) plasmid for monitoring IFN-β promoter activation (p125-Luc) was kindly provided by Takashi Fujita, Tokyo Metropolitan Institute of Medical Science, Japan [52]. The FF-Luc reporter construct for monitoring ISRE activation (p(9–27)4tkΔ(–39)lucter) [53] was kindly provided by Stephen Goodbourn, St. George's Hospital Medical School, London, UK. The control plasmid pRL-SV40 (Promega, http://www.promega.com/) encodes the renilla luciferase (REN-Luc) gene under control of the constitutive SV40 promoter. The negative control expression plasmid contained the reading frame of the N-terminus of the human MxA protein. To construct the coronavirus nsp1 expression plasmids, the MHV nts 1–951 (pMHV-nsp1), MHV nts 1–902 (pMHV-Δ49), MHV nts 1–851 (pMHV-Δ100), HCoV-229E nts 293–625 (pHCoV-229E-nsp1), and SARS-CoV nts 265–804 (pSARS-CoV-nsp1) were amplified by standard PCR techniques and cloned downstream of a CMV promoter between the SmaI and XhoI sites of the eukaryotic high-level expression plasmid pI.18 (kindly provided by Jim Robertson, National Institute for Biological Standards and Control, Hertfordshire, UK).

Transient transfections and reporter gene assays. Subconfluent cell monolayers of 293 cells seeded in 12-well plates were transfected with 250 ng p125-Luc reporter plasmid, 50 ng pRL-SV40, and 1 μg of expression plasmid in 200 μl of OPTIMEM (Gibco-BRL) containing 3.9 μl of Fugene HD (Roche, http://www.roche.com). At 8 h post transfection, cells were induced with either 0.2 μg of viral ssRNA containing 5′ triphosphates [54] (p125-Luc), 2.5 μg of poly(I:C) (Sigma), or 500 U/ml IFN-α (p(9–27)4tkΔ(–39)lucter), or left uninduced. After an incubation period of 16 h, cells were harvested and lysed in 100 μl of Reporter Lysis Buffer (Promega). An aliquot of 10 μl lysate was used to measure luciferase activity as decribed by the manufacturer (Promega).

Virus infections, determination of virus titers, and liver enzyme values. Mice were injected intraperitoneally or intracranially with indicated pfu of MHV A59 or intravenously with the indicated pfu of LCMV and sacrificed at the indicated time points. Organs were stored at −70 °C until further analysis. Blood was incubated at RT to coagulate, centrifuged, and serum was used for ALT measurements using a Hitachi 747 autoanalyzer (http://www.hitachi.com/). Peritoneal exudates cells (PECs) were isolated from the peritoneal cavity by flushing with 4 ml of ice-cold PBS. MHV titers were determined by standard plaque assay using L929 cells. LCMV titers in the spleens were determined 4 d after intravenous challenge in an LCMV infectious focus assay as previously described [55].

Histology, IFN-α ELISA, IFN-α treatment. Organs were fixed in 4% formalin and embedded in paraffin. Sections were stained with hematoxylin and eosin. Images were acquired using a Leica DMRA microscope (Leica, http://www.leica.com/) with a 25×/0.65 NA objective (total magnification, ×162). Images were processed using Adobe Photoshop (Adobe Systems, http://www.adobe.com). Mouse IFN-α concentration in cell culture supernatants was measured by ELISA (PBL Biomedical Laboratories, http://www.interferonsource.com/) according to the manufacturer's instructions. IFN-α treatment of cells prior to MHV infection was performed using universal type I IFN (IFN-αA/D, Sigma).

Intracellular cytokine staining. Specific ex vivo production of IFN-γ was determined by intracellular cytokine staining. Organs were removed at the indicated time points following infection with recombinant MHV. For intracellular cytokine staining, single cell suspensions of 1×10^6 splenocytes were incubated for 5 h at 37 °C in 96-well round-bottom plates in 200 μl of culture medium containing 25 U/ml IL-2 and 5 μg/ml Brefeldin A (Sigma). Cells were stimulated with phorbolmyristateacetate (PMA, 50 ng/ml) and ionomycin (500 ng/ml) (both purchased from Sigma) as positive control or left untreated as a negative control. For analysis of peptide-specific responses, cells were stimulated with 10^{-6} M GP33 peptide or 10^{-4} M MHV S598 peptide. The percentage of CD8$^+$ T cells producing IFN-γ was determined using a FACSCalibur flow cytometer (BD Biosciences). Both S598 (RCQIFANI) and GP33 (KAVYNFATC) peptides were purchased from Neosystem (http://www.neomps.com/).

Statistical analysis. All statistical analyses were performed with Prism 4.0 (GraphPad Software, http://www.graphpad.com/). Data were analyzed with the paired Student's *t*-test assuming that the values followed a Gaussian distribution. A p-value of < 0.05 was considered significant.

Supporting Information

Accession Numbers

The GenBank (http://www.ncbi.nlm.nih.gov/Genbank/) accession numbers for the viruses and sequences discussed in this paper are HCoV-229E (AF304460), MHV-A59 (AY700211), and SARS-CoV Frankfurt-1 (AY291315).

Acknowledgments

The authors thank Reinhard Maier for critical reading of the manuscript. We thank Philippe Krebs, Divine Makia, Klara Eriksson, Elke Scandella, Simone Miller, Beat Ryf, and Rita de Giuli for helpful discussions and/or excellent technical assistance.

Author contributions. FW, BL, and VT conceived and designed the experiments. RZ, LCB, TK, and GB performed the experiments. All authors analyzed the data. RZ, FW, BL, and VT wrote the paper.

Funding. This work was supported by the Swiss National Science Foundation, the European Commission (SARS-DTV SP22-CT-2004–511064), the Sino-German Center for Research promotion (GZ Nr. 239 (202/12), the Deutsche Forschungsgemeinschaft (We 2616/4), and in part by the US National Institutes of Health (5 R21 AI062246).

Competing interests. The authors have declared that no competing interests exist.

References

1. Weiss SR, Navas-Martin S (2005) Coronavirus pathogenesis and the emerging pathogen severe acute respiratory syndrome coronavirus. Microbiol Mol Biol Rev 69: 635–664.
2. Falsey AR, McCann RM, Hall WJ, Criddle MM, Formica MA, et al. (1997) The "common cold" in frail older persons: Impact of rhinovirus and coronavirus in a senior daycare center. J Am Geriatr Soc 45: 706–711.
3. van der Hoek L, Pyrc K, Berkhout B (2006) Human coronavirus NL63, a new respiratory virus. FEMS Microbiol Rev 30: 760–773.
4. Perlman S, Dandekar AA (2005) Immunopathogenesis of coronavirus infections: Implications for SARS. Nat Rev Immunol 5: 917–927.
5. Rota PA, Oberste MS, Monroe SS, Nix WA, Campagnoli R, et al. (2003) Characterization of a novel coronavirus associated with severe acute respiratory syndrome. Science 300: 1394–1399.
6. Marra MA, Jones SJ, Astell CR, Holt RA, Brooks-Wilson A, et al. (2003) The genome sequence of the SARS-associated coronavirus. Science 300: 1399–1404.
7. Fouchier RA, Kuiken T, Schutten M, van Amerongen G, van Doornum GJ, et al. (2003) Aetiology: Koch's postulates fulfilled for SARS virus. Nature 423: 240.
8. Li W, Shi Z, Yu M, Ren W, Smith C, et al. (2005) Bats are natural reservoirs of SARS-like coronaviruses. Science 310: 676–679.
9. Plotkin SA (2005) Vaccines: Past, present and future. Nat Med 11: S5–S11.
10. Lambert PH, Liu M, Siegrist CA (2005) Can successful vaccines teach us how to induce efficient protective immune responses? Nat Med 11: S54–S62.
11. Moore ZS, Seward JF, Lane JM (2006) Smallpox. Lancet 367: 425–435.
12. Racaniello VR (2006) One hundred years of poliovirus pathogenesis. Virology 344: 9–16.
13. Lefeuvre A, Marianneau P, Deubel V (2004) Current assessment of yellow fever and yellow fever vaccine. Curr Infect Dis Rep 6: 96–104.
14. Pulendran B, Ahmed R (2006) Translating innate immunity into immunological memory: Implications for vaccine development. Cell 124: 849–863.
15. Haller O, Kochs G, Weber F (2006) The interferon response circuit: Induction and suppression by pathogenic viruses. Virology 344: 119–130.
16. Richt JA, Lekcharoensuk P, Lager KM, Vincent AL, Loiacono CM, et al. (2006) Vaccination of pigs against swine influenza viruses by using an NS1-truncated modified live-virus vaccine. J Virol 80: 11009–11018.
17. Talon J, Salvatore M, O'Neill RE, Nakaya Y, Zheng H, et al. (2000) Influenza A and B viruses expressing altered NS1 proteins: A vaccine approach. Proc Natl Acad Sci U S A 97: 4309–4314.
18. Kamitani W, Narayanan K, Huang C, Lokugamage K, Ikegami T, et al. (2006) Severe acute respiratory syndrome coronavirus nsp1 protein suppresses host gene expression by promoting host mRNA degradation. Proc Natl Acad Sci U S A 103: 12885–12890.
19. Kopecky-Bromberg SA, Martinez-Sobrido L, Frieman M, Baric RA, Palese P (2007) Severe acute respiratory syndrome coronavirus open reading frame (ORF) 3b, ORF 6, and nucleocapsid proteins function as interferon antagonists. J Virol 81: 548–557.
20. Ye Y, Hauns K, Langland JO, Jacobs BL, Hogue BG (2007) Mouse hepatitis coronavirus A59 nucleocapsid protein is a type I interferon antagonist. J Virol 81: 2554–2563
21. Ziebuhr J (2005) The coronavirus replicase. Curr Top Microbiol Immunol 287: 57–94.
22. Snijder EJ, Bredenbeek PJ, Dobbe JC, Thiel V, Ziebuhr J, et al. (2003) Unique and conserved features of genome and proteome of SARS-coronavirus, an early split-off from the coronavirus group 2 lineage. J Mol Biol 331: 991–1004.
23. Almeida MS, Johnson MA, Herrmann T, Geralt M, Wuthrich K (2007) Novel {beta}-barrel fold in the NMR structure of the replicase nonstructural protein 1 from the SARS coronavirus. J Virol 81: 3151–61.
24. Coley SE, Lavi E, Sawicki SG, Fu L, Schelle B, et al. (2005) Recombinant mouse hepatitis virus strain A59 from cloned, full-length cDNA replicates to high titers in vitro and is fully pathogenic in vivo. J Virol 79: 3097–3106.
25. Brockway SM, Denison MR (2005) Mutagenesis of the murine hepatitis virus nsp1-coding region identifies residues important for protein processing, viral RNA synthesis, and viral replication. Virology 340: 209–223.
26. Freigang S, Probst HC, van den Broek M (2005) DC infection promotes antiviral CTL priming: The "Winkelried" strategy. Trends Immunol 26: 13–18.
27. Cervantes-Barragan L, Zust R, Weber F, Spiegel M, Lang KS, et al. (2007) Control of coronavirus infection through plasmacytoid dendritic-cell-derived type I interferon. Blood 109: 1131–1137.
28. Muller U, Steinhoff U, Reis LF, Hemmi S, Pavlovic J, et al. (1994) Functional role of type I and type II interferons in antiviral defense. Science 264: 1918–1921.
29. Oehen S, Junt T, Lopez-Macias C, Kramps TA (2000) Antiviral protection after DNA vaccination is short lived and not enhanced by CpG DNA. Immunology 99: 163–169.
30. Graham RL, Sims AC, Brockway SM, Baric RS, Denison MR (2005) The nsp2 replicase proteins of murine hepatitis virus and severe acute respiratory syndrome coronavirus are dispensable for viral replication. J Virol 79: 13399–13411.
31. Putics A, Filipowicz W, Hall J, Gorbalenya AE, Ziebuhr J (2005) ADP-ribose-1″-monophosphatase: A conserved coronavirus enzyme that is dispensable for viral replication in tissue culture. J Virol 79: 12721–12731.
32. Sperry SM, Kazi L, Graham RL, Baric RS, Weiss SR, et al. (2005) Single-amino-acid substitutions in open reading frame (ORF) 1b-nsp14 and ORF 2a proteins of the coronavirus mouse hepatitis virus are attenuating in mice. J Virol 79: 3391–3400.
33. McCray PB Jr, Pewe L, Wohlford-Lenane C, Hickey M, Manzel L, et al. (2007) Lethal infection of K18-hACE2 mice infected with severe acute respiratory syndrome coronavirus. J Virol 81: 813–821.
34. Roberts A, Deming D, Paddock CD, Cheng A, Yount B, et al. (2007) A mouse-adapted SARS-coronavirus causes disease and mortality in BALB/c Mice. PLoS Pathog 3: e5. doi:10.1371/journal.ppat.0030005
35. Tseng CT, Huang C, Newman P, Wang N, Narayanan K, et al. (2007) Severe acute respiratory syndrome coronavirus infection of mice transgenic for the human Angiotensin-converting enzyme 2 virus receptor. J Virol 81: 1162–1173.
36. Lassnig C, Sanchez CM, Egerbacher M, Walter I, Majer S, et al. (2005) Development of a transgenic mouse model susceptible to human coronavirus 229E. Proc Natl Acad Sci U S A 102: 8275–8280.
37. Cheung CY, Poon LL, Ng IH, Luk W, Sia SF, et al. (2005) Cytokine responses in severe acute respiratory syndrome coronavirus-infected macrophages in vitro: Possible relevance to pathogenesis. J Virol 79: 7819–7826.
38. de Groot-Mijnes JD, van Dun JM, van der Most RG, de Groot RJ (2005) Natural history of a recurrent feline coronavirus infection and the role of cellular immunity in survival and disease. J Virol 79: 1036–1044.
39. Law HK, Cheung CY, Ng HY, Sia SF, Chan YO, et al. (2005) Chemokine up-regulation in SARS-coronavirus-infected, monocyte-derived human dendritic cells. Blood 106: 2366–2374.
40. Thiel V, Karl N, Schelle B, Disterer P, Klagge I, et al. (2003) Multigene RNA vector based on coronavirus transcription. J Virol 77: 9790–9798.
41. Turner BC, Hemmila EM, Beauchemin N, Holmes KV (2004) Receptor-dependent coronavirus infection of dendritic cells. J Virol 78: 5486–5490.
42. Zhou H, Perlman S (2006) Preferential infection of mature dendritic cells by mouse hepatitis virus strain JHM. J Virol 80: 2506–2514.
43. Enjuanes L, Sola I, Alonso S, Escors D, Zuniga S (2005) Coronavirus reverse genetics and development of vectors for gene expression. Curr Top Microbiol Immunol 287: 161–197.
44. de Haan CA, Masters PS, Shen X, Weiss S, Rottier PJ (2002) The group-specific murine coronavirus genes are not essential, but their deletion, by reverse genetics, is attenuating in the natural host. Virology 296: 177–189.
45. Haijema BJ, Volders H, Rottier PJ (2004) Live, attenuated coronavirus vaccines through the directed deletion of group-specific genes provide protection against feline infectious peritonitis. J Virol 78: 3863–3871.
46. Ortego J, Sola I, Almazan F, Ceriani JE, Riquelme C, et al. (2003) Transmissible gastroenteritis coronavirus gene 7 is not essential but influences in vivo virus replication and virulence. Virology 308: 13–22.
47. Ortego J, Escors D, Laude H, Enjuanes L (2002) Generation of a replication-competent, propagation-deficient virus vector based on the transmissible gastroenteritis coronavirus genome. J Virol 76: 11518–11529.
48. Curtis KM, Yount B, Baric RS (2002) Heterologous gene expression from transmissible gastroenteritis virus replicon particles. J Virol 76: 1422–1434.
49. Eriksson KK, Makia D, Maier R, Cervantes L, Ludewig B, et al. (2006) Efficient transduction of dendritic cells using coronavirus-based vectors. Adv Exp Med Biol 581: 203–206.
50. Hertzig T, Scandella E, Schelle B, Ziebuhr J, Siddell SG, et al. (2004) Rapid identification of coronavirus replicase inhibitors using a selectable replicon RNA. J Gen Virol 85: 1717–1725.
51. Thiel V, Herold J, Schelle B, Siddell SG (2001) Infectious RNA transcribed in vitro from a cDNA copy of the human coronavirus genome cloned in vaccinia virus. J Gen Virol 82: 1273–1281.
52. Yoneyama M, Suhara W, Fukuhara Y, Fukuda M, Nishida E, et al. (1998) Direct triggering of the type I interferon system by virus infection:

Activation of a transcription factor complex containing IRF-3 and CBP/p300. EMBO J 17: 1087–1095.
53. King P, Goodbourn S (1998) STAT1 is inactivated by a caspase. J Biol Chem 273: 8699–8704.
54. Pichlmair A, Schulz O, Tan CP, Naslund TI, Liljestrom P, et al. (2006) RIG-I-mediated antiviral responses to single-stranded RNA bearing 5'-phosphates. Science 314: 997–1001.
55. Battegay M, Cooper S, Althage A, Banziger J, Hengartner H, et al. (1991) Quantification of lymphocytic choriomeningitis virus with an immunological focus assay in 24- or 96-well plates. J Virol Methods 33: 191–198.

7 Unpublished data

7.1 Introduction

With genome sizes of about 30 kb coronaviruses have the largest genomes of all known RNA viruses. RNA viruses have high error rates, and the resulting quasispecies may aid survival of the virus population in the presence of selective pressure. Therefore, RNA viruses have been proposed to replicate and evolve at the maximum limit of genetic variability. The replication of RNA virus genomes occurs within limits, concurrently producing quasispecies diversity important for adaptation to changing environments, while simultaneously preventing population extinction due to excessive mutation (202, 270). This precarious balance is thought to be maintained by interplay between RNA polymerase fidelity and error repair by RNA recombination since proofreading activities have not been identified in RNA viruses. For MHV a mutation rate of 2.5×10^{-6} has been calculated, which is, in comparison to other RNA viruses very low (75). It has been proposed that coronaviruses may have acquired a proofreading activity, possibly associated with nsp14 exoribonuclease activity that may be critical for genome expansion up to 30 kb (94, 232). Indeed, it has been shown, that a mutation in a conserved site of MHV nsp14 leads to decreased fidelity in replication (75). The mechanism on how nsp14 leads to increased fidelity remains to be elucidated, however it is likely that ExoN activity may directly mediate hydrolysis of an incorrect nucleotide from the 3' end of the nascent RNA chain, similar to the role of DE-D-D ExoN proofreading domains or subunits of DNA polymerases (18, 184). Mutations in HCoV-229E even led to a lethal phenotype (181). It is unclear why infectious ExoN mutants were recovered for MHV but not for HCoV-229E but it may be that the defects exceed the threshold for recovery of recombinant HCoV-229E. Besides nsp14 an additional ribonuclease (nsp15; endoribonuclease NendoU) has been reported for coronaviruses (232), however knowledge is up to date very limited. It is known, that mutations in the catalytic pocket have little effect on kinetics *in vitro* (134). Besides the above mentioned ribonuclease activities, coronaviruses express a third RNA-processing protein encoded in ORF1b, termed nsp16. Nsp16 has been predicted to possess 2'-O-methyltransferase activity and very recently this activity has been demonstrated for the feline coronavirus nsp16. (63, 85, 232, 272).

Although nsp14, nsp15, and nsp16 are part of the replicase complex, it has been shown at least for nsp14 and nsp15, that their ribonuclease activities are not strictly required for RNA synthesis. Therefore it is conceivable that these enzymes may play a role in host-pathogen interactions. To study the roles of nsp14-16 in virus replication we constructed MHV mutants bearing mutations in the respective conserved regions (75, 134, 222, 232, 237).

7.2 Results

7.2.1 The role of nsp14 in viral replication

In order to study functions of nsp14 for viral replication *in vitro* and *in vivo*, we aimed to construct recombinant viruses bearing mutations in conserved regions of nsp14 (Fig. 4A). Both conserved regions targeted by homologous recombination could be mutated and progeny virus rescued. Nsp14-mut1 was designed to harbor a single nucleotide mutation (C to T) at base 19401 thereby causing a substitution of a tyrosine at position 6398 through a histidine. This mutation has previously been associated with a pronounced attenuation *in vivo* but does not affect virus growth in tissue culture (75, 237) (Fig. 4B). Nsp14-mut2 bears 4 point mutations (A18427C, T18428A, A18433C, and A18434T) leading to two aa substitutions (Asp to Ala, and Glu to Ala) at position 6072 and 6074, respectively. These aa substitutions abolish the exonuclease activity (75, 237) and growth of the recombinant virus termed nsp14-mut2 was reduced in tissue culture (Fig. 4B). The differential growth kinetics of the two mutants suggest that nsp14 may actually possess two domains with distinctive functions. To further elucidate the important function(s) of nsp14 for virus replication and viral pathogenicity *in vivo*, 129Sv mice were infected intraperitoneally with different doses of wild-type MHV or MHV-nsp14-mut1. Both viruses replicated in the spleen, whereby MHV-nsp14-mut1 titers were consistently lower than wild-type virus titers (Figure 4C). Wild-type, but not mutant virus, was detectable in the liver at low and high dose (50 pfu and 5,000 pfu, respectively) (Figure 4C). The attenuation of the nsp14 mutant is also reflected in the low liver damage, measured as alanine 2-oxoglutarate-aminotransferase (ALT) levels in serum. To investigate the potential influence of nsp14 on innate immune responses, we infected type I IFN receptor-deficient ($IFNAR^{-/-}$) mice (186) with 5000 pfu of wild-type MHV or MHV-nsp14-mut1. Infection of $IFNAR^{-/-}$ mice with wild-type MHV led to high titers in all tested organs, indicating that signals transmitted via the IFNAR are crucial for preventing

uncontrolled spread of the virus (42). Replication of MHV-nsp14-mut1 in IFNAR$^{-/-}$ mice was partially restored and peak titers of approximately 10^6 pfu/g tissue have been detected in spleen and liver (Fig. 4D). Surprisingly, the mutant virus could finally be controlled in IFNAR$^{-/-}$ mice, presumably by the onset of adaptive immune responses around day 5 post infection (17).

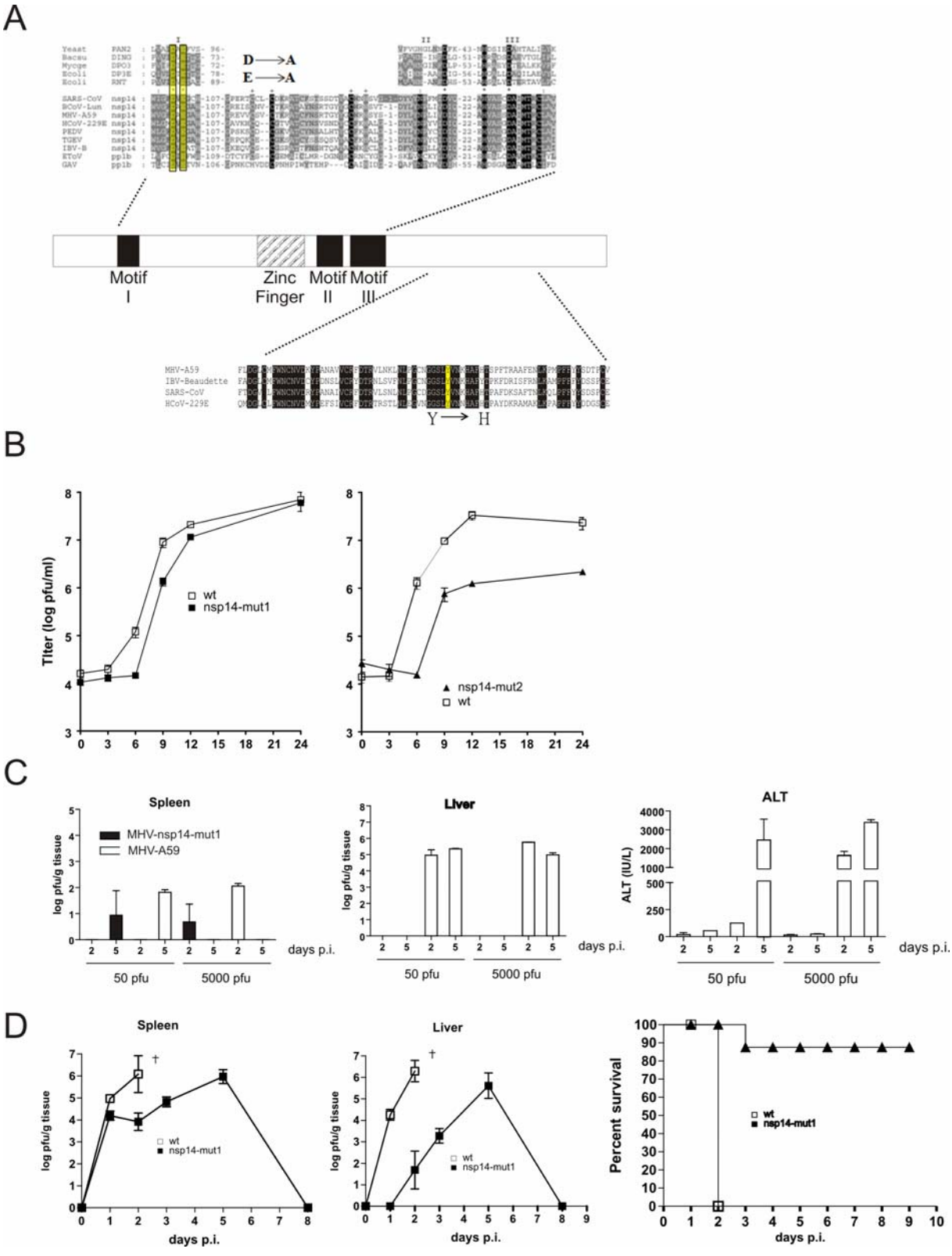

Fig. 4: Sequence alignment of nsp14 (A) and growth properties of recovered nsp14 mutant viruses (B-D) (A) Sequence alignment of nsp14**.** Mutated regions are highlighted in yellow and aa substitutions are denoted with an arrow. The upper panel shows the mutations introduced in MHV-nsp14-mut1, the lower one shows mutations introduced into MHV-nsp14-

mut2. Figure adapted from Snijder et al. (231). (B) Single step kinetics of MHV-nsp14-mut1 and MHV-nsp14-mut2, respectively in 17Cl1 cells. (C) 129Sv mice were infected with the indicated dose of MHV-nsp14-mut1 and viral titers in spleen and liver and ALT values were determined at the indicated time points p.i. (D) IFNAR$^{-/-}$ 129Sv mice were infected i.p. with 5000 pfu of MHV-A59 or MHV-nsp14-mut1 and viral titers in spleens and livers and the survival of mice were determined. † denotes death of mice.

7.2.2 The role of nsp15 in viral replication

To investigate the role of nsp15 in virus replication, we decided to inactivate the nsp15-encoded endonuclease activity (134). A highly conserved histidine at position 6781 was substituted by an alanine (Fig. 5A). As described before we found that the nsp15 mutant showed little defect in growth in tissue culture (Fig. 5B). We have commenced further experiments to elucidate if this mutation has an effect on viral pathogenicity.

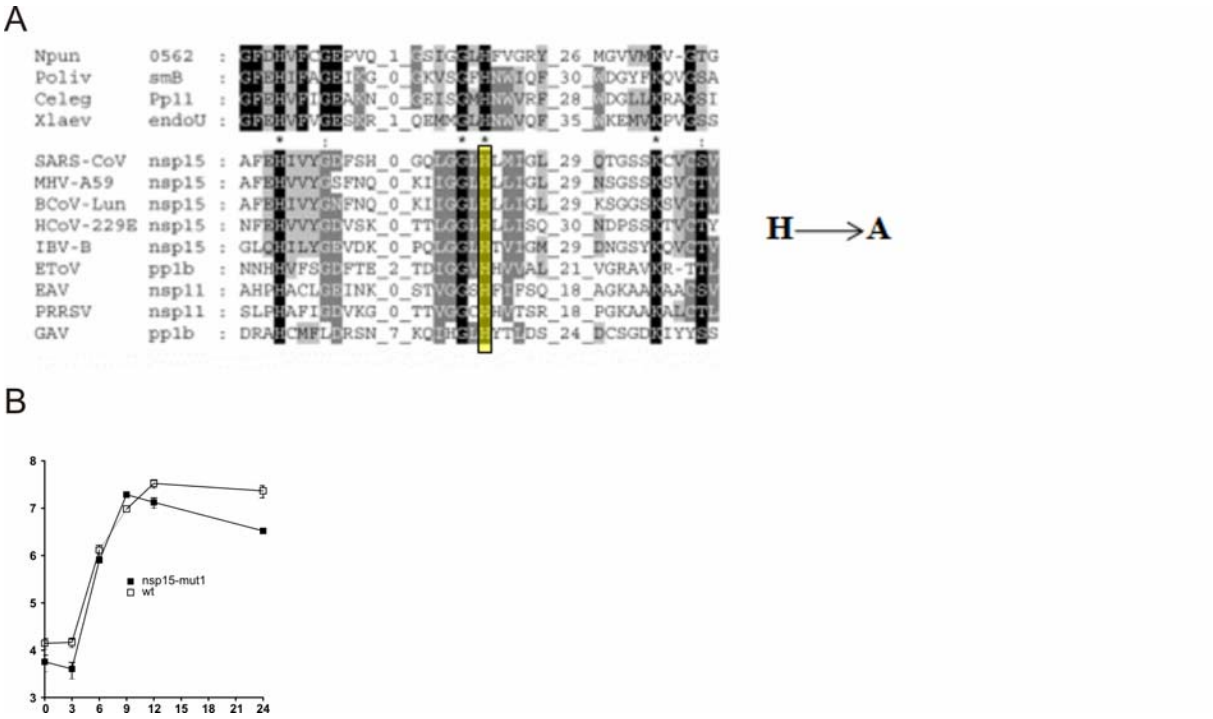

Fig. 5: Sequence alignment of nsp15 (A) and growth properties of recovered virus

(A) Sequence alignment of nsp15**.** Mutated regions are highlighted in yellow and aa substitutions are denoted with an arrow. Figure adapted from Snijder et al. (231). (B) Single step kinetics of MHV-nsp15 in 17Cl1 cells.

7.2.3 The role of nsp16 in viral replication

The third RNA modifying enzyme encoded by the coronavirus genome is the 2'-O RNA methyltransferase nsp16. We were interested to investigate the role of this enzyme in viral replication and generated two mutants harboring aa substitutions at position 6890 (proline to serine) or at position 7032 (leucine to proline) (Fig. 6A). These mutations have previously been associated with a temperature-sensitivity displaying an RNA(-) phenotype, i.e. with no detectable RNA synthesis at the restrictive temperature (222). The reconstructed ts mutant viruses grew to comparable levels as wt-A59 in tissue culture at 33° C and 37° C. However, replication is abolished at the restrictive temperature (Fig. 6B). Future studies are planned to elucidate if the observed ts phenotype is associated with the 2'-O methyltransferase activity of nsp16.

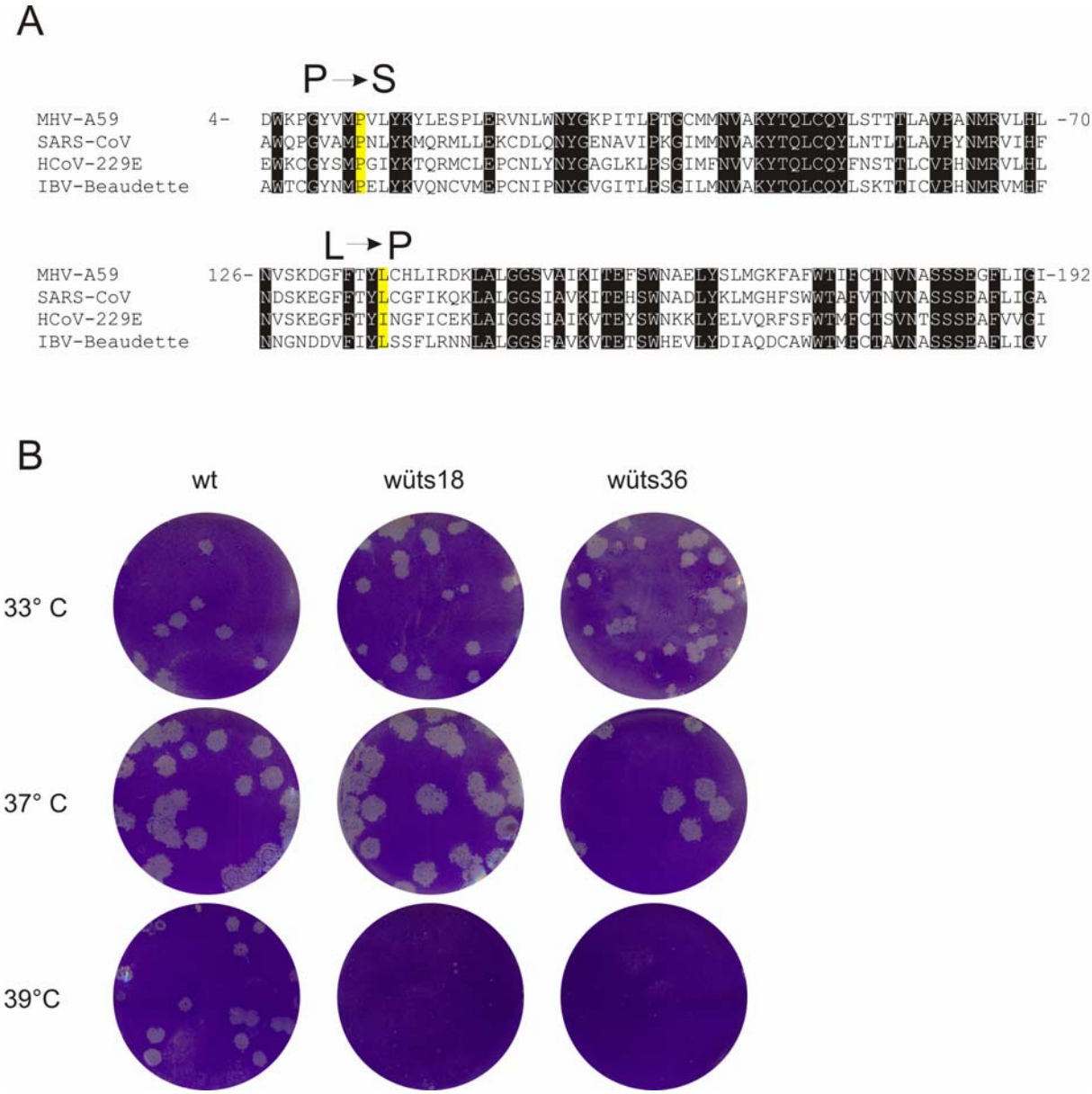

Fig. 6: Sequence alignment of nsp16 (A) and characterization of nsp16 temperature sensitive mutants

(A Sequence alignment of nsp16. Mutated regions are highlighted in yellow and aa substitutions are denoted with an arrow. The upper panel shows nsp16 mutant wüts18, whereas the lower panel shows nsp16 mutant wüts36 (B) Confluent L929 cells were infected with the indicated virus, incubated for 3 h at 33° C, washed with PBS, overlayed with a 1:1 mixture of 2% Avicel and 2xDMEM and incubated 28 h (39° C) or 48 h (33° C and 37° C). The overlay was then removed and cells were stained with crystal violet.

8 Discussion

8.1 Summary of own findings

The first article provides new insight into the genetic interaction between an essential pseudoknot in the MHV 3' UTR, replicase gene products nsp8 and nsp9, and the extreme 3' end of the genome. The analyses of a poorly replicating and genetically instable mutant virus (Alb391) containing a 6 nt insertion in loop 1 of the pseudoknot revealed a number of second site suppressor mutations that can compensate for the growth defect mediated by the initial 6 nt insertion. These second site mutations were found in nsp8 or nsp9, or at the penultimate nucleotide (A to G) at the extreme 3'-end of the MHV genome. Our data suggest, for the first time, an interaction of RNA-binding replicase gene products with *cis*-acting elements of the MHV 3'UTR. A new model of the secondary structure of the 3'UTR and how it might function in the initiation of minus strand RNA synthesis has been proposed (300).

The second article describes the importance of type I IFNs on MHV replication *in vitro*. We could demonstrate that type I IFNs are absolutely essential to combat MHV infection and furthermore, that pDCs are the major source of IFN-α early after infection. pDC depletion diminished IFN-α expression, allowed MHV to rapidly spread to multiple organs and increased the severity of MHV-induced acute viral hepatitis.

The third article provides evidence that nsp1 is an important pathogenicity factor. MHV encoding a truncated form of nsp1 was still able to replicate in tissue culture and in primary cells but was attenuated in the natural host. This attenuation was abolished in mice lacking the type I IFN receptor demonstrating that nsp1 interferes with host innate immune responses. Our finding, that the nsp1 mutant virus grew to high titers *in vitro* but was still able to replicate in secondary lymphoid organs and in professional antigen-presenting cells, such as macrophages and dendritic cells, led to the hypothesis that this mutant serves as an ideal attenuated vaccine candidate. Indeed, MHV-nsp1Δ99 encoding the immunodominant cytotoxic T lymphocyte (CTL) epitope (KAVYNFATC) of the lymphocytic choriomeningitis virus (LCMV) and the enhanced green fluorescent protein (GP33-GFP) fully protected against homologous MHV and partially against heterologous LCMV challenge (300).

The unpublished data show that nsp14 and nsp15 are dispensable on viral growth *in vitro*. We could confirm that MHV-nsp14-mut1 is greatly attenuated *in vivo*, suggesting that nsp14 may play an important role in the natural host. Nsp16 seems to be essential for viral replication, since temperature sensitive mutants do not show any replication at the restrictive temperature (39°C). Further studies are in progress to assess if the growth defect is associated with impaired methyltransferase activity.

8.2 Interactions of replicase gene products with 3' UTR

Initiation of coronavirus negative strand RNA synthesis occurs at the 3' end of the genomic RNA. However, it was still elusive, which 3'-*cis*-acting elements and which replicase gene products play a role in this process. In the work presented in the thesis we analyzed revertants of a highly defective MHV mutant, Alb391, containing a particular insertion, AACAAG, in loop 1 of the MHV 3'UTR pseudoknot. Three types of revertants were repeatedly identified. First, so-called "true" revertants had deleted or altered the 6 nt insertion. Second, we also found two types of second-site revertants mapping to two distinct regions of the genome. One class was represented by a single nucleotide change at the penultimate nucleotide upstream the 3'-poly(A) tail (A to G) and the second class of second-site revertants encoded point mutations in nsp8 or nsp9. These findings corroborate recent reports, where it has been shown that nsp8 and nsp9 have RNA-binding activity (76, 246). In addition nsp8 has been shown to possess RdRp activity that mediates the ability to synthesize short RNAs (120). Therefore, nsp8 has been proposed to function as a primase for the canonical coronavirus RdRp (nsp12). Despite the demonstrated RNA-binding activity of nsp8 and nsp9 it is currently not clear if RNA-binding is sequence specific. Our data strongly support the idea that MHV nsp8 and nsp9 interact with the pseudoknot of the 3' UTR. Based on our results we propose a new model for the initiation of negative strand synthesis that also includes the putative primase activity of nsp8 and a putative role for the molecular switch that has been previously proposed to consist of the 3'-UTR buldged stem loop and the adjacent pseudoknot structure (90, 120, 301).

In addition to the newly proposed model of RNA synthesis initiation we could demonstrate that only a very small part of the 3' UTR is absolutely required for RNA synthesis. Based on m-fold structural predictions we could pin down the essential

regions to no more than 160 nt of the 3' UTR, nearly discarding half of the 3' UTR. Our predictions were further supported by a viable MHV mutant ΔHVR3, where bases 30 to 170 have been discarded. Interestingly, the deleted region encompasses *in vitro* binding sites for a number of cell proteins including PTB, hnRNP A1, and heat shock proteins, previously reported to be important for viral replication. Our results demand for reconsideration of conclusions obtained from a previous study that the last 45 to 55 nts of the genome are required (165). Many mechanistic details of the initiation of negative-strand RNA remain to be elucidated. However, we hope this work will provide a starting point for further studies.

8.3 Coronavirus interaction with the type I IFN system

The innate immune response against coronavirus such as MHV has not yet been sufficiently characterized. Several studies could demonstrate that pretreatment with recombinant IFN-β or IFN-α can inhibit SARS-CoV replication (43, 238, 291) and diminish the severity of the disease (101, 167). However, neither peripheral-blood mono-nuclear cells, nor macrophages, nor monocyte-derived DCs respond to coronavirus infection with a significant IFN-α production (58, 130, 155, 212, 283, 289). In the presented work (42) we could demonstrate that pDCs can respond to coronaviral infection with a swift IFN induction and that TLR7 acts as the sensor for coronavirus RNA. The importance of pDCs was shown since widespread replication in various nonlymphoid organs, and the associated organ damage, is efficiently kept in check through pDC-derived type I IFNs. A characteristic of pDCs is the constitutively high expression of IFN regulatory factor-7 (IRF7) (115, 125), which directly stimulates IFN-α expression, independently of an IFN-β-mediated feedback loop (11).

Several members of the *Coronaviridae* family, including SARS-CoV and MHV, have recently been shown to avoid recognition by cytoplasmic pattern recognition receptors (PRR) such as RigI, Mda5 and TLR3 (42, 269, 292). All these proteins have been demonstrated to recognize viral RNA (1, 116, 136, 269) and respond with a subsequent IFN induction. How coronavirus shields itself from the recognition through these PRRs remains to be determined. We believe that coronavirus avoids

recognition through replication in a protected enviroment, the endoplasmatic reticulum-derived double membrane vesicles (97, 204).

8.4 The role of nsp1 in viral replication

Nsp1 is the first protein to be expressed in the coronavirus life cycle of group I and group II coronaviruses and is therefore expected to play an important role in viral replication. Surprisingly, large parts of the C-terminal end can be deleted without effect on growth *in vitro* indicating a different role of this enzyme (32). Within the sequence encoding for the N-terminal region of nsp1 there are most likely essential *cis*-acting elements required for replication. For MHV and BCoV DI RNAs it has been shown that parts of the nsp1-coding region play a pivotal role as *cis*-acting elements in the replication (34). We could show that nsp1 plays a critical role in virus-host interactions. When nsp1 was expressed *in vitro* together with a reporter plasmid encoding the luciferase under the control of the IFN-β, ISRE or the constitutive active SV40 promoter, the expression of the reporter diminished significantly. This was not the case when a truncated form of MHV nsp1 was expressed. These results are in accordance with a report by Kamitani et al. (133). Their suggestion that SARS-CoV nsp1 may play a role in SARS-CoV pathogenesis by promoting host cell mRNA degradation received support through our analysis of an MHV nsp1 mutant in a murine model. How the SARS-CoV (and probably MHV) nsp1 promotes the degeneration only of host cell RNA without affecting viral RNA still remains to be investigated.

IFN-α/β in addition to playing a key role in the innate control of virus replication, have been shown to potently enhance immune responses (156, 157, 206). Therefore virus have developed different strategies to evade the IFN activity, including sequestration of danger signals, targeting specific components of the IFN system such as members of the IFN regulatory factor (IRF) family or components of the JAK-STAT signaling pathway. For coronavirus a protein fulfilling one of these functions has not been described. Our results clearly demonstrate that nsp1 mainly affects IFN signaling pathways or other downstream events rather than directly the induction of IFN-α expression. pDCs infected with MHV-nsp1Δ99 produced the same amount of IFN-α as did wild-type MHV-infected pDCs. Macrophages and cDCs did not express

significant amounts of IFN-α with wild-type MHV or MHV-nsp1Δ99. However, treatment of macrophages with IFN-α revealed a more efficient reduction of MHV-nsp1Δ99 replication compared to wild-type MHV. This reduction could not be seen in pre-treated cDCs indicating that IFN has mainly a pivotal role on macrophages. This observation received support in a recent work from our laboratory (Cervantes et al. JEM, in revision) where we showed that IFNAR expression on macrophages and cDCs is essential to combat MHV infection in mice, whereas mice lacking the IFNAR on B-cells or T-cells did not show such serious effects.

In vivo experiments demonstrated the pivotal role of nsp1 on viral pathogenicity. Wild type mice infected with MHV-nsp1Δ99 did not show any signs of disease and progeny virus in the liver could only be isolated when high doses of MHV-nsp1Δ99 were applied. Interestingly the mutant virus retained the potential to replicate in the spleen. Even when the mutant virus was applied intracranially the mice survived, although a severe demyelination could be observed. The strong attenuation of MHV-nsp1Δ99 was abolished in mice lacking the IFNAR. $IFNAR^{-/-}$ mice were highly permissive for the mutant virus and organ titers almost reached those of wild type MHV infected $IFNAR^{-/-}$ mice. Nevertheless it should be noted that the mice infected with MHV-nsp1Δ99 survived longer than mice infected with wild-type MHV and the ALT values increased only late after infection. Therefore, further studies are required to precisely define the molecular targets and function(s) of coronavirus nsp1.

Nsp1 has been suggested as a group specific marker to differentiate group I coronaviruses from group II coronaviruses however our expression data denote a functional relationship between nsp1 molecules from both coronaviruses groups (232). Despite the apparent lack of any sequence homology (5, 232) nsp1 of HCoV-229E, a group I member, may represent a functional correlate to the nsp1 of group IIa/IIb coronaviruses. It would be interesting to address this question in future studies and recent progress in the establishment of mouse models for HCoV-229E (153) will enable research on this topic.

The modification of a pathogenicity factor represents and attractive attenuation strategy for the rational design of live coronavirus vaccines. MHV-nsp1Δ99 grows to high titers in cell culture, thereby facilitating vaccine production. It generates a strong, long lasting immune response that mediates protection against viral challenge. Because of its pronounced tropism for professional antigen presenting cells and the

induction of strong cytotoxic T cell (CTL) responses coronaviruses might be promising vectors for the expression of heterologous antigens (80, 81). Indeed experiments performed in our laboratory demonstrate, that coronaviruses have a high cloning capacity allowing the expression of several antigens and additional cytokines which boost the immune response. MHV-based vectors containing deletions of all accessory genes and the deletion of the structural envelope protein E has resulted in propagation-deficient, replication-competent vectors. The combination of these deletions together with the herein described truncation of the nsp1 protein, would lead to a vector considered to be “recombination proof”, because the deletions are located at opposite genomic regions. We therefore suggest that such a vector would be particular safe with the potential to express multiple heterologous antigens. In future studies it will be important to transfer this knowledge to the generation of vaccines for humans.

Taken together we describe a novel type of coronavirus vaccines based on impaired function of the replicase gene nsp1. We believe that our approach is applicable to most, if not all mammalian coronaviruses. This will enable the development of long-desired vaccines for important human and animal coronavirus-induced diseases.

9 Future perspectives

Reverse genetic systems have greatly facilitated the analysis of coronavirus replication at the molecular level. Much progress has been made in understanding the role of particular replicase gene products and *cis*-acting elements in viral replication. For a number of replicase-encoded gene products enzymatic functions have been predicted by sequence comparison and/or demonstrated by biochemical studies. Reverse genetics, as well as classical “forward” genetics, are currently used to place these functions into distinct processes within the viral replication cycle. Interestingly, some replicase gene products have been shown to be dispensable for viral RNA synthesis, and therefore, several questions concerning the role of these replicase gene products have arisen:

- To which extend do replicase gene products contribute to host cell tropism and viral pathogenicity?
- Are replicase proteins specifically altering host cell gene expression, and how are specific cellular signaling pathways blocked or induced?
- Are replicase-encoded pathogenicity factors conserved amongst all coronaviruses or are some of them virus- and/or host specific?

To answer these questions it will be important to combine bioinformatic, biochemical and structural approaches with classical and reverse genetic techniques in order to produce and characterize informative virus mutants. Furthermore, these studies have to be expanded to the analysis of virus-host interactions on the cellular level, but also on the level of the host organism. Therefore, we expect that MHV as a mouse pathogen will continue to provide an excellent model to study coronavirus replication and pathogenesis as both, the virus and the host can be genetically modified.

10 References

1. **Alexopoulou, L., A. C. Holt, R. Medzhitov, and R. A. Flavell.** 2001. Recognition of double-stranded RNA and activation of NF-kappaB by Toll-like receptor 3. Nature **413:**732-8.
2. **Almazan, F., M. L. Dediego, C. Galan, D. Escors, E. Alvarez, J. Ortego, I. Sola, S. Zuniga, S. Alonso, J. L. Moreno, A. Nogales, C. Capiscol, and L. Enjuanes.** 2006. Construction of a severe acute respiratory syndrome coronavirus infectious cDNA clone and a replicon to study coronavirus RNA synthesis. J Virol **80:**10900-6.
3. **Almazan, F., C. Galan, and L. Enjuanes.** 2004. The nucleoprotein is required for efficient coronavirus genome replication. J Virol **78:**12683-8.
4. **Almazan, F., J. M. Gonzalez, Z. Penzes, A. Izeta, E. Calvo, J. Plana-Duran, and L. Enjuanes.** 2000. Engineering the largest RNA virus genome as an infectious bacterial artificial chromosome. Proc Natl Acad Sci U S A **97:**5516-21.
5. **Almeida, M. S., M. A. Johnson, T. Herrmann, M. Geralt, and K. Wuthrich.** 2007. Novel beta-barrel fold in the nuclear magnetic resonance structure of the replicase nonstructural protein 1 from the severe acute respiratory syndrome coronavirus. J Virol **81:**3151-61.
6. **Anand, K., G. J. Palm, J. R. Mesters, S. G. Siddell, J. Ziebuhr, and R. Hilgenfeld.** 2002. Structure of coronavirus main proteinase reveals combination of a chymotrypsin fold with an extra alpha-helical domain. Embo J **21:**3213-24.
7. **Arbely, E., Z. Khattari, G. Brotons, M. Akkawi, T. Salditt, and I. T. Arkin.** 2004. A highly unusual palindromic transmembrane helical hairpin formed by SARS coronavirus E protein. J Mol Biol **341:**769-79.
8. **Asselin-Paturel, C., A. Boonstra, M. Dalod, I. Durand, N. Yessaad, C. Dezutter-Dambuyant, A. Vicari, A. O'Garra, C. Biron, F. Briere, and G. Trinchieri.** 2001. Mouse type I IFN-producing cells are immature APCs with plasmacytoid morphology. Nat Immunol **2:**1144-50.
9. **Banner, L. R., J. G. Keck, and M. M. Lai.** 1990. A clustering of RNA recombination sites adjacent to a hypervariable region of the peplomer gene of murine coronavirus. Virology **175:**548-55.
10. **Baranov, P. V., C. M. Henderson, C. B. Anderson, R. F. Gesteland, J. F. Atkins, and M. T. Howard.** 2005. Programmed ribosomal frameshifting in decoding the SARS-CoV genome. Virology **332:**498-510.
11. **Barchet, W., M. Cella, B. Odermatt, C. Asselin-Paturel, M. Colonna, and U. Kalinke.** 2002. Virus-induced interferon alpha production by a dendritic cell subset in the absence of feedback signaling in vivo. J Exp Med **195:**507-16.
12. **Baric, R. S., K. Fu, M. C. Schaad, and S. A. Stohlman.** 1990. Establishing a genetic recombination map for murine coronavirus strain A59 complementation groups. Virology **177:**646-56.
13. **Baric, R. S., and A. C. Sims.** 2005. Development of mouse hepatitis virus and SARS-CoV infectious cDNA constructs. Curr Top Microbiol Immunol **287:**229-52.
14. **Barretto, N., D. Jukneliene, K. Ratia, Z. Chen, A. D. Mesecar, and S. C. Baker.** 2006. Deubiquitinating activity of the SARS-CoV papain-like protease. Adv Exp Med Biol **581:**37-41.

15. **Barretto, N., D. Jukneliene, K. Ratia, Z. Chen, A. D. Mesecar, and S. C. Baker.** 2005. The papain-like protease of severe acute respiratory syndrome coronavirus has deubiquitinating activity. J Virol **79:**15189-98.
16. **Baudoux, P., C. Carrat, L. Besnardeau, B. Charley, and H. Laude.** 1998. Coronavirus pseudoparticles formed with recombinant M and E proteins induce alpha interferon synthesis by leukocytes. J Virol **72:**8636-43.
17. **Bergmann, C. C., T. E. Lane, and S. A. Stohlman.** 2006. Coronavirus infection of the central nervous system: host-virus stand-off. Nat Rev Microbiol **4:**121-32.
18. **Bernad, A., L. Blanco, J. M. Lazaro, G. Martin, and M. Salas.** 1989. A conserved 3'----5' exonuclease active site in prokaryotic and eukaryotic DNA polymerases. Cell **59:**219-28.
19. **Bhardwaj, K., L. Guarino, and C. C. Kao.** 2004. The severe acute respiratory syndrome coronavirus Nsp15 protein is an endoribonuclease that prefers manganese as a cofactor. J Virol **78:**12218-24.
20. **Bhardwaj, K., S. Palaninathan, J. M. Alcantara, L. L. Yi, L. Guarino, J. C. Sacchettini, and C. C. Kao.** 2008. Structural and functional analyses of the severe acute respiratory syndrome coronavirus endoribonuclease Nsp15. J Biol Chem **283:**3655-64.
21. **Bonilla, P. J., S. A. Hughes, J. D. Pinon, and S. R. Weiss.** 1995. Characterization of the leader papain-like proteinase of MHV-A59: identification of a new in vitro cleavage site. Virology **209:**489-97.
22. **Bonilla, P. J., S. A. Hughes, and S. R. Weiss.** 1997. Characterization of a second cleavage site and demonstration of activity in trans by the papain-like proteinase of the murine coronavirus mouse hepatitis virus strain A59. J Virol **71:**900-9.
23. **Bos, E. C., W. Luytjes, H. V. van der Meulen, H. K. Koerten, and W. J. Spaan.** 1996. The production of recombinant infectious DI-particles of a murine coronavirus in the absence of helper virus. Virology **218:**52-60.
24. **Bost, A. G., R. H. Carnahan, X. T. Lu, and M. R. Denison.** 2000. Four proteins processed from the replicase gene polyprotein of mouse hepatitis virus colocalize in the cell periphery and adjacent to sites of virion assembly. J Virol **74:**3379-87.
25. **Bredenbeek, P. J., C. J. Pachuk, A. F. Noten, J. Charite, W. Luytjes, S. R. Weiss, and W. J. Spaan.** 1990. The primary structure and expression of the second open reading frame of the polymerase gene of the coronavirus MHV-A59; a highly conserved polymerase is expressed by an efficient ribosomal frameshifting mechanism. Nucleic Acids Res **18:**1825-32.
26. **Brian, D. A., and R. S. Baric.** 2005. Coronavirus genome structure and replication. Curr Top Microbiol Immunol **287:**1-30.
27. **Brierley, I., M. E. Boursnell, M. M. Binns, B. Bilimoria, V. C. Blok, T. D. Brown, and S. C. Inglis.** 1987. An efficient ribosomal frame-shifting signal in the polymerase-encoding region of the coronavirus IBV. Embo J **6:**3779-85.
28. **Brierley, I., P. Digard, and S. C. Inglis.** 1989. Characterization of an efficient coronavirus ribosomal frameshifting signal: requirement for an RNA pseudoknot. Cell **57:**537-47.
29. **Brierley, I., A. J. Jenner, and S. C. Inglis.** 1992. Mutational analysis of the "slippery-sequence" component of a coronavirus ribosomal frameshifting signal. J Mol Biol **227:**463-79.

30. **Brierley, I., N. J. Rolley, A. J. Jenner, and S. C. Inglis.** 1991. Mutational analysis of the RNA pseudoknot component of a coronavirus ribosomal frameshifting signal. J Mol Biol **220:**889-902.
31. **Brockway, S. M., C. T. Clay, X. T. Lu, and M. R. Denison.** 2003. Characterization of the expression, intracellular localization, and replication complex association of the putative mouse hepatitis virus RNA-dependent RNA polymerase. J Virol **77:**10515-27.
32. **Brockway, S. M., and M. R. Denison.** 2005. Mutagenesis of the murine hepatitis virus nsp1-coding region identifies residues important for protein processing, viral RNA synthesis, and viral replication. Virology **340:**209-23.
33. **Brockway, S. M., X. T. Lu, T. R. Peters, T. S. Dermody, and M. R. Denison.** 2004. Intracellular localization and protein interactions of the gene 1 protein p28 during mouse hepatitis virus replication. J Virol **78:**11551-62.
34. **Brown, C. G., K. S. Nixon, S. D. Senanayake, and D. A. Brian.** 2007. An RNA stem-loop within the bovine coronavirus nsp1 coding region is a cis-acting element in defective interfering RNA replication. J Virol **81:**7716-24.
35. **Budzilowicz, C. J., and S. R. Weiss.** 1987. In vitro synthesis of two polypeptides from a nonstructural gene of coronavirus mouse hepatitis virus strain A59. Virology **157:**509-15.
36. **Casais, R., M. Davies, D. Cavanagh, and P. Britton.** 2005. Gene 5 of the avian coronavirus infectious bronchitis virus is not essential for replication. J Virol **79:**8065-78.
37. **Casais, R., V. Thiel, S. G. Siddell, D. Cavanagh, and P. Britton.** 2001. Reverse genetics system for the avian coronavirus infectious bronchitis virus. J Virol **75:**12359-69.
38. **Cavanagh, D.** 2007. Coronavirus avian infectious bronchitis virus. Vet Res **38:**281-97.
39. **Cavanagh, D.** 1997. Nidovirales: a new order comprising Coronaviridae and Arteriviridae. Arch Virol **142:**629-33.
40. **Cavanagh, P. B. a. D.** 2007. Avain coronavirus diseases and infectious bronchitis virus vaccine development. In: Coronaviruses: Molecular and Cellular Biology pp161-183, Edited by Volker Thiel. Norfolk: Caister academic press.
41. **Cella, M., D. Jarrossay, F. Facchetti, O. Alebardi, H. Nakajima, A. Lanzavecchia, and M. Colonna.** 1999. Plasmacytoid monocytes migrate to inflamed lymph nodes and produce large amounts of type I interferon. Nat Med **5:**919-23.
42. **Cervantes-Barragan, L., R. Zust, F. Weber, M. Spiegel, K. S. Lang, S. Akira, V. Thiel, and B. Ludewig.** 2007. Control of coronavirus infection through plasmacytoid dendritic-cell-derived type I interferon. Blood **109:**1131-7.
43. **Cinatl, J., B. Morgenstern, G. Bauer, P. Chandra, H. Rabenau, and H. W. Doerr.** 2003. Treatment of SARS with human interferons. Lancet **362:**293-4.
44. **Clementz, M. A., A. Kanjanahaluethai, T. E. O'Brien, and S. C. Baker.** 2008. Mutation in murine coronavirus replication protein nsp4 alters assembly of double membrane vesicles. Virology.
45. **Coley, S. E., E. Lavi, S. G. Sawicki, L. Fu, B. Schelle, N. Karl, S. G. Siddell, and V. Thiel.** 2005. Recombinant mouse hepatitis virus strain A59 from cloned, full-length cDNA replicates to high titers in vitro and is fully pathogenic in vivo. J Virol **79:**3097-106.

46. **Cologna, R., J. F. Spagnolo, and B. G. Hogue.** 2000. Identification of nucleocapsid binding sites within coronavirus-defective genomes. Virology **277:**235-49.
47. **Corse, E., and C. E. Machamer.** 2000. Infectious bronchitis virus E protein is targeted to the Golgi complex and directs release of virus-like particles. J Virol **74:**4319-26.
48. **Cowley, J. A., C. M. Dimmock, K. M. Spann, and P. J. Walker.** 2000. Gill-associated virus of Penaeus monodon prawns: an invertebrate virus with ORF1a and ORF1b genes related to arteri- and coronaviruses. J Gen Virol **81:**1473-84.
49. **Cui, J., N. Han, D. Streicker, G. Li, X. Tang, Z. Shi, Z. Hu, G. Zhao, A. Fontanet, Y. Guan, L. Wang, G. Jones, H. E. Field, P. Daszak, and S. Zhang.** 2007. Evolutionary Relationships between Bat Coronaviruses and Their Hosts. Emerg Infect Dis **13:**1526-1532.
50. **Curtis, K. M., B. Yount, and R. S. Baric.** 2002. Heterologous gene expression from transmissible gastroenteritis virus replicon particles. J Virol **76:**1422-34.
51. **Chan-Yeung, M., G. C. Ooi, D. S. Hui, P. L. Ho, and K. W. Tsang.** 2003. Severe acute respiratory syndrome. Int J Tuberc Lung Dis **7:**1117-30.
52. **Chang, R. Y., and D. A. Brian.** 1996. cis Requirement for N-specific protein sequence in bovine coronavirus defective interfering RNA replication. J Virol **70:**2201-7.
53. **Chang, R. Y., M. A. Hofmann, P. B. Sethna, and D. A. Brian.** 1994. A cis-acting function for the coronavirus leader in defective interfering RNA replication. J Virol **68:**8223-31.
54. **Chen, H., A. Gill, B. K. Dove, S. R. Emmett, C. F. Kemp, M. A. Ritchie, M. Dee, and J. A. Hiscox.** 2005. Mass spectroscopic characterization of the coronavirus infectious bronchitis virus nucleoprotein and elucidation of the role of phosphorylation in RNA binding by using surface plasmon resonance. J Virol **79:**1164-79.
55. **Chen, P., M. Jiang, T. Hu, Q. Liu, X. S. Chen, and D. Guo.** 2007. Biochemical characterization of exoribonuclease encoded by SARS coronavirus. J Biochem Mol Biol **40:**649-55.
56. **Chen, Z., Y. Wang, K. Ratia, A. D. Mesecar, K. D. Wilkinson, and S. C. Baker.** 2007. Proteolytic processing and deubiquitinating activity of papain-like proteases of human coronavirus NL63. J Virol **81:**6007-18.
57. **Cheng, A., W. Zhang, Y. Xie, W. Jiang, E. Arnold, S. G. Sarafianos, and J. Ding.** 2005. Expression, purification, and characterization of SARS coronavirus RNA polymerase. Virology **335:**165-76.
58. **Cheung, C. Y., L. L. Poon, I. H. Ng, W. Luk, S. F. Sia, M. H. Wu, K. H. Chan, K. Y. Yuen, S. Gordon, Y. Guan, and J. S. Peiris.** 2005. Cytokine responses in severe acute respiratory syndrome coronavirus-infected macrophages in vitro: possible relevance to pathogenesis. J Virol **79:**7819-26.
59. **Dalton, K., R. Casais, K. Shaw, K. Stirrups, S. Evans, P. Britton, T. D. Brown, and D. Cavanagh.** 2001. cis-acting sequences required for coronavirus infectious bronchitis virus defective-RNA replication and packaging. J Virol **75:**125-33.
60. **de Haan, C. A., P. S. Masters, X. Shen, S. Weiss, and P. J. Rottier.** 2002. The group-specific murine coronavirus genes are not essential, but their deletion, by reverse genetics, is attenuating in the natural host. Virology **296:**177-89.

61. **de Haan, C. A., M. Smeets, F. Vernooij, H. Vennema, and P. J. Rottier.** 1999. Mapping of the coronavirus membrane protein domains involved in interaction with the spike protein. J Virol **73:**7441-52.
62. **de Haan, C. A., L. van Genne, J. N. Stoop, H. Volders, and P. J. Rottier.** 2003. Coronaviruses as vectors: position dependence of foreign gene expression. J Virol **77:**11312-23.
63. **Decroly, E., I. Imbert, B. Coutard, M. Bouvet, B. Selisko, K. Alvarez, A. E. Gorbalenya, E. J. Snijder, and B. Canard.** 2008. Coronavirus nonstructural protein 16 is a cap-0 binding enzyme possessing (nucleoside-2'O)-methyltransferase activity. J Virol.
64. **DeDiego, M. L., E. Alvarez, F. Almazan, M. T. Rejas, E. Lamirande, A. Roberts, W. J. Shieh, S. R. Zaki, K. Subbarao, and L. Enjuanes.** 2007. A severe acute respiratory syndrome coronavirus that lacks the E gene is attenuated in vitro and in vivo. J Virol **81:**1701-13.
65. **Delmas, B., J. Gelfi, R. L'Haridon, L. K. Vogel, H. Sjostrom, O. Noren, and H. Laude.** 1992. Aminopeptidase N is a major receptor for the entero-pathogenic coronavirus TGEV. Nature **357:**417-20.
66. **den Boon, J. A., E. J. Snijder, E. D. Chirnside, A. A. de Vries, M. C. Horzinek, and W. J. Spaan.** 1991. Equine arteritis virus is not a togavirus but belongs to the coronaviruslike superfamily. J Virol **65:**2910-20.
67. **Denison, M. R., P. W. Zoltick, S. A. Hughes, B. Giangreco, A. L. Olson, S. Perlman, J. L. Leibowitz, and S. R. Weiss.** 1992. Intracellular processing of the N-terminal ORF 1a proteins of the coronavirus MHV-A59 requires multiple proteolytic events. Virology **189:**274-84.
68. **Devaraj, S. G., N. Wang, Z. Chen, Z. Chen, M. Tseng, N. Barretto, R. Lin, C. J. Peters, C. T. Tseng, S. C. Baker, and K. Li.** 2007. Regulation of IRF-3-dependent innate immunity by the papain-like protease domain of the severe acute respiratory syndrome coronavirus. J Biol Chem **282:**32208-21.
69. **Dominguez, S. R., T. J. O'Shea, L. M. Oko, and K. V. Holmes.** 2007. Detection of group 1 coronaviruses in bats in North America. Emerg Infect Dis **13:**1295-300.
70. **Donaldson, E. F., R. L. Graham, A. C. Sims, M. R. Denison, and R. S. Baric.** 2007. Analysis of murine hepatitis virus strain A59 temperature-sensitive mutant TS-LA6 suggests that nsp10 plays a critical role in polyprotein processing. J Virol **81:**7086-98.
71. **Donaldson, E. F., A. C. Sims, R. L. Graham, M. R. Denison, and R. S. Baric.** 2007. Murine hepatitis virus replicase protein nsp10 is a critical regulator of viral RNA synthesis. J Virol **81:**6356-68.
72. **Drosten, C., W. Preiser, S. Gunther, H. Schmitz, and H. W. Doerr.** 2003. Severe acute respiratory syndrome: identification of the etiological agent. Trends Mol Med **9:**325-7.
73. **Dveksler, G. S., M. N. Pensiero, C. W. Dieffenbach, C. B. Cardellichio, A. A. Basile, P. E. Elia, and K. V. Holmes.** 1993. Mouse hepatitis virus strain A59 and blocking antireceptor monoclonal antibody bind to the N-terminal domain of cellular receptor. Proc Natl Acad Sci U S A **90:**1716-20.
74. **Eaton, B. T.** 2001. Introduction to Current focus on Hendra and Nipah viruses. Microbes Infect **3:**277-8.
75. **Eckerle, L. D., X. Lu, S. M. Sperry, L. Choi, and M. R. Denison.** 2007. High fidelity of murine hepatitis virus replication is decreased in nsp14 exoribonuclease mutants. J Virol **81:**12135-44.

76. **Egloff, M. P., F. Ferron, V. Campanacci, S. Longhi, C. Rancurel, H. Dutartre, E. J. Snijder, A. E. Gorbalenya, C. Cambillau, and B. Canard.** 2004. The severe acute respiratory syndrome-coronavirus replicative protein nsp9 is a single-stranded RNA-binding subunit unique in the RNA virus world. Proc Natl Acad Sci U S A **101:**3792-6.
77. **Egloff, M. P., H. Malet, A. Putics, M. Heinonen, H. Dutartre, A. Frangeul, A. Gruez, V. Campanacci, C. Cambillau, J. Ziebuhr, T. Ahola, and B. Canard.** 2006. Structural and functional basis for ADP-ribose and poly(ADP-ribose) binding by viral macro domains. J Virol **80:**8493-502.
78. **Eleouet, J. F., D. Rasschaert, P. Lambert, L. Levy, P. Vende, and H. Laude.** 1995. Complete sequence (20 kilobases) of the polyprotein-encoding gene 1 of transmissible gastroenteritis virus. Virology **206:**817-22.
79. **Enjuanes, L., I. Sola, S. Alonso, D. Escors, and S. Zuniga.** 2005. Coronavirus reverse genetics and development of vectors for gene expression. Curr Top Microbiol Immunol **287:**161-97.
80. **Eriksson, K. K., D. Makia, R. Maier, L. Cervantes, B. Ludewig, and V. Thiel.** 2006. Efficient transduction of dendritic cells using coronavirus-based vectors. Adv Exp Med Biol **581:**203-6.
81. **Eriksson, K. K., D. Makia, R. Maier, B. Ludewig, and V. Thiel.** 2006. Towards a coronavirus-based HIV multigene vaccine. Clin Dev Immunol **13:**353-60.
82. **Escors, D., A. Izeta, C. Capiscol, and L. Enjuanes.** 2003. Transmissible gastroenteritis coronavirus packaging signal is located at the 5' end of the virus genome. J Virol **77:**7890-902.
83. **Esper, F., C. Weibel, D. Ferguson, M. L. Landry, and J. S. Kahn.** 2005. Evidence of a novel human coronavirus that is associated with respiratory tract disease in infants and young children. J Infect Dis **191:**492-8.
84. **Fang, S., B. Chen, F. P. Tay, B. S. Ng, and D. X. Liu.** 2007. An arginine-to-proline mutation in a domain with undefined functions within the helicase protein (Nsp13) is lethal to the coronavirus infectious bronchitis virus in cultured cells. Virology **358:**136-47.
85. **Feder, M., J. Pas, L. S. Wyrwicz, and J. M. Bujnicki.** 2003. Molecular phylogenetics of the RrmJ/fibrillarin superfamily of ribose 2'-O-methyltransferases. Gene **302:**129-38.
86. **Fischer, F., D. Peng, S. T. Hingley, S. R. Weiss, and P. S. Masters.** 1997. The internal open reading frame within the nucleocapsid gene of mouse hepatitis virus encodes a structural protein that is not essential for viral replication. J Virol **71:**996-1003.
87. **Fouchier, R. A., N. G. Hartwig, T. M. Bestebroer, B. Niemeyer, J. C. de Jong, J. H. Simon, and A. D. Osterhaus.** 2004. A previously undescribed coronavirus associated with respiratory disease in humans. Proc Natl Acad Sci U S A **101:**6212-6.
88. **Frieman, M., B. Yount, M. Heise, S. A. Kopecky-Bromberg, P. Palese, and R. S. Baric.** 2007. Severe acute respiratory syndrome coronavirus ORF6 antagonizes STAT1 function by sequestering nuclear import factors on the rough endoplasmic reticulum/Golgi membrane. J Virol **81:**9812-24.
89. **Gloza-Rausch, F., A. Ipsen, A. Seebens, M. Gottsche, M. Panning, J. Felix Drexler, N. Petersen, A. Annan, K. Grywna, M. Muller, S. Pfefferle, and C. Drosten.** 2008. Detection and Prevalence Patterns of Group I Coronaviruses in Bats, Northern Germany. Emerg Infect Dis **14:**626-631.

90. **Goebel, S. J., B. Hsue, T. F. Dombrowski, and P. S. Masters.** 2004. Characterization of the RNA components of a putative molecular switch in the 3' untranslated region of the murine coronavirus genome. J Virol **78:**669-82.
91. **Goebel, S. J., T. B. Miller, C. J. Bennett, K. A. Bernard, and P. S. Masters.** 2007. A hypervariable region within the 3' cis-acting element of the murine coronavirus genome is nonessential for RNA synthesis but affects pathogenesis. J Virol **81:**1274-87.
92. **Gonzalez, J. M., Z. Penzes, F. Almazan, E. Calvo, and L. Enjuanes.** 2002. Stabilization of a full-length infectious cDNA clone of transmissible gastroenteritis coronavirus by insertion of an intron. J Virol **76:**4655-61.
93. **Gorbalenya, A. E., A. P. Donchenko, V. M. Blinov, and E. V. Koonin.** 1989. Cysteine proteases of positive strand RNA viruses and chymotrypsin-like serine proteases. A distinct protein superfamily with a common structural fold. FEBS Lett **243:**103-14.
94. **Gorbalenya, A. E., L. Enjuanes, J. Ziebuhr, and E. J. Snijder.** 2006. Nidovirales: evolving the largest RNA virus genome. Virus Res **117:**17-37.
95. **Gorbalenya, A. E., E. V. Koonin, A. P. Donchenko, and V. M. Blinov.** 1989. Two related superfamilies of putative helicases involved in replication, recombination, repair and expression of DNA and RNA genomes. Nucleic Acids Res **17:**4713-30.
96. **Gorbalenya, A. E., E. J. Snijder, and W. J. Spaan.** 2004. Severe acute respiratory syndrome coronavirus phylogeny: toward consensus. J Virol **78:**7863-6.
97. **Gosert, R., A. Kanjanahaluethai, D. Egger, K. Bienz, and S. C. Baker.** 2002. RNA replication of mouse hepatitis virus takes place at double-membrane vesicles. J Virol **76:**3697-708.
98. **Graham, R. L., and M. R. Denison.** 2006. Replication of murine hepatitis virus is regulated by papain-like proteinase 1 processing of nonstructural proteins 1, 2, and 3. J Virol **80:**11610-20.
99. **Graham, R. L., A. C. Sims, R. S. Baric, and M. R. Denison.** 2006. The nsp2 proteins of mouse hepatitis virus and SARS coronavirus are dispensable for viral replication. Adv Exp Med Biol **581:**67-72.
100. **Graham, R. L., A. C. Sims, S. M. Brockway, R. S. Baric, and M. R. Denison.** 2005. The nsp2 replicase proteins of murine hepatitis virus and severe acute respiratory syndrome coronavirus are dispensable for viral replication. J Virol **79:**13399-411.
101. **Haagmans, B. L., T. Kuiken, B. E. Martina, R. A. Fouchier, G. F. Rimmelzwaan, G. van Amerongen, D. van Riel, T. de Jong, S. Itamura, K. H. Chan, M. Tashiro, and A. D. Osterhaus.** 2004. Pegylated interferon-alpha protects type 1 pneumocytes against SARS coronavirus infection in macaques. Nat Med **10:**290-3.
102. **Haijema, B. J., H. Volders, and P. J. Rottier.** 2004. Live, attenuated coronavirus vaccines through the directed deletion of group-specific genes provide protection against feline infectious peritonitis. J Virol **78:**3863-71.
103. **Haijema, B. J., H. Volders, and P. J. Rottier.** 2003. Switching species tropism: an effective way to manipulate the feline coronavirus genome. J Virol **77:**4528-38.
104. **Harcourt, B. H., D. Jukneliene, A. Kanjanahaluethai, J. Bechill, K. M. Severson, C. M. Smith, P. A. Rota, and S. C. Baker.** 2004. Identification of severe acute respiratory syndrome coronavirus replicase products and characterization of papain-like protease activity. J Virol **78:**13600-12.

105. **Hasoksuz, M., S. Lathrop, M. A. Al-dubaib, P. Lewis, and L. J. Saif.** 1999. Antigenic variation among bovine enteric coronaviruses (BECV) and bovine respiratory coronaviruses (BRCV) detected using monoclonal antibodies. Arch Virol **144:**2441-7.
106. **Hasoksuz, M., S. L. Lathrop, K. L. Gadfield, and L. J. Saif.** 1999. Isolation of bovine respiratory coronaviruses from feedlot cattle and comparison of their biological and antigenic properties with bovine enteric coronaviruses. Am J Vet Res **60:**1227-33.
107. **He, R., A. Leeson, M. Ballantine, A. Andonov, L. Baker, F. Dobie, Y. Li, N. Bastien, H. Feldmann, U. Strocher, S. Theriault, T. Cutts, J. Cao, T. F. Booth, F. A. Plummer, S. Tyler, and X. Li.** 2004. Characterization of protein-protein interactions between the nucleocapsid protein and membrane protein of the SARS coronavirus. Virus Res **105:**121-5.
108. **Hegyi, A., and J. Ziebuhr.** 2002. Conservation of substrate specificities among coronavirus main proteases. J Gen Virol **83:**595-9.
109. **Herold, J., and S. G. Siddell.** 1993. An 'elaborated' pseudoknot is required for high frequency frameshifting during translation of HCV 229E polymerase mRNA. Nucleic Acids Res **21:**5838-42.
110. **Herrewegh, A. A., H. Vennema, M. C. Horzinek, P. J. Rottier, and R. J. de Groot.** 1995. The molecular genetics of feline coronaviruses: comparative sequence analysis of the ORF7a/7b transcription unit of different biotypes. Virology **212:**622-31.
111. **Hertzog, P. J., L. A. O'Neill, and J. A. Hamilton.** 2003. The interferon in TLR signaling: more than just antiviral. Trends Immunol **24:**534-9.
112. **Hodgson, T., P. Britton, and D. Cavanagh.** 2006. Neither the RNA nor the proteins of open reading frames 3a and 3b of the coronavirus infectious bronchitis virus are essential for replication. J Virol **80:**296-305.
113. **Hofmann, H., K. Pyrc, L. van der Hoek, M. Geier, B. Berkhout, and S. Pohlmann.** 2005. Human coronavirus NL63 employs the severe acute respiratory syndrome coronavirus receptor for cellular entry. Proc Natl Acad Sci U S A **102:**7988-93.
114. **Hofmann, M. A., P. B. Sethna, and D. A. Brian.** 1990. Bovine coronavirus mRNA replication continues throughout persistent infection in cell culture. J Virol **64:**4108-14.
115. **Honda, K., H. Yanai, H. Negishi, M. Asagiri, M. Sato, T. Mizutani, N. Shimada, Y. Ohba, A. Takaoka, N. Yoshida, and T. Taniguchi.** 2005. IRF-7 is the master regulator of type-I interferon-dependent immune responses. Nature **434:**772-7.
116. **Hornung, V., J. Ellegast, S. Kim, K. Brzozka, A. Jung, H. Kato, H. Poeck, S. Akira, K. K. Conzelmann, M. Schlee, S. Endres, and G. Hartmann.** 2006. 5'-Triphosphate RNA is the ligand for RIG-I. Science **314:**994-7.
117. **Huang, P., and M. M. Lai.** 2001. Heterogeneous nuclear ribonucleoprotein a1 binds to the 3'-untranslated region and mediates potential 5'-3'-end cross talks of mouse hepatitis virus RNA. J Virol **75:**5009-17.
118. **Huang, Y., Z. Y. Yang, W. P. Kong, and G. J. Nabel.** 2004. Generation of synthetic severe acute respiratory syndrome coronavirus pseudoparticles: implications for assembly and vaccine production. J Virol **78:**12557-65.
119. **Hurst, K. R., L. Kuo, C. A. Koetzner, R. Ye, B. Hsue, and P. S. Masters.** 2005. A major determinant for membrane protein interaction localizes to the carboxy-terminal domain of the mouse coronavirus nucleocapsid protein. J Virol **79:**13285-97.

120. **Imbert, I., J. C. Guillemot, J. M. Bourhis, C. Bussetta, B. Coutard, M. P. Egloff, F. Ferron, A. E. Gorbalenya, and B. Canard.** 2006. A second, non-canonical RNA-dependent RNA polymerase in SARS coronavirus. Embo J **25:**4933-42.
121. **Imbert, I., E. J. Snijder, M. Dimitrova, J. C. Guillemot, P. Lecine, and B. Canard.** 2008. The SARS-Coronavirus PLnc domain of nsp3 as a replication/transcription scaffolding protein. Virus Res.
122. **Ivanov, K. A., T. Hertzig, M. Rozanov, S. Bayer, V. Thiel, A. E. Gorbalenya, and J. Ziebuhr.** 2004. Major genetic marker of nidoviruses encodes a replicative endoribonuclease. Proc Natl Acad Sci U S A **101:**12694-9.
123. **Ivanov, K. A., V. Thiel, J. C. Dobbe, Y. van der Meer, E. J. Snijder, and J. Ziebuhr.** 2004. Multiple enzymatic activities associated with severe acute respiratory syndrome coronavirus helicase. J Virol **78:**5619-32.
124. **Ivanov, K. A., and J. Ziebuhr.** 2004. Human coronavirus 229E nonstructural protein 13: characterization of duplex-unwinding, nucleoside triphosphatase, and RNA 5'-triphosphatase activities. J Virol **78:**7833-8.
125. **Izaguirre, A., B. J. Barnes, S. Amrute, W. S. Yeow, N. Megjugorac, J. Dai, D. Feng, E. Chung, P. M. Pitha, and P. Fitzgerald-Bocarsly.** 2003. Comparative analysis of IRF and IFN-alpha expression in human plasmacytoid and monocyte-derived dendritic cells. J Leukoc Biol **74:**1125-38.
126. **Izeta, A., C. Smerdou, S. Alonso, Z. Penzes, A. Mendez, J. Plana-Duran, and L. Enjuanes.** 1999. Replication and packaging of transmissible gastroenteritis coronavirus-derived synthetic minigenomes. J Virol **73:**1535-45.
127. **Jacks, T., H. D. Madhani, F. R. Masiarz, and H. E. Varmus.** 1988. Signals for ribosomal frameshifting in the Rous sarcoma virus gag-pol region. Cell **55:**447-58.
128. **Jacobs, L., B. A. van der Zeijst, and M. C. Horzinek.** 1986. Characterization and translation of transmissible gastroenteritis virus mRNAs. J Virol **57:**1010-5.
129. **Jia, W., S. P. Mondal, and S. A. Naqi.** 2002. Genetic and antigenic diversity in avian infectious bronchitis virus isolates of the 1940s. Avian Dis **46:**437-41.
130. **Jones, B. M., E. S. Ma, J. S. Peiris, P. C. Wong, J. C. Ho, B. Lam, K. N. Lai, and K. W. Tsang.** 2004. Prolonged disturbances of in vitro cytokine production in patients with severe acute respiratory syndrome (SARS) treated with ribavirin and steroids. Clin Exp Immunol **135:**467-73.
131. **Joseph, J. S., K. S. Saikatendu, V. Subramanian, B. W. Neuman, A. Brooun, M. Griffith, K. Moy, M. K. Yadav, J. Velasquez, M. J. Buchmeier, R. C. Stevens, and P. Kuhn.** 2006. Crystal structure of nonstructural protein 10 from the severe acute respiratory syndrome coronavirus reveals a novel fold with two zinc-binding motifs. J Virol **80:**7894-901.
132. **Joseph, J. S., K. S. Saikatendu, V. Subramanian, B. W. Neuman, M. J. Buchmeier, R. C. Stevens, and P. Kuhn.** 2007. Crystal structure of a monomeric form of severe acute respiratory syndrome coronavirus endonuclease nsp15 suggests a role for hexamerization as an allosteric switch. J Virol **81:**6700-8.
133. **Kamitani, W., K. Narayanan, C. Huang, K. Lokugamage, T. Ikegami, N. Ito, H. Kubo, and S. Makino.** 2006. Severe acute respiratory syndrome coronavirus nsp1 protein suppresses host gene expression by promoting host mRNA degradation. Proc Natl Acad Sci U S A **103:**12885-90.

134. **Kang, H., K. Bhardwaj, Y. Li, S. Palaninathan, J. Sacchettini, L. Guarino, J. L. Leibowitz, and C. C. Kao.** 2007. Biochemical and genetic analyses of murine hepatitis virus Nsp15 endoribonuclease. J Virol **81:**13587-97.
135. **Kanjanahaluethai, A., Z. Chen, D. Jukneliene, and S. C. Baker.** 2007. Membrane topology of murine coronavirus replicase nonstructural protein 3. Virology **361:**391-401.
136. **Kato, H., O. Takeuchi, S. Sato, M. Yoneyama, M. Yamamoto, K. Matsui, S. Uematsu, A. Jung, T. Kawai, K. J. Ishii, O. Yamaguchi, K. Otsu, T. Tsujimura, C. S. Koh, C. Reis e Sousa, Y. Matsuura, T. Fujita, and S. Akira.** 2006. Differential roles of MDA5 and RIG-I helicases in the recognition of RNA viruses. Nature **441:**101-5.
137. **Keck, J. G., G. K. Matsushima, S. Makino, J. O. Fleming, D. M. Vannier, S. A. Stohlman, and M. M. Lai.** 1988. In vivo RNA-RNA recombination of coronavirus in mouse brain. J Virol **62:**1810-3.
138. **Keck, J. G., L. H. Soe, S. Makino, S. A. Stohlman, and M. M. Lai.** 1988. RNA recombination of murine coronaviruses: recombination between fusion-positive mouse hepatitis virus A59 and fusion-negative mouse hepatitis virus 2. J Virol **62:**1989-98.
139. **Kim, K. H., K. Narayanan, and S. Makino.** 1998. Characterization of coronavirus DI RNA packaging. Adv Exp Med Biol **440:**347-53.
140. **Kim, Y. N., Y. S. Jeong, and S. Makino.** 1993. Analysis of cis-acting sequences essential for coronavirus defective interfering RNA replication. Virology **197:**53-63.
141. **Koetzner, C. A., M. M. Parker, C. S. Ricard, L. S. Sturman, and P. S. Masters.** 1992. Repair and mutagenesis of the genome of a deletion mutant of the coronavirus mouse hepatitis virus by targeted RNA recombination. J Virol **66:**1841-8.
142. **Kopecky-Bromberg, S. A., L. Martinez-Sobrido, M. Frieman, R. A. Baric, and P. Palese.** 2007. Severe acute respiratory syndrome coronavirus open reading frame (ORF) 3b, ORF 6, and nucleocapsid proteins function as interferon antagonists. J Virol **81:**548-57.
143. **Kopecky-Bromberg, S. A., L. Martinez-Sobrido, and P. Palese.** 2006. 7a protein of severe acute respiratory syndrome coronavirus inhibits cellular protein synthesis and activates p38 mitogen-activated protein kinase. J Virol **80:**785-93.
144. **Kuo, L., G. J. Godeke, M. J. Raamsman, P. S. Masters, and P. J. Rottier.** 2000. Retargeting of coronavirus by substitution of the spike glycoprotein ectodomain: crossing the host cell species barrier. J Virol **74:**1393-406.
145. **Kuo, L., K. R. Hurst, and P. S. Masters.** 2007. Exceptional flexibility in the sequence requirements for coronavirus small envelope protein function. J Virol **81:**2249-62.
146. **Kuo, L., and P. S. Masters.** 2002. Genetic evidence for a structural interaction between the carboxy termini of the membrane and nucleocapsid proteins of mouse hepatitis virus. J Virol **76:**4987-99.
147. **Kuo, L., and P. S. Masters.** 2003. The small envelope protein E is not essential for murine coronavirus replication. J Virol **77:**4597-608.
148. **Kusters, J. G., E. J. Jager, H. G. Niesters, and B. A. van der Zeijst.** 1990. Sequence evidence for RNA recombination in field isolates of avian coronavirus infectious bronchitis virus. Vaccine **8:**605-8.
149. **Lai, M. M., C. D. Patton, R. S. Baric, and S. A. Stohlman.** 1983. Presence of leader sequences in the mRNA of mouse hepatitis virus. J Virol **46:**1027-33.

150. **Lai, M. M., C. D. Patton, and S. A. Stohlman.** 1982. Further characterization of mRNA's of mouse hepatitis virus: presence of common 5'-end nucleotides. J Virol **41:**557-65.
151. **Lai, M. M., and S. A. Stohlman.** 1981. Comparative analysis of RNA genomes of mouse hepatitis viruses. J Virol **38:**661-70.
152. **Lapps, W., B. G. Hogue, and D. A. Brian.** 1987. Sequence analysis of the bovine coronavirus nucleocapsid and matrix protein genes. Virology **157:**47-57.
153. **Lassnig, C., C. M. Sanchez, M. Egerbacher, I. Walter, S. Majer, T. Kolbe, P. Pallares, L. Enjuanes, and M. Muller.** 2005. Development of a transgenic mouse model susceptible to human coronavirus 229E. Proc Natl Acad Sci U S A **102:**8275-80.
154. **Lau, S. K., P. C. Woo, C. C. Yip, H. Tse, H. W. Tsoi, V. C. Cheng, P. Lee, B. S. Tang, C. H. Cheung, R. A. Lee, L. Y. So, Y. L. Lau, K. H. Chan, and K. Y. Yuen.** 2006. Coronavirus HKU1 and other coronavirus infections in Hong Kong. J Clin Microbiol **44:**2063-71.
155. **Law, H. K., C. Y. Cheung, H. Y. Ng, S. F. Sia, Y. O. Chan, W. Luk, J. M. Nicholls, J. S. Peiris, and Y. L. Lau.** 2005. Chemokine up-regulation in SARS-coronavirus-infected, monocyte-derived human dendritic cells. Blood **106:**2366-74.
156. **Le Bon, A., G. Schiavoni, G. D'Agostino, I. Gresser, F. Belardelli, and D. F. Tough.** 2001. Type i interferons potently enhance humoral immunity and can promote isotype switching by stimulating dendritic cells in vivo. Immunity **14:**461-70.
157. **Le Bon, A., and D. F. Tough.** 2002. Links between innate and adaptive immunity via type I interferon. Curr Opin Immunol **14:**432-6.
158. **Lee, H. J., C. K. Shieh, A. E. Gorbalenya, E. V. Koonin, N. La Monica, J. Tuler, A. Bagdzhadzhyan, and M. M. Lai.** 1991. The complete sequence (22 kilobases) of murine coronavirus gene 1 encoding the putative proteases and RNA polymerase. Virology **180:**567-82.
159. **Leibowitz, J. L., S. R. Weiss, E. Paavola, and C. W. Bond.** 1982. Cell-free translation of murine coronavirus RNA. J Virol **43:**905-13.
160. **Li, H. P., P. Huang, S. Park, and M. M. Lai.** 1999. Polypyrimidine tract-binding protein binds to the leader RNA of mouse hepatitis virus and serves as a regulator of viral transcription. J Virol **73:**772-7.
161. **Li, H. P., X. Zhang, R. Duncan, L. Comai, and M. M. Lai.** 1997. Heterogeneous nuclear ribonucleoprotein A1 binds to the transcription-regulatory region of mouse hepatitis virus RNA. Proc Natl Acad Sci U S A **94:**9544-9.
162. **Li, L., H. Kang, P. Liu, N. Makkinje, S. T. Williamson, J. L. Leibowitz, and D. P. Giedroc.** 2008. Structural lability in stem-loop 1 drives a 5' UTR-3' UTR interaction in coronavirus replication. J Mol Biol **377:**790-803.
163. **Li, W., M. J. Moore, N. Vasilieva, J. Sui, S. K. Wong, M. A. Berne, M. Somasundaran, J. L. Sullivan, K. Luzuriaga, T. C. Greenough, H. Choe, and M. Farzan.** 2003. Angiotensin-converting enzyme 2 is a functional receptor for the SARS coronavirus. Nature **426:**450-4.
164. **Lin, Y. J., and M. M. Lai.** 1993. Deletion mapping of a mouse hepatitis virus defective interfering RNA reveals the requirement of an internal and discontiguous sequence for replication. J Virol **67:**6110-8.
165. **Lin, Y. J., C. L. Liao, and M. M. Lai.** 1994. Identification of the cis-acting signal for minus-strand RNA synthesis of a murine coronavirus: implications

for the role of minus-strand RNA in RNA replication and transcription. J Virol **68:**8131-40.

166. **Lin, Y. J., X. Zhang, R. C. Wu, and M. M. Lai.** 1996. The 3' untranslated region of coronavirus RNA is required for subgenomic mRNA transcription from a defective interfering RNA. J Virol **70:**7236-40.
167. **Loutfy, M. R., L. M. Blatt, K. A. Siminovitch, S. Ward, B. Wolff, H. Lho, D. H. Pham, H. Deif, E. A. LaMere, M. Chang, K. C. Kain, G. A. Farcas, P. Ferguson, M. Latchford, G. Levy, J. W. Dennis, E. K. Lai, and E. N. Fish.** 2003. Interferon alfacon-1 plus corticosteroids in severe acute respiratory syndrome: a preliminary study. Jama **290:**3222-8.
168. **Luytjes, W., H. Gerritsma, and W. J. Spaan.** 1996. Replication of synthetic defective interfering RNAs derived from coronavirus mouse hepatitis virus-A59. Virology **216:**174-83.
169. **Maeda, J., A. Maeda, and S. Makino.** 1999. Release of coronavirus E protein in membrane vesicles from virus-infected cells and E protein-expressing cells. Virology **263:**265-72.
170. **Makino, S., N. Fujioka, and K. Fujiwara.** 1985. Structure of the intracellular defective viral RNAs of defective interfering particles of mouse hepatitis virus. J Virol **54:**329-36.
171. **Makino, S., J. G. Keck, S. A. Stohlman, and M. M. Lai.** 1986. High-frequency RNA recombination of murine coronaviruses. J Virol **57:**729-37.
172. **Makino, S., F. Taguchi, and K. Fujiwara.** 1984. Defective interfering particles of mouse hepatitis virus. Virology **133:**9-17.
173. **Masters, P. S.** 1992. Localization of an RNA-binding domain in the nucleocapsid protein of the coronavirus mouse hepatitis virus. Arch Virol **125:**141-60.
174. **Masters, P. S.** 2006. The molecular biology of coronaviruses. Adv Virus Res **66:**193-292.
175. **Masters, P. S.** 1999. Reverse genetics of the largest RNA viruses. Adv Virus Res **53:**245-64.
176. **Masters, P. S., M. M. Parker, C. S. Ricard, C. Duchala, M. F. Frana, K. V. Holmes, and L. S. Sturman.** 1990. Structure and function studies of the nucleocapsid protein of mouse hepatitis virus. Adv Exp Med Biol **276:**239-46.
177. **Masters, P. S., and P. J. Rottier.** 2005. Coronavirus reverse genetics by targeted RNA recombination. Curr Top Microbiol Immunol **287:**133-59.
178. **Matthes, N., J. R. Mesters, B. Coutard, B. Canard, E. J. Snijder, R. Moll, and R. Hilgenfeld.** 2006. The non-structural protein Nsp10 of mouse hepatitis virus binds zinc ions and nucleic acids. FEBS Lett **580:**4143-9.
179. **Matthews, A. E., S. R. Weiss, and Y. Paterson.** 2002. Murine hepatitis virus--a model for virus-induced CNS demyelination. J Neurovirol **8:**76-85.
180. **Mendez, A., C. Smerdou, A. Izeta, F. Gebauer, and L. Enjuanes.** 1996. Molecular characterization of transmissible gastroenteritis coronavirus defective interfering genomes: packaging and heterogeneity. Virology **217:**495-507.
181. **Minskaia, E., T. Hertzig, A. E. Gorbalenya, V. Campanacci, C. Cambillau, B. Canard, and J. Ziebuhr.** 2006. Discovery of an RNA virus 3'->5' exoribonuclease that is critically involved in coronavirus RNA synthesis. Proc Natl Acad Sci U S A **103:**5108-13.
182. **Molenkamp, R., and W. J. Spaan.** 1997. Identification of a specific interaction between the coronavirus mouse hepatitis virus A59 nucleocapsid protein and packaging signal. Virology **239:**78-86.

183. **Mortola, E., and P. Roy.** 2004. Efficient assembly and release of SARS coronavirus-like particles by a heterologous expression system. FEBS Lett **576:**174-8.
184. **Moser, M. J., W. R. Holley, A. Chatterjee, and I. S. Mian.** 1997. The proofreading domain of Escherichia coli DNA polymerase I and other DNA and/or RNA exonuclease domains. Nucleic Acids Res **25:**5110-8.
185. **Muller, M. A., J. T. Paweska, P. A. Leman, C. Drosten, K. Grywna, A. Kemp, L. Braack, K. Sonnenberg, M. Niedrig, and R. Swanepoel.** 2007. Coronavirus antibodies in African bat species. Emerg Infect Dis **13:**1367-70.
186. **Muller, U., U. Steinhoff, L. F. Reis, S. Hemmi, J. Pavlovic, R. M. Zinkernagel, and M. Aguet.** 1994. Functional role of type I and type II interferons in antiviral defense. Science **264:**1918-21.
187. **Nakano, H., M. Yanagita, and M. D. Gunn.** 2001. CD11c(+)B220(+)Gr-1(+) cells in mouse lymph nodes and spleen display characteristics of plasmacytoid dendritic cells. J Exp Med **194:**1171-8.
188. **Napthine, S., J. Liphardt, A. Bloys, S. Routledge, and I. Brierley.** 1999. The role of RNA pseudoknot stem 1 length in the promotion of efficient -1 ribosomal frameshifting. J Mol Biol **288:**305-20.
189. **Narayanan, K., C. J. Chen, J. Maeda, and S. Makino.** 2003. Nucleocapsid-independent specific viral RNA packaging via viral envelope protein and viral RNA signal. J Virol **77:**2922-7.
190. **Narayanan, K., C. Huang, K. Lokugamage, W. Kamitani, T. Ikegami, C. T. Tseng, and S. Makino.** 2008. Severe Acute Respiratory Syndrome Coronavirus Nsp1 Suppresses Host Gene Expression, Including Type I Interferon, in Infected Cells. J Virol.
191. **Narayanan, K., A. Maeda, J. Maeda, and S. Makino.** 2000. Characterization of the coronavirus M protein and nucleocapsid interaction in infected cells. J Virol **74:**8127-34.
192. **Narayanan, K., and S. Makino.** 2001. Cooperation of an RNA packaging signal and a viral envelope protein in coronavirus RNA packaging. J Virol **75:**9059-67.
193. **Narayanan, K., and S. Makino.** 2001. Characterization of nucleocapsid-M protein interaction in murine coronavirus. Adv Exp Med Biol **494:**577-82.
194. **Nelson, G. W., and S. A. Stohlman.** 1993. Localization of the RNA-binding domain of mouse hepatitis virus nucleocapsid protein. J Gen Virol **74 (Pt 9):**1975-9.
195. **Nguyen, K. B., W. T. Watford, R. Salomon, S. R. Hofmann, G. C. Pien, A. Morinobu, M. Gadina, J. J. O'Shea, and C. A. Biron.** 2002. Critical role for STAT4 activation by type 1 interferons in the interferon-gamma response to viral infection. Science **297:**2063-6.
196. **Oostra, M., E. G. te Lintelo, M. Deijs, M. H. Verheije, P. J. Rottier, and C. A. de Haan.** 2007. Localization and membrane topology of coronavirus nonstructural protein 4: involvement of the early secretory pathway in replication. J Virol **81:**12323-36.
197. **Ortego, J., D. Escors, H. Laude, and L. Enjuanes.** 2002. Generation of a replication-competent, propagation-deficient virus vector based on the transmissible gastroenteritis coronavirus genome. J Virol **76:**11518-29.
198. **Ortego, J., I. Sola, F. Almazan, J. E. Ceriani, C. Riquelme, M. Balasch, J. Plana, and L. Enjuanes.** 2003. Transmissible gastroenteritis coronavirus gene 7 is not essential but influences in vivo virus replication and virulence. Virology **308:**13-22.

199. **Peiris, J. S., S. T. Lai, L. L. Poon, Y. Guan, L. Y. Yam, W. Lim, J. Nicholls, W. K. Yee, W. W. Yan, M. T. Cheung, V. C. Cheng, K. H. Chan, D. N. Tsang, R. W. Yung, T. K. Ng, and K. Y. Yuen.** 2003. Coronavirus as a possible cause of severe acute respiratory syndrome. Lancet **361:**1319-25.
200. **Pene, F., A. Merlat, A. Vabret, F. Rozenberg, A. Buzyn, F. Dreyfus, A. Cariou, F. Freymuth, and P. Lebon.** 2003. Coronavirus 229E-related pneumonia in immunocompromised patients. Clin Infect Dis **37:**929-32.
201. **Penzes, Z., K. Tibbles, K. Shaw, P. Britton, T. D. Brown, and D. Cavanagh.** 1994. Characterization of a replicating and packaged defective RNA of avian coronavirus infectious bronchitis virus. Virology **203:**286-93.
202. **Pfeiffer, J. K., and K. Kirkegaard.** 2005. Increased fidelity reduces poliovirus fitness and virulence under selective pressure in mice. PLoS Pathog **1:**e11.
203. **Plant, E. P., G. C. Perez-Alvarado, J. L. Jacobs, B. Mukhopadhyay, M. Hennig, and J. D. Dinman.** 2005. A three-stemmed mRNA pseudoknot in the SARS coronavirus frameshift signal. PLoS Biol **3:**e172.
204. **Prentice, E., W. G. Jerome, T. Yoshimori, N. Mizushima, and M. R. Denison.** 2004. Coronavirus replication complex formation utilizes components of cellular autophagy. J Biol Chem **279:**10136-41.
205. **Prentice, E., J. McAuliffe, X. Lu, K. Subbarao, and M. R. Denison.** 2004. Identification and characterization of severe acute respiratory syndrome coronavirus replicase proteins. J Virol **78:**9977-86.
206. **Proietti, E., L. Bracci, S. Puzelli, T. Di Pucchio, P. Sestili, E. De Vincenzi, M. Venditti, I. Capone, I. Seif, E. De Maeyer, D. Tough, I. Donatelli, and F. Belardelli.** 2002. Type I IFN as a natural adjuvant for a protective immune response: lessons from the influenza vaccine model. J Immunol **169:**375-83.
207. **Putics, A., W. Filipowicz, J. Hall, A. E. Gorbalenya, and J. Ziebuhr.** 2005. ADP-ribose-1"-monophosphatase: a conserved coronavirus enzyme that is dispensable for viral replication in tissue culture. J Virol **79:**12721-31.
208. **Raamsman, M. J., J. K. Locker, A. de Hooge, A. A. de Vries, G. Griffiths, H. Vennema, and P. J. Rottier.** 2000. Characterization of the coronavirus mouse hepatitis virus strain A59 small membrane protein E. J Virol **74:**2333-42.
209. **Raman, S., P. Bouma, G. D. Williams, and D. A. Brian.** 2003. Stem-loop III in the 5' untranslated region is a cis-acting element in bovine coronavirus defective interfering RNA replication. J Virol **77:**6720-30.
210. **Raman, S., and D. A. Brian.** 2005. Stem-loop IV in the 5' untranslated region is a cis-acting element in bovine coronavirus defective interfering RNA replication. J Virol **79:**12434-46.
211. **Ratia, K., K. S. Saikatendu, B. D. Santarsiero, N. Barretto, S. C. Baker, R. C. Stevens, and A. D. Mesecar.** 2006. Severe acute respiratory syndrome coronavirus papain-like protease: structure of a viral deubiquitinating enzyme. Proc Natl Acad Sci U S A **103:**5717-22.
212. **Reghunathan, R., M. Jayapal, L. Y. Hsu, H. H. Chng, D. Tai, B. P. Leung, and A. J. Melendez.** 2005. Expression profile of immune response genes in patients with Severe Acute Respiratory Syndrome. BMC Immunol **6:**2.
213. **Ricagno, S., M. P. Egloff, R. Ulferts, B. Coutard, D. Nurizzo, V. Campanacci, C. Cambillau, J. Ziebuhr, and B. Canard.** 2006. Crystal structure and mechanistic determinants of SARS coronavirus nonstructural protein 15 define an endoribonuclease family. Proc Natl Acad Sci U S A **103:**11892-7.

214. **Robbins, S. G., M. F. Frana, J. J. McGowan, J. F. Boyle, and K. V. Holmes.** 1986. RNA-binding proteins of coronavirus MHV: detection of monomeric and multimeric N protein with an RNA overlay-protein blot assay. Virology **150:**402-10.
215. **Rota, P. A., M. S. Oberste, S. S. Monroe, W. A. Nix, R. Campagnoli, J. P. Icenogle, S. Penaranda, B. Bankamp, K. Maher, M. H. Chen, S. Tong, A. Tamin, L. Lowe, M. Frace, J. L. DeRisi, Q. Chen, D. Wang, D. D. Erdman, T. C. Peret, C. Burns, T. G. Ksiazek, P. E. Rollin, A. Sanchez, S. Liffick, B. Holloway, J. Limor, K. McCaustland, M. Olsen-Rasmussen, R. Fouchier, S. Gunther, A. D. Osterhaus, C. Drosten, M. A. Pallansch, L. J. Anderson, and W. J. Bellini.** 2003. Characterization of a novel coronavirus associated with severe acute respiratory syndrome. Science **300:**1394-9.
216. **Roth-Cross, J. K., L. Martinez-Sobrido, E. P. Scott, A. Garcia-Sastre, and S. R. Weiss.** 2007. Inhibition of the alpha/beta interferon response by mouse hepatitis virus at multiple levels. J Virol **81:**7189-99.
217. **Saikatendu, K. S., J. S. Joseph, V. Subramanian, T. Clayton, M. Griffith, K. Moy, J. Velasquez, B. W. Neuman, M. J. Buchmeier, R. C. Stevens, and P. Kuhn.** 2005. Structural basis of severe acute respiratory syndrome coronavirus ADP-ribose-1''-phosphate dephosphorylation by a conserved domain of nsP3. Structure **13:**1665-75.
218. **Salanueva, I. J., J. L. Carrascosa, and C. Risco.** 1999. Structural maturation of the transmissible gastroenteritis coronavirus. J Virol **73:**7952-64.
219. **Sanchez, C. M., A. Izeta, J. M. Sanchez-Morgado, S. Alonso, I. Sola, M. Balasch, J. Plana-Duran, and L. Enjuanes.** 1999. Targeted recombination demonstrates that the spike gene of transmissible gastroenteritis coronavirus is a determinant of its enteric tropism and virulence. J Virol **73:**7607-18.
220. **Sawicki, S. G., and D. L. Sawicki.** 1990. Coronavirus transcription: subgenomic mouse hepatitis virus replicative intermediates function in RNA synthesis. J Virol **64:**1050-6.
221. **Sawicki, S. G., and D. L. Sawicki.** 1995. Coronaviruses use discontinuous extension for synthesis of subgenome-length negative strands. Adv Exp Med Biol **380:**499-506.
222. **Sawicki, S. G., D. L. Sawicki, D. Younker, Y. Meyer, V. Thiel, H. Stokes, and S. G. Siddell.** 2005. Functional and genetic analysis of coronavirus replicase-transcriptase proteins. PLoS Pathog **1:**e39.
223. **Schelle, B., N. Karl, B. Ludewig, S. G. Siddell, and V. Thiel.** 2005. Selective replication of coronavirus genomes that express nucleocapsid protein. J Virol **79:**6620-30.
224. **Schwarz, B., E. Routledge, and S. G. Siddell.** 1990. Murine coronavirus nonstructural protein ns2 is not essential for virus replication in transformed cells. J Virol **64:**4784-91.
225. **Sethna, P. B., M. A. Hofmann, and D. A. Brian.** 1991. Minus-strand copies of replicating coronavirus mRNAs contain antileaders. J Virol **65:**320-5.
226. **Sethna, P. B., S. L. Hung, and D. A. Brian.** 1989. Coronavirus subgenomic minus-strand RNAs and the potential for mRNA replicons. Proc Natl Acad Sci U S A **86:**5626-30.
227. **Seybert, A., C. C. Posthuma, L. C. van Dinten, E. J. Snijder, A. E. Gorbalenya, and J. Ziebuhr.** 2005. A complex zinc finger controls the enzymatic activities of nidovirus helicases. J Virol **79:**696-704.
228. **Shi, S. T., J. J. Schiller, A. Kanjanahaluethai, S. C. Baker, J. W. Oh, and M. M. Lai.** 1999. Colocalization and membrane association of murine hepatitis

virus gene 1 products and De novo-synthesized viral RNA in infected cells. J Virol **73:**5957-69.

229. **Siddell, S., D. Sawicki, Y. Meyer, V. Thiel, and S. Sawicki.** 2001. Identification of the mutations responsible for the phenotype of three MHV RNA-negative ts mutants. Adv Exp Med Biol **494:**453-8.
230. **Siddell, S. G., J. Ziebuhr, and E. J. Snijder.** 2005. Coronaviruses, torovirues and arteriviruses, p. in press. *In* B. W. J. Mahy and V. ter Meulen (ed.), Topley and Wilson's Microbiology and Microbial Infections, 10th ed, vol. 1 and 2. Edward Arnold, London.
231. **Siegal, F. P., N. Kadowaki, M. Shodell, P. A. Fitzgerald-Bocarsly, K. Shah, S. Ho, S. Antonenko, and Y. J. Liu.** 1999. The nature of the principal type 1 interferon-producing cells in human blood. Science **284:**1835-7.
232. **Snijder, E. J., P. J. Bredenbeek, J. C. Dobbe, V. Thiel, J. Ziebuhr, L. L. Poon, Y. Guan, M. Rozanov, W. J. Spaan, and A. E. Gorbalenya.** 2003. Unique and conserved features of genome and proteome of SARS-coronavirus, an early split-off from the coronavirus group 2 lineage. J Mol Biol **331:**991-1004.
233. **Snijder, E. J., J. A. den Boon, P. J. Bredenbeek, M. C. Horzinek, R. Rijnbrand, and W. J. Spaan.** 1990. The carboxyl-terminal part of the putative Berne virus polymerase is expressed by ribosomal frameshifting and contains sequence motifs which indicate that toro- and coronaviruses are evolutionarily related. Nucleic Acids Res **18:**4535-42.
234. **Snijder, E. J., Y. van der Meer, J. Zevenhoven-Dobbe, J. J. Onderwater, J. van der Meulen, H. K. Koerten, and A. M. Mommaas.** 2006. Ultrastructure and origin of membrane vesicles associated with the severe acute respiratory syndrome coronavirus replication complex. J Virol **80:**5927-40.
235. **Sola, I., J. L. Moreno, S. Zuniga, S. Alonso, and L. Enjuanes.** 2005. Role of nucleotides immediately flanking the transcription-regulating sequence core in coronavirus subgenomic mRNA synthesis. J Virol **79:**2506-16.
236. **Sparks, J. S., X. Lu, and M. R. Denison.** 2007. Genetic analysis of Murine hepatitis virus nsp4 in virus replication. J Virol **81:**12554-63.
237. **Sperry, S. M., L. Kazi, R. L. Graham, R. S. Baric, S. R. Weiss, and M. R. Denison.** 2005. Single-amino-acid substitutions in open reading frame (ORF) 1b-nsp14 and ORF 2a proteins of the coronavirus mouse hepatitis virus are attenuating in mice. J Virol **79:**3391-400.
238. **Spiegel, M., A. Pichlmair, L. Martinez-Sobrido, J. Cros, A. Garcia-Sastre, O. Haller, and F. Weber.** 2005. Inhibition of Beta interferon induction by severe acute respiratory syndrome coronavirus suggests a two-step model for activation of interferon regulatory factor 3. J Virol **79:**2079-86.
239. **St-Jean, J. R., M. Desforges, F. Almazan, H. Jacomy, L. Enjuanes, and P. J. Talbot.** 2006. Recovery of a neurovirulent human coronavirus OC43 from an infectious cDNA clone. J Virol **80:**3670-4.
240. **Stadler, K., V. Masignani, M. Eickmann, S. Becker, S. Abrignani, H. D. Klenk, and R. Rappuoli.** 2003. SARS--beginning to understand a new virus. Nat Rev Microbiol **1:**209-18.
241. **Stark, G. R., I. M. Kerr, B. R. Williams, R. H. Silverman, and R. D. Schreiber.** 1998. How cells respond to interferons. Annu Rev Biochem **67:**227-64.
242. **Stertz, S., M. Reichelt, M. Spiegel, T. Kuri, L. Martinez-Sobrido, A. Garcia-Sastre, F. Weber, and G. Kochs.** 2007. The intracellular sites of early replication and budding of SARS-coronavirus. Virology **361:**304-15.

243. **Stohlman, S. A., R. S. Baric, G. N. Nelson, L. H. Soe, L. M. Welter, and R. J. Deans.** 1988. Specific interaction between coronavirus leader RNA and nucleocapsid protein. J Virol **62:**4288-95.
244. **Storz, J., C. W. Purdy, X. Lin, M. Burrell, R. E. Truax, R. E. Briggs, G. H. Frank, and R. W. Loan.** 2000. Isolation of respiratory bovine coronavirus, other cytocidal viruses, and Pasteurella spp from cattle involved in two natural outbreaks of shipping fever. J Am Vet Med Assoc **216:**1599-604.
245. **Su, D., Z. Lou, F. Sun, Y. Zhai, H. Yang, R. Zhang, A. Joachimiak, X. C. Zhang, M. Bartlam, and Z. Rao.** 2006. Dodecamer structure of severe acute respiratory syndrome coronavirus nonstructural protein nsp10. J Virol **80:**7902-8.
246. **Sutton, G., E. Fry, L. Carter, S. Sainsbury, T. Walter, J. Nettleship, N. Berrow, R. Owens, R. Gilbert, A. Davidson, S. Siddell, L. L. Poon, J. Diprose, D. Alderton, M. Walsh, J. M. Grimes, and D. I. Stuart.** 2004. The nsp9 replicase protein of SARS-coronavirus, structure and functional insights. Structure **12:**341-53.
247. **Tang, X. C., J. X. Zhang, S. Y. Zhang, P. Wang, X. H. Fan, L. F. Li, G. Li, B. Q. Dong, W. Liu, C. L. Cheung, K. M. Xu, W. J. Song, D. Vijaykrishna, L. L. Poon, J. S. Peiris, G. J. Smith, H. Chen, and Y. Guan.** 2006. Prevalence and genetic diversity of coronaviruses in bats from China. J Virol **80:**7481-90.
248. **Tekes, G., R. Hofmann-Lehmann, I. Stallkamp, V. Thiel, and H. J. Thiel.** 2008. Genome organization and reverse genetic analysis of a type I feline coronavirus. J Virol **82:**1851-9.
249. **ten Dam, E. B., C. W. Pleij, and L. Bosch.** 1990. RNA pseudoknots: translational frameshifting and readthrough on viral RNAs. Virus Genes **4:**121-36.
250. **Teng, H., J. D. Pinon, and S. R. Weiss.** 1999. Expression of murine coronavirus recombinant papain-like proteinase: efficient cleavage is dependent on the lengths of both the substrate and the proteinase polypeptides. J Virol **73:**2658-66.
251. **Theofilopoulos, A. N., R. Baccala, B. Beutler, and D. H. Kono.** 2005. Type I interferons (alpha/beta) in immunity and autoimmunity. Annu Rev Immunol **23:**307-36.
252. **Thiel, V., Buch.** 2007. Coronaviruses: Molecular and Cellular Biology
253. **Thiel, V., J. Herold, B. Schelle, and S. G. Siddell.** 2001. Infectious RNA transcribed in vitro from a cDNA copy of the human coronavirus genome cloned in vaccinia virus. J Gen Virol **82:**1273-81.
254. **Thiel, V., J. Herold, B. Schelle, and S. G. Siddell.** 2001. Viral replicase gene products suffice for coronavirus discontinuous transcription. J Virol **75:**6676-81.
255. **Thiel, V., K. A. Ivanov, A. Putics, T. Hertzig, B. Schelle, S. Bayer, B. Weissbrich, E. J. Snijder, H. Rabenau, H. W. Doerr, A. E. Gorbalenya, and J. Ziebuhr.** 2003. Mechanisms and enzymes involved in SARS coronavirus genome expression. J Gen Virol **84:**2305-15.
256. **Thiel, V., and S. G. Siddell.** 2005. Reverse genetics of coronaviruses using vaccinia virus vectors. Curr Top Microbiol Immunol **287:**199-227.
257. **Thiel, V., and F. Weber.** 2008. Interferon and cytokine responses to SARS-coronavirus infection. Cytokine Growth Factor Rev **19:**121-32.
258. **Tooze, J., S. Tooze, and G. Warren.** 1984. Replication of coronavirus MHV-A59 in sac- cells: determination of the first site of budding of progeny virions. Eur J Cell Biol **33:**281-93.

259. **Tooze, J., S. A. Tooze, and S. D. Fuller.** 1987. Sorting of progeny coronavirus from condensed secretory proteins at the exit from the trans-Golgi network of AtT20 cells. J Cell Biol **105:**1215-26.
260. **Tresnan, D. B., R. Levis, and K. V. Holmes.** 1996. Feline aminopeptidase N serves as a receptor for feline, canine, porcine, and human coronaviruses in serogroup I. J Virol **70:**8669-74.
261. **Van Den Born, E., A. P. Gultyaev, and E. J. Snijder.** 2004. Secondary structure and function of the 5'-proximal region of the equine arteritis virus RNA genome. Rna **10:**424-37.
262. **van der Hoek, L.** 2007. Human coronaviruses: what do they cause? Antivir Ther **12:**651-8.
263. **van der Hoek, L., K. Pyrc, M. F. Jebbink, W. Vermeulen-Oost, R. J. Berkhout, K. C. Wolthers, P. M. Wertheim-van Dillen, J. Kaandorp, J. Spaargaren, and B. Berkhout.** 2004. Identification of a new human coronavirus. Nat Med **10:**368-73.
264. **van der Meer, Y., E. J. Snijder, J. C. Dobbe, S. Schleich, M. R. Denison, W. J. Spaan, and J. K. Locker.** 1999. Localization of mouse hepatitis virus nonstructural proteins and RNA synthesis indicates a role for late endosomes in viral replication. J Virol **73:**7641-57.
265. **van der Most, R. G., P. J. Bredenbeek, and W. J. Spaan.** 1991. A domain at the 3' end of the polymerase gene is essential for encapsidation of coronavirus defective interfering RNAs. J Virol **65:**3219-26.
266. **van Marle, G., J. C. Dobbe, A. P. Gultyaev, W. Luytjes, W. J. Spaan, and E. J. Snijder.** 1999. Arterivirus discontinuous mRNA transcription is guided by base pairing between sense and antisense transcription-regulating sequences. Proc Natl Acad Sci U S A **96:**12056-61.
267. **van Marle, G., W. Luytjes, R. G. van der Most, T. van der Straaten, and W. J. Spaan.** 1995. Regulation of coronavirus mRNA transcription. J Virol **69:**7851-6.
268. **Vennema, H., G. J. Godeke, J. W. Rossen, W. F. Voorhout, M. C. Horzinek, D. J. Opstelten, and P. J. Rottier.** 1996. Nucleocapsid-independent assembly of coronavirus-like particles by co-expression of viral envelope protein genes. Embo J **15:**2020-8.
269. **Versteeg, G. A., P. J. Bredenbeek, S. H. van den Worm, and W. J. Spaan.** 2007. Group 2 coronaviruses prevent immediate early interferon induction by protection of viral RNA from host cell recognition. Virology **361:**18-26.
270. **Vignuzzi, M., J. K. Stone, J. J. Arnold, C. E. Cameron, and R. Andino.** 2006. Quasispecies diversity determines pathogenesis through cooperative interactions in a viral population. Nature **439:**344-8.
271. **Vijgen, L., E. Keyaerts, E. Moes, I. Thoelen, E. Wollants, P. Lemey, A. M. Vandamme, and M. Van Ranst.** 2005. Complete genomic sequence of human coronavirus OC43: molecular clock analysis suggests a relatively recent zoonotic coronavirus transmission event. J Virol **79:**1595-604.
272. **von Grotthuss, M., L. S. Wyrwicz, and L. Rychlewski.** 2003. mRNA cap-1 methyltransferase in the SARS genome. Cell **113:**701-2.
273. **Voss, D., A. Kern, E. Traggiai, M. Eickmann, K. Stadler, A. Lanzavecchia, and S. Becker.** 2006. Characterization of severe acute respiratory syndrome coronavirus membrane protein. FEBS Lett **580:**968-73.
274. **Wang, L. F., Z. Shi, S. Zhang, H. Field, P. Daszak, and B. T. Eaton.** 2006. Review of bats and SARS. Emerg Infect Dis **12:**1834-40.

275. **Wathelet, M. G., M. Orr, M. B. Frieman, and R. S. Baric.** 2007. Severe acute respiratory syndrome coronavirus evades antiviral signaling: role of nsp1 and rational design of an attenuated strain. J Virol **81:**11620-33.
276. **Williams, G. D., R. Y. Chang, and D. A. Brian.** 1999. A phylogenetically conserved hairpin-type 3' untranslated region pseudoknot functions in coronavirus RNA replication. J Virol **73:**8349-55.
277. **Winter, C., C. Schwegmann-Wessels, D. Cavanagh, U. Neumann, and G. Herrler.** 2006. Sialic acid is a receptor determinant for infection of cells by avian Infectious bronchitis virus. J Gen Virol **87:**1209-16.
278. **Woo, P. C., S. K. Lau, C. M. Chu, K. H. Chan, H. W. Tsoi, Y. Huang, B. H. Wong, R. W. Poon, J. J. Cai, W. K. Luk, L. L. Poon, S. S. Wong, Y. Guan, J. S. Peiris, and K. Y. Yuen.** 2005. Characterization and complete genome sequence of a novel coronavirus, coronavirus HKU1, from patients with pneumonia. J Virol **79:**884-95.
279. **Xu, X., Y. Liu, S. Weiss, E. Arnold, S. G. Sarafianos, and J. Ding.** 2003. Molecular model of SARS coronavirus polymerase: implications for biochemical functions and drug design. Nucleic Acids Res **31:**7117-30.
280. **Yang, C. W., Y. N. Yang, P. H. Liang, C. M. Chen, W. L. Chen, H. Y. Chang, Y. S. Chao, and S. J. Lee.** 2007. Novel small-molecule inhibitors of transmissible gastroenteritis virus. Antimicrob Agents Chemother **51:**3924-31.
281. **Yang, H., M. Yang, Y. Ding, Y. Liu, Z. Lou, Z. Zhou, L. Sun, L. Mo, S. Ye, H. Pang, G. F. Gao, K. Anand, M. Bartlam, R. Hilgenfeld, and Z. Rao.** 2003. The crystal structures of severe acute respiratory syndrome virus main protease and its complex with an inhibitor. Proc Natl Acad Sci U S A **100:**13190-5.
282. **Yeager, C. L., R. A. Ashmun, R. K. Williams, C. B. Cardellichio, L. H. Shapiro, A. T. Look, and K. V. Holmes.** 1992. Human aminopeptidase N is a receptor for human coronavirus 229E. Nature **357:**420-2.
283. **Yilla, M., B. H. Harcourt, C. J. Hickman, M. McGrew, A. Tamin, C. S. Goldsmith, W. J. Bellini, and L. J. Anderson.** 2005. SARS-coronavirus replication in human peripheral monocytes/macrophages. Virus Res **107:**93-101.
284. **Younker, D. R., and S. G. Sawicki.** 1998. Negative strand RNA synthesis by temperature-sensitive mutants of mouse hepatitis virus. Adv Exp Med Biol **440:**221-6.
285. **Yount, B., K. M. Curtis, and R. S. Baric.** 2000. Strategy for systematic assembly of large RNA and DNA genomes: transmissible gastroenteritis virus model. J Virol **74:**10600-11.
286. **Yount, B., K. M. Curtis, E. A. Fritz, L. E. Hensley, P. B. Jahrling, E. Prentice, M. R. Denison, T. W. Geisbert, and R. S. Baric.** 2003. Reverse genetics with a full-length infectious cDNA of severe acute respiratory syndrome coronavirus. Proc Natl Acad Sci U S A **100:**12995-3000.
287. **Yount, B., M. R. Denison, S. R. Weiss, and R. S. Baric.** 2002. Systematic assembly of a full-length infectious cDNA of mouse hepatitis virus strain A59. J Virol **76:**11065-78.
288. **Yount, B., R. S. Roberts, A. C. Sims, D. Deming, M. B. Frieman, J. Sparks, M. R. Denison, N. Davis, and R. S. Baric.** 2005. Severe acute respiratory syndrome coronavirus group-specific open reading frames encode nonessential functions for replication in cell cultures and mice. J Virol **79:**14909-22.

289. **Yu, S. Y., Y. W. Hu, X. Y. Liu, W. Xiong, Z. T. Zhou, and Z. H. Yuan.** 2005. Gene expression profiles in peripheral blood mononuclear cells of SARS patients. World J Gastroenterol **11:**5037-43.
290. **Zhai, Y., F. Sun, X. Li, H. Pang, X. Xu, M. Bartlam, and Z. Rao.** 2005. Insights into SARS-CoV transcription and replication from the structure of the nsp7-nsp8 hexadecamer. Nat Struct Mol Biol **12:**980-6.
291. **Zheng, B., M. L. He, K. L. Wong, C. T. Lum, L. L. Poon, Y. Peng, Y. Guan, M. C. Lin, and H. F. Kung.** 2004. Potent inhibition of SARS-associated coronavirus (SCOV) infection and replication by type I interferons (IFN-alpha/beta) but not by type II interferon (IFN-gamma). J Interferon Cytokine Res **24:**388-90.
292. **Zhou, H., and S. Perlman.** 2006. Preferential infection of mature dendritic cells by mouse hepatitis virus strain JHM. J Virol **80:**2506-14.
293. **Zhou, M., A. K. Williams, S. I. Chung, L. Wang, and E. W. Collisson.** 1996. The infectious bronchitis virus nucleocapsid protein binds RNA sequences in the 3' terminus of the genome. Virology **217:**191-9.
294. **Ziebuhr, J.** 2005. The coronavirus replicase. Curr Top Microbiol Immunol **287:**57-94.
295. **Ziebuhr, J., B. Schelle, N. Karl, E. Minskaia, S. Bayer, S. G. Siddell, A. E. Gorbalenya, and V. Thiel.** 2007. Human coronavirus 229E papain-like proteases have overlapping specificities but distinct functions in viral replication. J Virol **81:**3922-32.
296. **Ziebuhr, J., E. J. Snijder, and A. E. Gorbalenya.** 2000. Virus-encoded proteinases and proteolytic processing in the Nidovirales. J Gen Virol **81:**853-79.
297. **Ziebuhr, J., V. Thiel, and A. E. Gorbalenya.** 2001. The autocatalytic release of a putative RNA virus transcription factor from its polyprotein precursor involves two paralogous papain-like proteases that cleave the same peptide bond. J Biol Chem **276:**33220-32.
298. **Zuniga, S., I. Sola, S. Alonso, and L. Enjuanes.** 2004. Sequence motifs involved in the regulation of discontinuous coronavirus subgenomic RNA synthesis. J Virol **78:**980-94.
299. **Zuniga, S., I. Sola, J. L. Moreno, P. Sabella, J. Plana-Duran, and L. Enjuanes.** 2007. Coronavirus nucleocapsid protein is an RNA chaperone. Virology **357:**215-27.
300. **Zust, R., L. Cervantes-Barragan, T. Kuri, G. Blakqori, F. Weber, B. Ludewig, and V. Thiel.** 2007. Coronavirus non-structural protein 1 is a major pathogenicity factor: implications for the rational design of coronavirus vaccines. PLoS Pathog **3:**e109.
301. **Zust, R., T. B. Miller, S. J. Goebel, V. Thiel, and P. S. Masters.** 2008. Genetic interactions between an essential 3' cis-acting RNA pseudoknot, replicase gene products, and the extreme 3' end of the mouse coronavirus genome. J Virol **82:**1214-28.

11 Curriculum Vitae

Name: ZUEST

First name: Roland

Date of Birth: 10.04.1978

Place of Birth: Antananarivo, Madagaskar

Place of origin: Lutzenberg, AR

Education

1994-1998 Gymnasium in Heerbrugg, 1998, Maturatypus B

1998-2002 Masterstudies in molecular biology at the Biocenter, University of Basel, Switzerland

2003 Diploma thesis “Expression profiling of Abf1p regulated genes in *S. cerevisiae* using oligonucleotide microarrays” supervised by Prof. Dr. Michael Primig, Biocenter, Basel

2004-2008 Ph.D. thesis: “Reverse Genetic Analysis of Coronavirus Replication” at the Research Department, Cantonal Hospital St. Gallen, Supervisor: PD Dr. Volker Thiel, Research Department St. Gallen; Komitee: Prof. Dr. Michael O. Hottiger and Prof Dr. Michael O. Hengartner, University of Zürich

Original Publications

Cervantes-Barragan, L., **R. Zust**, F. Weber, M. Spiegel, K. S. Lang, S. Akira, V. Thiel, and B. Ludewig. 2007. Control of coronavirus infection through plasmacytoid dendritic-cell-derived type I interferon. Blood 109:1131-7.

Zust, R., L. Cervantes-Barragan, T. Kuri, G. Blakqori, F. Weber, B. Ludewig, and V. Thiel. 2007. Coronavirus non-structural protein 1 is a major pathogenicity factor: implications for the rational design of coronavirus vaccines. PLoS Pathog 3:e109.

Zust, R., T. B. Miller, S. J. Goebel, V. Thiel, and P. S. Masters. 2008. Genetic interactions between an essential 3' cis-acting RNA pseudoknot, replicase gene products, and the extreme 3' end of the mouse coronavirus genome. J Virol 82:1214-28.

Cervantes-Barragán, L., Kalinke U., **Zust R.**, Reizis B., López-Macías C., Thiel V., and Ludewig B. 2008. Type I interferon-mediated protection of macrophages and dendritic cells secures control of murine coronavirus infection, JEM, in revision

Meetings and Congresses attended

Züst R, Miller T., Goebel S., Masters P., and Thiel V.
Genetic Interactions between an Essential 3' cis-Acting RNA Pseudoknot, Replicase Gene Products, and the Extreme 3' End of the Mouse Coronavirus Genome
Deutsche Gesellschaft für Virologie, Annual Meeting, Heidelberg, 5.-8. March 2008

Züst R, Cervantes-Barragán L, Kuri T, Blakqori G, Weber F, Ludewig B. and Thiel V.
Identification of Coronavirus Non-Structural Protein 1 as a Major Pathogenicity Factor Implications for the Rational Design of Live Attenuated Coronavirus Vaccines.
Third European Congress of Virology, Nürberg,1-5. September 2007 (Poster presentation, poster nominated for award as 2nd among 900 shown.)

Züst R, Cervantes-Barragán L, Kuri T, Blakqori G, Weber F, Ludewig B. and Thiel V.
Identification of Coronavirus Non-Structural Protein 1 as a Major Pathogenicity Factor Implications for the Rational Design of Live Attenuated Coronavirus Vaccines
Annual Congress SGAI-SSAI, Basel, 19.-20. April, 2007 (Poster presentation)

Züst R, Cervantes-Barragán L, Kuri T, Blakqori G, Weber F, Ludewig B. and Thiel V.
Interaction of mouse hepatitis non-strutural protein 1 with innate immune effector pathways XIX. meeting of the swiss immunology PhD. students at Schloss Wolfsberg, Ermatingen, 26.-28. March 2007 (oral presentation)

Züst R, Cervantes-Barragán L, Kuri T, Blakqori G, Weber F, Ludewig B. and Thiel V.
Rational Design of Live Attenuated Coronavirus Vaccines
Microorganisms and Innate Immunity, Annual Congress of the Swiss Society of Microbiology, Interlaken,1.-2. March 2007 (oral presentation)

Züst, R., Cervantes, L., Weber, F., Ludewig, B., Thiel, V.
Effect of murine coronavirus non-structural protein 1 on innate immune responses (poster presentation).
EMDS (European Macrophage and Dendritic Cell Society), Freiburg (Deutschland) 05.-07. Oktober 2006

Züst, R., Cervantes, L., Ludewig, B., Thiel, V.
Effect of mouse hepatitis virus non-structural protein 1 on type I interferon responses in murine dendritic cells (poster presentation) .
XVIII. meeting of the swiss immunology PhD. students at Schloss Wolfsberg, Ermatingen 20.-22 March 2006

12 Acknowledgements

I would like to thank to PD. Dr. Volker Thiel and PD. Dr. Ludewig Burkhard for giving me the opportunity to work in their lab, for stimulating discussions and for a very friendly atmosphere exceeding the common boss-worker relationship.

Especially my supervisor Volker deserves a huge laud for having endless patience and for explaining even complex things uncomplicated. Also thanks to the frequently used “Volkers export and import service” and to many funny times in the office (I still don’t cope with the defeat in the continental race).

Furthermore I’d like to thank to all members of the lab who generated a very nice atmosphere. Thanks to Reinhard, Lucas, Divine and Simone for coming together for sports activities and special training of the “talking muscles”. Some long chat sessions with Simone in Kieser will be unforgettable.

Thanks to all the nice girls in the lab. I enjoyed the stimulating discussion with Bea, and I’m glad to read, that my statements were all right ;-). Also thanks to Elke, Rita, Sonja and Vroni for simply being friends.

Also thank to Harinda for being the driving force in organizing all the TGIFs and BBQs.

Very special thank to my girlfriend Luisa who helped me with all immunological problems and for supporting (and standing) me during the most stressful time. Special thanks for our delightful discussions which were thank goodness not only concerning work.

I would also like to thank the thesis committee Prof. Dr. Michael O. Hottiger and Prof. Dr. Michael Hengartner for taking the time to read and evaluate my thesis.

I’m grateful to my family and friends for their support and usually not so big interest in my work (fortunately, to keep a healthful balance).